RECURSIVE FILTERS AND POLYPHASE DISTANCE RELAYS

A Thesis

Submitted to the Faculty of Graduate Studies and Research
in Partial Fulfilment of the Requirements
for the Degree of

Master of Science

in the Department of Electrical Engineering
University of Saskatchewan

by

Kulwant Singh Nanuan
Saskatoon, Saskatchewan
July 1981

ACKNOWLEDGEMENTS

The author expresses his gratitude and appreciation to Dr. M. S. Sachdev for his guidance throughout the course of this work. His advice and assistance in the preparation of this thesis is thankfully acknowledged.

Special thanks are extended to his wife, Ravinder, for her encouragement during the study.

Financial assistance provided by the National Science and Engineering Research Council through grant No. A7249 is thankfully acknowledged.

UNIVERSITY OF SASKATCHEWAN

Electrical Engineering Abstract 81A211

RECURSIVE FILTERS AND POLYPHASE DISTANCE RELAYS

Student: Kulwant Singh Nanuan Supervisor: Dr. M. S. Sachdev

M.Sc. Thesis Presented to the

College of Graduate Studies and Research

July 1981

ABSTRACT

Distance relays, alone and in conjuction with communication channels, are used to protect modern EHV transmission lines. These relays check the electrical distance from a relay location to the fault and decide whether the fault is inside or outside the relay's assigned protected zone.

Presently, distance relays use electromechanical devices or electronic (solid-state, analog) circuits as relay structures. The cost of both the electromechanical and solid-state analog systems has been increasing rapidly during the last fifteen years. On the other hand, the cost of digital processors has been rapidly decreasing. It seems that the use of digital processors for control and protection systems is at the verge of becoming economically viable.

This thesis reviews the developments in the area of digital relaying and polyphase distance relays. Procedures for designing digital lowpass and bandpass recursive filters are outlined. Feasibility of using the designed recursive filters in digital distance relays is then examined. The studies indicate that using recursive filters for processing fault data does not necessarily permit relaying decisions to be made in shorter times. Lowpass recursive filters do, however, stabilize the calculated impedances and would, therefore, be useful in determining the locations of faults. Possibility of using the general exponential smoothing technique for processing power system voltages and currents is also investigated. A generic polyphase distance relay suitable for implementation on a microprocessor is designed. Also included is a brief description of the relay software and logic. The performance of the relay was tested in the real time-mode; some test results are also included.

TABLE OF CONTENTS

LIST OF FIGURES

LIST OF TABLES

1. INTRODUCTION

1.1 Background

Equipment for generation, transmission and distribution of electric power in a utility represents huge investments. For optimum returns the power system must be operated at peak efficiency and should be protected from avoidable interruptions and equipment damage. Some equipment damage is generally expected because of inherent defects in the equipment and external disturbing factors. The inherent defects are due to inadequate design, substandard materials and improper manufacture or installation procedures. The external disturbances include lightning storms, switching surges and conductor vibrations. Both, the inherent defects and external disturbances manifest in breakdowns which are in most cases, short circuits from a phase to ground. These and other types of shunt faults can seriously damage the equipment of the power system and cause loss of revenue to the utility. These faults can also damage the equipment of the customers and cause loss of their productivity.

1.2 Protection

The electrical equipment such as generators, transformers, buses, transmission lines and motors are invariably protected by relays and breakers. The protective relays are designed to detect the presence of a fault,

determine its location and initiate opening of circuit breakers which would isolate the damaged equipment from the rest of the system.

The philosophy generally used in relay applications is to divide the power system into protective zones; each zone is protected by a system of relays. A zone of protection normally includes a generator, a transformer, a bus, a transmission line, a distribution line or a motor. In the event of a fault in a zone, its relays open circuit breakers which isolate the zone thus protecting the remaining power system from being damaged and avoiding complete shutdown of the system. In addition to primary protection, backup protection is also provided. Backup relays isolate the faulted zone and an adjoining zone, in many applications, if the primary protection fails to isolate the faulted zone.

1.3 Protection of Transmission Lines

A power line can be protected by overcurrent, pilot or distance relays or by a combination of these relays. Overcurrent relays are relatively simple devices which are generally used for protecting distribution circuits. Two factors dictate this choice. One of the factors is economics; costlier relay systems cannot be economically justified for application on distribution circuits. The second factor is that, on distribution circuits, short

circuit currents are considerably larger than load currents and selectivity can be achieved by using time delay devices.

Many present day generating stations are located in remote areas which are far away from load centres. Long transmission lines are used to transmit energy from these generating stations to the load centres. For adequate transmission capability, the transmission lines are generally rated at 500 kV and above (EHV). Economics has dictated increased energy interchange between power systems causing them to operate close to their stability limits. This and other factors have forced the power industry to develop and use fast acting relays and circuit breakers. Presently one cycle (at 60 Hz) relays and three cycle breakers are being commonly used on EHV lines. Distance or pilot relays are, therefore, used to detect faults instead of overcurrent relays.

Pilot relays utilize currents and voltages at both ends of a protected line and communication channels are, therefore, required for transmitting information concerning currents or power flow direction from one end of the line to the other end. The information transfer is possible by using wire pilot, carrier pilot or microwave pilot channels. Pilot relays can provide high speed protection for 100 percent of the protected line but for security reasons, intentional time delays are incorporated. For long EHV

lines, admittance relays with communication channels are generally preferred over the current or power flow monitoring systems.

A distance relay estimates from line voltages and currents, the electrical distance from the relay location to the fault. A measured distance is then compared with the relay setting to determine if the fault is in the protected zone or not. If a fault is in the protected zone, the relay operates and issues a command to trip line breaker/breakers; otherwise the relay does not issue the trip command.

1.4 Digital Processor Relays

Earlier distance relays were designed using electromagnetic induction devices, such as, induction cup and balanced beam. The advent of transistor technology stimulated the development of solid-state relays. Their acceptance by the utility industry has been gradually increasing. The cost of analog (solid-state) systems has, however, been increasing during the last fifteen years. On the contrary, the cost of digital systems has been decreasing rapidly. It seems that the costs of programmable digital devices have reduced to a level where processor based relays can become cost effective compared to electromechanical and solid-state relays[37].

The protection of transmission lines is known to be the most challenging problem in the area of protection by programmable digital processors and has received attention from many researchers[38]. Walker et. al.[42] showed that the first and the largest high frequency component of the voltage and current wave forms during a system fault is the function of the distance of the fault from a relay location if the source impedance is neglected. The concept was implemented in the form of special purpose hardware which used bandpass filters to extract components in the 500 Hz to 10 kHz range from the system inputs. The frequency of the largest high frequency component was measured and used to determine the location of the fault on the protected line. After the initial phase of this work, a frequency modulated radar technique was used in the prototype hardware which was tested by measuring distances to faults on power lines when the lines were de-energized and, in one set of experiments, when the line was energized. Rockefeller[34] reported the feasibility of using a single computer for protecting all the equipment in an EHV substation and the transmission lines emanating from it. The problems of using a digital computer for performing all the protection functions in a subststion are clearly stated in this paper. The concept of using a single computer along with its backup for the protection of a substation has been discarded in favour of using individual relaying microprocessors for each major element. Gilcrest et. al.[14] described the first digital

computer based distance relay which was developed as a joint Pacific Gas and Electric Co. and the Westinghouse Electric Company project. The relay was installed on the 230 kV Tesla-Bellota line of the Pacific Gas and Electric Co. A Westinghouse P-2000 digital computer was used in this system to provide phase and ground distance protection. Initially the computer was not required to trip the line but only provided files of the phenomena observed and decisions arrived at. Later the computer was allowed to trip breakers and considerable field experience was gained. Hope et. al.[17] tested the use of Fourier transform and correlation approaches by calculating impedances as seen from a line terminal during a simulated fault. A sampling rate of 1440 Hz was used in these studies. Carr and Jackson[8] also used Fourier transform approach but used 240 Hz sampling rate in their digital distance relay design. In this design an attempt was made to coordinate the analog and digital filter designs. Digitized fault data was used to test the proposed approach and to demonstrate its feasibility. Horton[18] used Walsh functions in a digital distance relay. This work did not proceed beyond the initial exploration stage. In 1971, the American Electric Power Corporation started their digital relaying project jointly with the IBM Corporation. Feasibility of a substation computer was investigated by Phadke et. al.[31]. Alarm, monitoring, data logging, control, oscillography and relaying programs were developed. The specific relaying functions developed and tested include

three phase distance protection, high set current relaying, directional relaying, breaker failure protection and automatic reclosing. In the second phase, Phadke and colleagues[32] developed and tested an impedance protection approach using symmetrical components. The significant feature of this approach is that a single performance equation identifies all types of shunt faults. The performance of the relay was tested by checking its response to staged single phase to ground faults. Sachdev and Baribeau[36] in their distance relay design used digital filters which were designed using least error squares approach. The relay takes into account the effect of pre-fault load currents on fault currents and detects three phase, two phase, two phases to ground and single phase to ground faults. Memory action is included to discriminate close-in line faults from close-in faults on adjacent lines. In 1973 the General Electric Company established a joint project with the Philadelphia Electric Company for investigating the feasibility of using digital computer techniques in protecting transmission lines. Breingan et. al.[6] reported the development and design philosophy of this approach. The relays based on this design were installed at both ends of a 116 km, 500 kV transmission line of the Philadelphia Electric Company system. Over-reaching directional trip logic was included. The system remained in operation in a monitoring mode for a year. Staged fault tests were conducted to check the adequacy and suitability

of the system. Research in this area is being presently pursued by many utilities, manufacturers and universities.

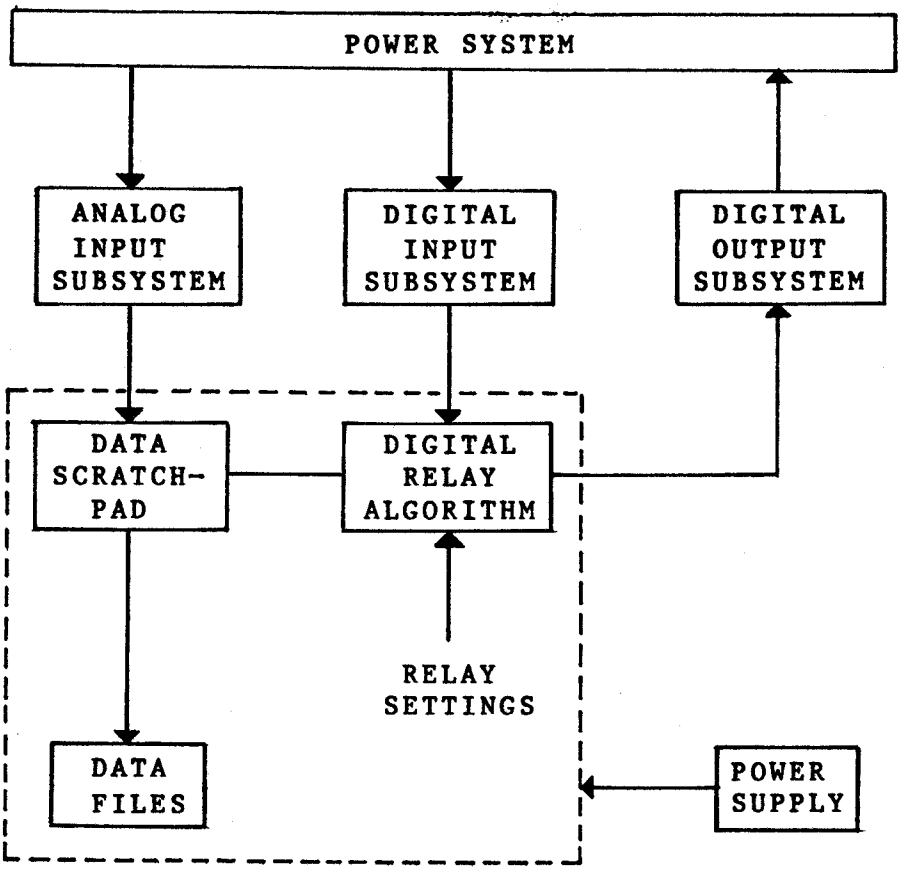

Figure 1.1 Functional block diagram of a digital processor relay

1.5 Functional Blocks of a Digital Processor Relay

A digital processor based relay can be conceptually described by functional blocks shown in Figure 1.1. Analog and digital subsystems, a digital processor, a power supply and input-output devices are the major functional blocks in

this system. The analog input subsystem receives low level signals, which represent system currents and voltages and transforms them to equivalent digital numbers. The digital input subsystem receives contact and voltage sense information; status changes of switches etc. The decisions of the digital relay are conveyed to the power system through a digital output subsystem. The digital processor includes data scratch pad, historical data files and digital processing unit. Because a failure of power supply would cause the loss of data and software programs residing in the processor at that time, use of read only and non-volatile memory is essential. It is also essential that the software programs be automatically reactivated on restoration of power supply after it has been once interrupted. The work reported in this project concerns with the design of filters, their use to process sampled voltages and currents at the relay location and developing a digital relay logic. These functions would normally be performed by the digital processor in the conceptual relay shown in Figure 1.1.

1.6 Objectives of the Project

The major objectives of the work reported in this thesis are:

(i) to investigate the suitability of recursive filters

for digital distance protection of transmission lines,

(ii) to investigate the benefits of polyphase distance relays and

(iii) to design and implement a generic polyphase distance relay.

Before commencing work towards these objectives, previous developments in the areas of digital protection of transmission lines and polyphase distance relays were reviewed.

1.7 Thesis Outline

This thesis is organized in eight chapters and appendices. The first chapter provides a very brief review of the areas relevant to the project and outlines the material presented in the thesis.

Many relaying algorithms have been proposed in the past. These algorithms process the digitized voltage and current samples to determine the magnitudes and phase angles of the voltage and current phasors. Five key algorithms are briefly outlined in Chapter 2. Procedures for designing distance relays and the background of polyphase distance relays are also reviewed in that chapter.

The algorithms reviewed in Chapter 2 use non-recursive filters to determine the equivalent fundamental frequency phasors from sampled voltages and currents. Recursive filters can also be used to process sampled data. Procedures for designing lowpass and bandpass recursive filters are described in Chapter 3. Numerical examples illustrating these procedures are included. The parameters of some of the designed recursive filters are tabulated and their frequency responses are demonstrated.

Chapter 4 demonstrates the use of recursive filters designed in Chapter 3. Simulated fault voltages and currents are processed by the designed bandpass filters. The outputs of the filters are processed by the sample and derivative and the least error squares algorithms. Apparent impedances and their phase angles are then calculated. The effectiveness of lowpass recursive filters in smoothing the repeatedly calculated impedances is also demonstrated.

Chapter 5 describes general exponential smoothing and single exponential smoothing techniques. These techniques are recursive in character. The general exponential smoothing is used to process the sampled voltages and currents. Single exponential smoothing technique is used to smooth the calculated impedances.

The developments of polyphase distance relays are outlined in Chapter 6. A generic polyphase distance relay system is selected and its digital equivalent is designed. Flowcharts describing details of the relay logic are included. The relay was implemented on the PDP 11/60 mini-computer and was tested in the real time mode. Some test results are also presented in Chapter 6.

Chapter 7 presents a brief summary and conclusions of the studies reported in this thesis. A list of references is given in Chapter 8. The references are listed in alphabetical order of the last name of the first author.

Chapter 9 includes five appendices. Appendix A discusses the reliability of the digital relaying algorithms. The z-transform technique is briefly presented in Appendix B. Equations for the three-sample least error squares algorithm are derived in Appendix C. Coefficients of the 6X9 least error squares algorithm and some additional test results of the studies reported in Chapter 4 are also given in that appendix. Appendix D presents the derivation of general exponential smoothing equations and some additional test results of the studies reported in Chapter 5. A technique for modifying the filter coefficients to obtain the phasor IZ_r directly from the sampled values of the current is given in Appendix E.

2. DISTANCE RELAYS AND DIGITAL RELAYING ALGORITHMS

A brief introduction on relays used for protecting transmission lines has been given in Chapter 1. The reasons for preferring distance relays over the overcurrent relays for transmission line protection have been given in that chapter. Developments of electromechanical and solid-state distance relays and their digital versions have also been outlined. The objective of this project stated in Chapter 1 is to briefly review the state of the art of distance protection with specific emphasis on their implementation in digital processor software packages. This chapter, therefore, reviews the principles of operation of distance relays and procedures for designing admittance relays. Previously published literature on digital distance relaying algorithms is also reviewed.

2.1 Distance relays

A distance relay operates if the impedance (voltage to current ratio) as seen from the relay location appears to be less than a pre-specified value. This concept takes advantage of the fact that magnitude of the voltage (V) to current (I) ratio is smaller during faults than the magnitude of this ratio during normal operating conditions. The argument of the V/I ratio is usually more than 60 degrees during faults but is considerably less during normal

loads.

The magnitudes of impedances seen by relays protecting long EHV lines may not be substantially different during faults and normal loading of the lines but the arguments of the impedances are quite different. A.R. van C. Warrington[43] used the phase angle criterion to distinguish faults from normal operating conditions.

Distance relays can be classified by the shape of their characteristics in the impedance or admittance plane. The major categories are:

(i) Impedance relay; circular characteristic in the impedance plane with centre of the circle at the origin.

(ii) Offset impedance relay; circular characteristic in the impedance plane with centre of the circle offset from the origin.

(iii) Admittance relay; circular characteristic in the impedance plane with the circle passing through the origin.

(iv) Reactance relay; straight line characteristic

in the impedance plane - characteristic is parallel to the resistance axis.

(v) Other characteristics; such as parabolic, hyperbolic, quadrilateral etc.

Reactance relays are suitable for protecting short lines whereas admittance and quadrilateral relays are specifically suitable for protecting long lines. A relay of the type categorized above usually monitors one voltage and one current of a three phase line. In distance protection systems seven relays are usually used for each zone of EHV lines; three relays monitoring phase to neutral voltages and line currents, three relays monitoring line to line voltages and differences between line currents of the corresponding phases and one relay to detect three phase faults. These relays usually belong to one of the five categories listed above. The most commonly used relays on the EHV transmission lines are the admittance (mho) relays. Procedures for designing these relays are briefly given in the following subsection.

2.1.1 Admittance relay design

The development of an admittance relay was first reported in 1943[43]. This relay consisted of amplitude and phase comparators. The amplitude comparator checked if the

magnitude of the apparent impedance was less than the set value and the phase comparator distinguished faults from normal load conditions. Figure 2.1 depicts the characteristics of three admittance relays in the impedance plane. Each characteristic represents a protective relay; the circles M_1, M_2 and M_3 represent the first, second and third zones of the protected line. Normally a relay operates when the tip of the impedance vector, determined from a voltage and a current at the relay location, is inside the relay characteristic. Should the tip of the impedance vector be outside the characteristic, the relay would block. Since impedance as seen from the relay location depends on the operating conditions, an appropriate characteristic enables the relay to distinguish line faults from other operating conditions. An admittance relay characteristic can be achieved by systems using either amplitude or phase comparators. Some of the possible design alternatives are now discussed.

The characteristics of an admittance relay have been shown in Figure 2.1. A characteristic of this form can be defined by the mathematical inequality:

$$\left|\frac{Z_1}{2}\right| > \left|Z - \frac{Z_1}{2}\right| \qquad (2.1)$$

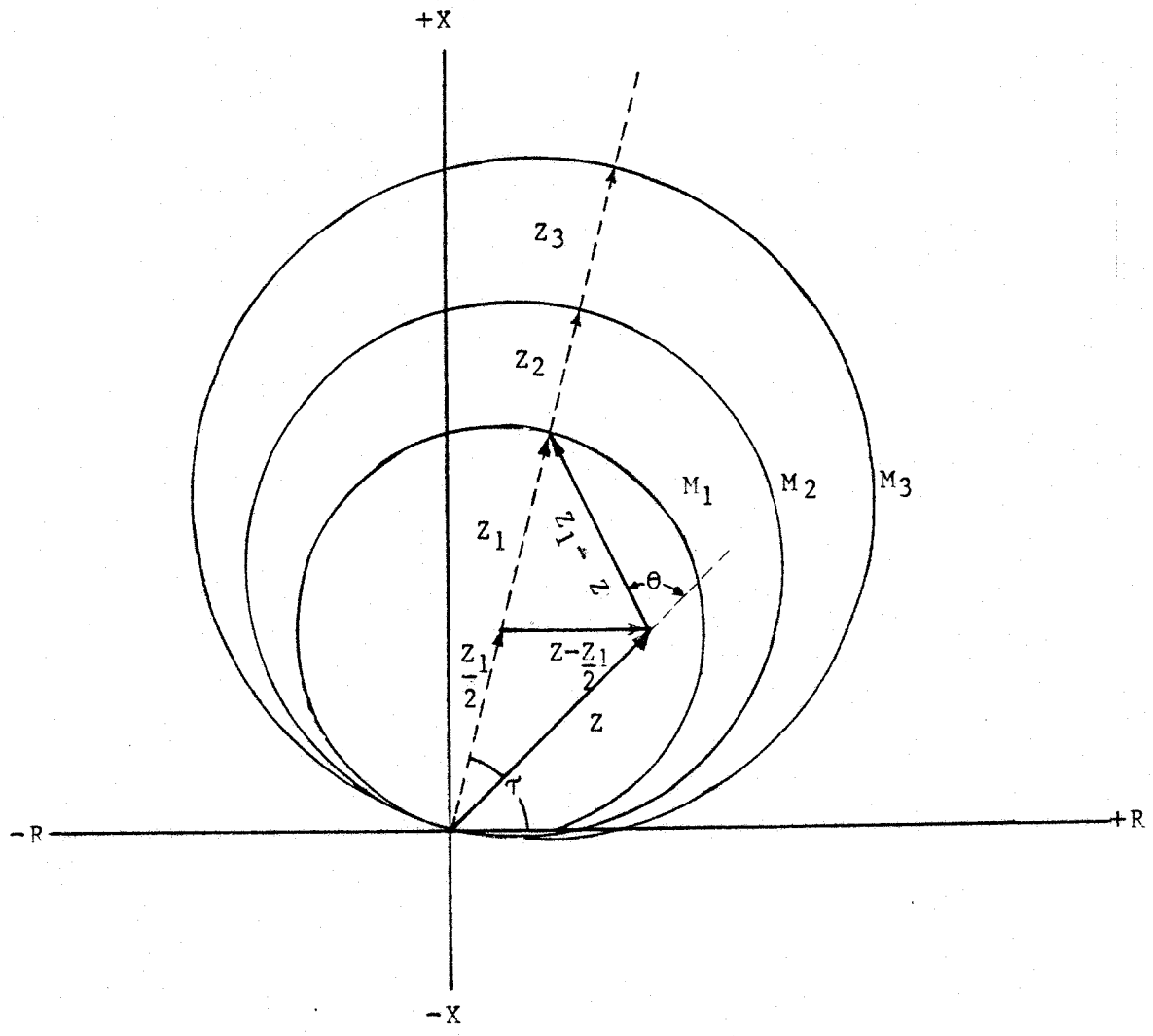

Figure 2.1 Operating characteristics of a mho type distance relay

where:

Z_1 is the set reach of the relay

Z is the impedance seen by the relay = $|V/I|$

Multiplying both sides of this equation by the current, I, at the relay location, the following inequality is obtained:

$$|Z_1 I| > |2ZI - Z_1 I| \qquad (2.2)$$

During a fault ZI is the voltage, V, at the relay location and Equation 2.2, therefore, transforms to:

$$|Z_1 I| > |2V - Z_1 I| \qquad (2.3)$$

Electromagnetic, electric or magnetic amplitude comparison devices can be used to implement the design based on Equation 2.3.

Another alternative approach to admittance relay design would be to use phase comparison. Consider the impedances Z and (Z_1-Z) shown in Figure 2.1. The angle, θ, between the impedances is less than 90 degrees if the tip of Z is in the defined characteristic. The angle θ is 90 degrees when the tip of the impedance Z is on the characteristic circle. If the tip of the impedance Z is outside the characteristic circle, angle θ is more than 90 degrees. The relay

characteristic can, therefore, be defined as follows:

$$-90^{o} < \theta < 90^{o} \qquad (2.4)$$

Since θ is the angle between Z and $(Z_1 - Z)$, it is also the angle between phasors IZ and $(IZ_1 - IZ)$ which are V and $(IZ_1 - V)$ phasors. A cosine type phase comparator energised by V and $(IZ_1 - V)$ can be used to implement the desired relay characteristic.

2.1.2 Polarized mho relays

Voltages of the faulted phase or phases at the relay location reduce to zero during close-in faults. The impedance measured by the admittance (mho) relay is also zero but it is not possible to directly determine whether the fault is on bus side or line side of the relay. This serious shortcoming of mho relays can result in incorrect relay operations or failures to operate. To alleviate this problem, polarized mho relays were developed. Brief details of their design are given in References 10,16, 19, 20, 30 and 44. The general approach in these references is either to use memory action or to polarize the relay with voltages of the sound phase or phases. These modifications are quite effective and during close-in faults, the relays generally operate only if the fault is on the line side of the relay.

2.1.3 Polyphase relays

The distance relays which use amplitude or phase comparators are called single phase relays. Distance relay systems presently used on EHV transmission lines consist of six or seven such comparators to cater all types of transmission line faults in one zone. The protection systems using these relays are, therefore, quite complex. To reduce this complexity, polyphase relays were developed. A single polyphase relay unit[29,32] or a set of two or three relay units[4,9,30,35,39] can respond to all types of line faults. The development of the polyphase distance relays, their principles of operation, design and digital implementation are reported in some detail in Chapter 6.

2.2 Review of Literature on the Relaying Algorithms

Distance relays in general and mho relays in particular have been discussed in the last section. Presently, electromechanical or solid state mho relays are used for protecting EHV lines. The digital technology has rapidly progressed during the last fifteen years and it seems that analog systems can now be replaced by digital systems. Engineers and researchers have suggested digital algorithms which can form the basis for decision making in digital relays. The previously suggested algorithms are reviewed in this section and three of these algorithms are used in the

work reported later in this thesis.

The relaying algorithms calculate apparent impedances from the digitized samples of voltages and currents observed at the relay location. These algorithms either calculate the magnitude of the apparent impedance and its phase angle or the resistance and reactance (sometimes inductance) as seen from the relay location. The algorithms reported so far can be divided into the following general categories.

(i) Sample and derivative approach
(ii) Sinusoidal curve fitting approach
(iii) Fourier-analysis and walsh-analysis notch filters
(iv) Least error squares curve fitting approach
(v) Differential equations approach

Brief description of these algorithms follows.

2.2.1 Sample and derivative approach

Mann and Morrison[24] proposed that the peak value of a voltage or current signal can be calculated from its sampled value and the rate of change of the signal at the instant the sample is taken. If the signal is clean and is composed of a fundamental frequency component only, the desired

signal and its derivative may be defined as follows:

$$v_k = V_p \sin(wt_k + \theta_v) \tag{2.5}$$

$$v'_k = w V_p \cos(wt_k + \theta_v) \tag{2.6}$$

Using trigonometric identities, peak value and phase angle of the signal can be obtained as follows:

$$\begin{aligned} V_{pk}^2 &= \{V_p \sin(wt_k + \theta_v)\}^2 + \{V_p \cos(wt_k + \theta_v)\}^2 \\ &= (v_k)^2 + (v'_k/w)^2 \end{aligned} \tag{2.7}$$

$$wt_k + \theta_v = \tan^{-1}\left(\frac{\sin(wt_k + \theta_v)}{\cos(wt_k + \theta_v)}\right) = \tan^{-1}\left(\frac{wv_k}{v'_k}\right) \tag{2.8}$$

where:

v_k is the value of the signal at instant k

v'_k is the first derivative of v_k at instant k

If the signals are sampled at regular intervals of time, ΔT, the first derivative of v_k can be obtained using the Stirling's three point equation:

$$v'_k = \frac{1}{(2\Delta T)}(v_{k+1} - v_{k-1}) \tag{2.9}$$

A modification of the sample and derivative approach was used in the Westinghouse - Pacific Gas and Electric Company's Prodar 70 project[12]. The first and second derivatives of the signals were used instead of the samples and first derivatives. If a signal is of a single frequency

sinusoid (as in Equation 2.5), its second derivative is given by:

$$v''_k = - w^2 V_p \sin(wt_k + \theta_v) \qquad (2.10)$$

The peak value of the signal and its phase angle can be obtained from Equations 2.6 and 2.10 as follows:

$$V_{pk}^2 = \left[\frac{v'_k}{w}\right]^2 + \left[\frac{v''_k}{w^2}\right]^2 \qquad (2.11)$$

$$wt_k + \theta_v = \tan^{-1}\left(\frac{-v''_k}{wv'_k}\right) \qquad (2.12)$$

In this project v'_k was determined using Equation 2.9 and v''_k was calculated using Equation 2.13.

$$v''_k = \frac{1}{(\Delta T)^2}(v_{k+1} - 2v_k + v_{k-1}) \qquad (2.13)$$

2.2.2 Sinusoidal curve fitting approach

This approach was proposed by Gilbert et. al.[14] of the Pennsylvania Power and Light Company. In this approach the input data was considered to contain signals of fundamental frequency components only. It was shown that the peak value and the real and imaginary components of a signal can be obtained from three sampled values. It was further shown that apparent resistances and reactances can be obtained

from the sampled data by using the following equations.

$$R = \frac{2v_{k-1}\ i_{k-1} - v_k\ i_{k-2} - v_{k-2}\ i_k}{2(i_{k-1}^2 - i_{k-2}\ i_k)} \qquad (2.14)$$

$$X = \frac{v_{k-1}\ i_k - v_k\ i_{k-1}}{(i_{k-1}^2 - i_{k-2}\ i_k)\ \csc(\theta)} \qquad (2.15)$$

where: $\theta = 2\pi f \Delta T$

2.2.3 Fourier analysis

Ramamoorthy[33] proposed that fundamental frequency components can be extracted from the voltages and currents by correlating data with reference sine and cosine functions. The correlation procedure consists of using Equations 2.16 and 2.17 for obtaining the real and imaginary components of a voltage. From these components, peak value and phase angle of a voltage can be obtained using Equation 2.18.

$$V_c = \frac{1}{N}\left[v_{k-N} + v_k + 2\sum_{m=1}^{N-1} v_{k-(N/2)+m}\ \cos(2\pi m/N)\right] \qquad (2.16)$$

$$V_s = \frac{1}{N}\left[2\sum_{m=1}^{N-1} v_{k-(N/2)+m}\ \sin(2\pi m/N)\right] \qquad (2.17)$$

where:

N is the number of samples per cycle

V_c is the real component of the voltage signal

V_s is the imaginary component of the voltage signal

$$V_p = \sqrt{V_c^2 + V_s^2} \qquad \theta_v = \tan^{-1}(V_s / V_c) \qquad (2.18)$$

Similarly the real and imaginary components of currents are calculated.

From the peak values and phase angles of voltages and currents, apparent impedances can be calculated. The real and reactive components can be directly calculated from the real and imaginary components of voltages and currents. The following equations can be used for this purpose.

$$R = \frac{V_s I_s + V_c I_c}{I_s^2 + I_c^2} \qquad (2.19)$$

$$X = \frac{V_s I_c - V_c I_s}{I_s^2 + I_c^2} \qquad (2.20)$$

This algorithm takes a full cycle (60 Hz basis) of the post-fault data to provide some meaningful results.

2.2.4 Fourier algorithm with shortened window

Phadke et. al.[31] suggested that the response time of a digital relay can be reduced by using half cycle Fourier

analysis. The quality of filtering, however, deteriorates due to the decrease of the window size. The basic technique in this case is the same as the full cycle Fourier method except that the data window is shortened to one half cycle plus one sample. The real and imaginary components of a signal are obtained by using the following equations:

$$V_c = \frac{4}{N} \sum_{m=1}^{N/2} v_{k-(N/2)+m} \cos(2\pi m/N) \qquad (2.21)$$

$$V_s = \frac{4}{N} \sum_{m=1}^{N/2} v_{k-(N/2)+m} \sin(2\pi m/N) \qquad (2.22)$$

The real and imaginary components of the voltage and current phasors are then used to calculate impedances and their phase angles as in the case of Fourier analysis described above. This approach provides results in lesser time but the quality of the results suffers because the filtering provided by this method is considerably inferior.

2.2.5 Least error squares approach

Luckett[21] proposed the use of the least error squares approach for finding peak values and phase angles of power system voltages and currents. Sachdev and Baribeau[36] reported further developments in this approach. They demonstrated that computations for the least error squares curve fitting need not be performed in the on-line mode and then used the suggested method in a digital distance relay design.

Sachdev and Baribeau's[36] approach consists of first selecting a mathematical model for the signals which are required to be processed. The following model was considered in Reference 36.

$$V(t) = K e^{-t/T} + \sum_{m=1}^{N} K_m \sin(mwt + \theta_m) \qquad (2.23)$$

where:

K is the magnitude of the d.c. offset

T is the time constant of the signal

K_m is the magnitude of the mth harmonic

θ_m is the phase angle of the mth harmonic

The authors assumed that analog filtering would be used to band limit the inputs to the relay; effectively eliminating the fifth and higher harmonics from fault currents and voltages. The second and fourth harmonic components were assumed to be negligible. The term $e^{-t/T}$ was expanded using the first two terms of its Taylor series expansion and the trigonometric terms were expanded using trigonometric identities. The substitution reduced Equation 2.23 to the form when time $t = t_1$.

$$V(t_1) = K - Kt_1/T + K_1\sin(\theta_1)\cos(wt_1) + K_1\cos(\theta_1)\sin(wt_1) + K_3\sin(\theta_3)\cos(3wt_1) + K_3\cos(\theta_3)\sin(3wt_1) \qquad (2.24)$$

This equation was rewritten as Equation 2.25 by making the

following substitutions.

$x_1 = K$ $\qquad a_1 = 1$

$x_2 = -K/T$ $\qquad a_2 = t_1$

$x_3 = K_1 \cos(\theta_1)$ $\qquad a_3 = \sin(wt_1)$

$x_4 = K_1 \sin(\theta_1)$ $\qquad a_4 = \cos(wt_1)$

$x_5 = K_3 \cos(\theta_3)$ $\qquad a_5 = \sin(3wt_1)$

$x_6 = K_3 \sin(\theta_3)$ $\qquad a_6 = \cos(3wt_1)$

$$V(t) = a_1x_1 + a_2x_2 + a_3x_3 + a_4x_4 + a_5x_5 + a_6x_6 \qquad (2.25)$$

After a small interval of time ΔT has elapsed the time t_1 advances to $t_2 = t_1 + \Delta T$ and another voltage sample is obtained. The new voltage sample can also be written in the form of Equation 2.25. If p samples are obtained and expressed in the form of Equation 2.25, the following equation would be available.

$$[A]\ [X] = [V] \qquad (2.26)$$

pxq qx1 px1

where: q is the number of unknowns in each equation and
p is greater than q

The vector of unknowns [X] was determined using Equation 2.27. The elements of the left pseudoinverse of [A] were determined off-line which reduced the on-line computations considerably.

$$[X] = [A]^{\dagger}[V]$$

qx1 qxp pxl

$$[A]^{\dagger} = \left[[A]^{T}[A]\right]^{-1}[A]^{T} \qquad (2.27)$$

qxp qxp pxq qxp

$\left[[A]^{T}[A]\right]^{-1}[A]^{T}$ is the left psedoinverse of the matrix [A]. The above approach was used to extract the fundamental frequency components of voltages and currents from raw data.

A particular case of Equation 2.26 was reported to be the 6X9 algorithm; p=9 and q=6. In this case a set of nine equations in six unknowns were established. The unknowns included two terms for the d.c. offset, two terms for the fundamental component and two terms for the third harmonic component. The 6X9 algorithm has been used in this project; the results are reported in the subsequent chapters.

2.2.6 Differential equations approach

McInnes and Morrison[25] proposed that during faults a transmission line can be modelled as a series R-L circuit. The voltage at the relay location should, therefore, satisfy the following equation:

$$v = Ri + Ldi/dt \qquad (2.28)$$

Solution for the R and L parameters can be obtained by integration over two successive time periods or by solving two simultaneous equations. Reference 25 used the later approach and obtained R and L by using the following equations.

$$R = \frac{(v_{k-1} + v_k)(i_{k-1} + i_{k-2}) - (v_{k-1} + v_{k-2})(i_k - i_{k-1})}{(i_{k-1} + i_k)(i_{k-1} - i_{k-2}) - (i_{k-1} + i_{k-2})(i_k - i_{k-1})} \quad (2.29)$$

$$L = \frac{h(v_{k-1} + v_{k-2})(i_{k-1} + i_k) - (v_{k-1} + v_k)(i_{k-1} + i_{k-2})}{2(i_{k-1} + i_k)(i_{k-1} - i_{k-2}) - (i_{k-1} + i_{k-2})(i_k - i_{k-1})} \quad (2.30)$$

In Equation 2.28 the effect of shunt capacitance has been neglected. The model is, therefore, not valid for long EHV lines whose shunt capacitances are large and cannot be neglected. The algorithm, however, has the advantage that the d.c. offsets do not affect the results.

The relaying algorithms were tested for reliability; the test results are reported in Appendix A. One cycle Fourier and the 6X9 least error squares algorithms were also used in the project for calculating apparent impedances and their phase angles from fault currents and voltages. The results are given in Chapter 4.

2.3 Summary

Distance relays in general and admittance relays in particular have been described. Procedures for designing admittance relays using amplitude and phase comparators have been outlined. Polarized mho relays and the concept of polyphase distance relays have been briefly discussed. Digital algorithms developed in the last decade have also been briefly presented.

3. DIGITAL RECURSIVE FILTERS

The relaying algorithms reviewed in Chapter 2 use non-recursive filters to suppress the undesired frequencies present in the power system voltage and current signals. Another possible approach is to use recursive filters for processing fault voltages and currents. The theory of recursive filters and a procedure for designing these filters are described in this chapter. Design procedures for both lowpass and bandpass recursive filters are presented. Coefficients of filters for various cut off frequencies and sampling rates were calculated; the calculated coefficients are tabulated. Frequency responses of some of the digital filters are also given.

3.1 Introduction to Recursive Filter Theory

A digital filter is a process or device which accepts a sequence of numbers as input and processes it to produce another sequence of numbers as output. Digital filters can be either constructed as special purpose hardware devices or as software algorithms for use in programmable digital processors.

Digital filters implemented as computer software have some advantages over the analogue filters and filters using

digital hardware[1]. A few of the advantages are:

(i) The outputs of digital filters are somewhat inaccurate due to rounding and truncation errors but the inaccuracies can be controlled by choosing suitable word lengths. On the other hand, the analogue components cannot be easily made to a tolerance of less than about one percent which affects the accuracy of the outputs and causes the outputs to contain some noise.

(ii) The design of a digital filter can be altered by re-writing a section of the software program and in most cases by changing the coefficients of the filter.

(iii) The characteristics of a digital filter software remain unaltered over the useful life of the equipment.

Digital filters were, therefore, designed for implementation as software programs in this project.

3.1.1 Background

The general equation describing a digital filter can be written as[15]:

$$Y_n = \sum_{m=0}^{N} A_m X_{n-m} - \sum_{m=1}^{N} B_m Y_{n-m} \qquad (3.1)$$

where:

X_n is the nth input signal

Y_n is the nth output signal

A_m and B_m are the coefficients of the filter

N is the order of the filter

It is obvious that a digital filter is a linear combination of equally spaced numerical values, X_n's of some function X(t) and the computed values of output Y_n's. When a new sample becomes available, the index n is incremented and a new output is calculated. If all the A_m and B_m coefficients are not zero, the filter is classified as a recursive filter. Should all the B_m coefficients be zero, the filter is classified as a non-recursive filter.

A desired characteristics (bandwidth) can be achieved by a recursive filter whose order is much lower than the order of the non-recursive filter required to achieve the same effect. Recursive filters are, therefore, more economical in terms of computation time and computer memory

than non-recursive filters of similar characteristics.

Two simple examples of recursive filters are[15]:

$$Y_{n+1} = Y_n + \frac{1}{2}(X_{n+1} + X_n) \qquad (3.2)$$

$$Y_{n+1} = Y_{n-1} + \frac{1}{3}(X_{n+1} + X_n + X_{n-1}) \qquad (3.3)$$

Equation 3.2 uses the trapezoidal rule and Equation 3.3 uses the Simpsons formula. These equations indicate that a recursive filter remembers all the past data because each new output is obtained by using the previous output and the latest two or three samples of the input data.

Recursive filters are also called Infinite Impulse Response Filters (IIR) because they remember all the past information and produce from a single input, outputs for all times in the future.

For practical reasons, only finite length digital filters are used in practice. It is, however, not possible to compute the outputs near the ends of the input data strings. This disadvantage is not serious for long sequences of data points, but presents a serious problem for fairly short sequences. For example, a full cycle Fourier filter will start providing output only after one cycle. The practice of supplying a sequence of zero values beyond one or both ends of data can lead to substantially

inaccurate outputs.

3.2 Transfer Function of Recursive Filters

The background of digital filters has been briefly described in Section 3.1. Advantages of digital recursive filters have also been outlined. Filters are usually described by their transfer functions. In this section transfer function of recursive filters is derived.

The general equation for a recursive filter is already given as Equation 3.1 which is reproduced here:

$$Y_n = \sum_{m=0}^{N} A_m \; X_{n-m} - \sum_{m=1}^{N} B_m \; Y_{n-m} \qquad (3.4)$$

The input and output of a digital filter can be expressed in the exponential forms as follows:

$$X_n = C_i \; e^{(j2\pi f n \Delta T)}$$

$$Y_n = C_o \; e^{(j2\pi f n \Delta T + \theta)} \qquad (3.5)$$

The transfer function, H(f), for the filter can now be defined as:

$$H(f) = \frac{C_o}{C_i} = \frac{\sum_{m=0}^{N} A_m \; e^{(-j2\pi f m \Delta T) + \theta}}{1 + \sum_{m=1}^{N} B_m \; e^{-j2\pi f m \Delta T}} \qquad (3.6)$$

where: θ is the phase shift by which the output lags the input

It is obvious from the equation that the gain of a filter of this kind increases rapidly as the denominator approaches zero. This results in the recursive filters having a narrow transition band.

3.3 Design of Digital Recursive Filters

The transfer function of recursive filters has been derived in Section 3.2. Using the derived transfer function, procedures for designing lowpass Butterworth recursive filters are presented in this section.

The most commonly used types of recursive filters are:

(i) Butterworth filters

(ii) Chebyshev filters

The Butterworth and the Chebyshev filters have their own advantages and drawbacks. The gain of a Chebyshev filter often decreases more rapidly in the stop band than the gain of a Butterworth filter of the same order. The gain characteristics of the Chebyshev filters, however, have ripples in the passband which may be undesirable in many applications. The gain characteristics of Butterworth filters do not have such ripples. Because of this property

of the Butterwoth filters, it was decided to design and test the performance of such filters. A procedure for designing Butterworth filters is, therefore, described in this section.

There are two principle approaches to the design of recursive digital filters. One method is to produce a suitable analogue filter design and then transform this to obtain a corresponding digital filter design. This method is useful for those working in the area of analogue filter design but otherwise it introduces unnecessary complications. The other approach, which has been adopted in this project, is to design a suitable digital filter directly.

Consider Equation 3.4 which can be rewritten in the form:

$$Y_n = (A_0 X_n + A_1 X_{n-1} + A_2 X_{n-2} + \ldots\ldots\ldots) - (B_1 Y_{n-1} + B_2 Y_{n-2} + \ldots\ldots\ldots\ldots) \qquad (3.7)$$

Using the z-transform technique, (for brief details of the z-transform, see Appendix B) the transfer function of the digital filters can be expressed in the form of Equation 3.8 by substituting X_{n-m} with $X(z)z^{-m}$.

$$Y(z)(1 + B_1 z^{-1} + B_2 z^{-2} + \ldots\ldots\ldots\ldots\ldots) = X(z)(A_0 + A_1 z^{-1} + A_2 z^{-2} + \ldots\ldots\ldots) \quad (3.8)$$

H(z), the transfer function of the filter is now given by:

$$H(z) = \frac{Y(z)}{X(z)} = \frac{(A_0 + A_1 z^{-1} + A_2 z^{-2} + \ldots\ldots\ldots)}{(1 + B_1 z^{-1} + B_2 z^{-2} + \ldots\ldots\ldots)}$$

$$= \frac{\sum_{m=0}^{N} A_m z^{-m}}{\sum_{m=0}^{N} B_m z^{-m}} \quad ; \quad B_0 = 1 \quad (3.9)$$

By definition $z^{-1} = e^{-jw\Delta T} = \cos(w\Delta T) - j \sin(w\Delta T)$. Using this substitution in Equation 3.9, the transfer function can be expressed as[5]:

$$H(w) = \frac{\sum_{m=0}^{N} A_m \cos(mw\Delta T) - j \sum_{m=0}^{N} A_m \sin(mw\Delta T)}{\sum_{m=0}^{N} B_m \cos(mw\Delta T) - j \sum_{m=0}^{N} B_m \sin(mw\Delta T)} \quad (3.10)$$

The real parts of the numerator and denominator are summations of the cosines of angles which are multiples of ($w\Delta T$) and can be expressed as polynomials in $\cos(w\Delta T)$. The imaginary parts are, however, summations of sines of the angles which are multiples of $w\Delta T$. These can be expressed as a product of $\sin(w\Delta T)$ and polynomials in $\cos(w\Delta T)$. Making

substitutions in Equation 3.10, the following equation is obtained[5]:

$$H(w) = \frac{\sum_{m=0}^{N} c_m \cos^m(w\Delta T) - j \sin(w\Delta T) \sum_{m=0}^{N} d_m \cos^m(w\Delta T)}{\sum_{m=0}^{N} e_m \cos^m(w\Delta T) - j \sin(w\Delta T) \sum_{m=0}^{N} f_m \cos^m(w\Delta T)} \qquad (3.11)$$

The magnitude of H(w) can be expressed in the following form:

$$|H(w)|^2 = \frac{(\sum_{m=0}^{N} c_m \cos^m(w\Delta T))^2 + (1-\cos^2(w\Delta T))(\sum_{m=0}^{N} d_m \cos^m(w\Delta T))^2}{(\sum_{m=0}^{N} e_m \cos^m(w\Delta T))^2 + (1-\cos^2(w\Delta T))(\sum_{m=0}^{N} f_m \cos^m(w\Delta T))^2}$$

$$= \frac{\sum_{m=0}^{N} G_m \cos^m(w\Delta T)}{\sum_{m=0}^{N} F_m \cos^m(w\Delta T)} \qquad (3.12)$$

Since, $\cos(w\Delta T) = \frac{1 - \tan^2(w\Delta T/2)}{1 + \tan^2(w\Delta T/2)}$, $|H(w)|^2$ is given by:

$$|H(w)|^2 = \frac{\sum_{m=0}^{N} C_m \tan^{2m}(w\Delta T/2)}{\sum_{m=0}^{N} D_m \tan^{2m}(w\Delta T/2)} \qquad (3.13)$$

C_m and D_m are real coefficients. The square of the gain of the filter can now be expressed as a real rational function

in $\tan^2(w\Delta T/2)$. Equation 3.13 can be re-written in the form:

$$|H(w)|^2 = \frac{1}{1 + b^2 \; P^2(w)}$$

or

$$|H(w)| = \sqrt{\frac{1}{1 + b^2 \; P^2(w)}} \qquad (3.14)$$

where:

a and b are real constants

$$P^2(w) = \sum_{m=0}^{N} a_m \; \tan^{2m}(w\Delta T/2)$$

3.3.1 Design of lowpass Butterworth filters

The theory of recursive digital filters has been discussed in the last section. In this section a procedure for designing Butterworth digital filters is examined. One of the options available is to use only the last term of the polynomial $P^2(w)$ in Equation 3.14. This provides a filter whose gain is given by[5]:

$$|H(w)| = \frac{1}{\sqrt{1 + a \; \tan^{2N}(w\Delta T/2)}} \qquad (3.15)$$

Since the gain of the filter reduces by 3 dB at the cut off frequency, w_c, the constant 'a' must be equal to

$\left[\tan^{2N}(w_c\Delta T/2)\right]^{-1}$. Using this value for the constant 'a', the gain of the filter is given by:

$$|H(w)| = \frac{1}{\sqrt{1 + \left[\frac{\tan(w\Delta T/2)}{\tan(w_c \Delta T/2)}\right]^{2N}}} \qquad (3.16)$$

It is obvious from Equation 3.16 that:

(i) $|H(0)| = 1$

(ii) $|H(w_c)| = 1/\sqrt{2}$

(iii) $|H(\pi/\Delta T)| = 0$

It can be shown that the gain of the filter described by Equation 3.16 decreases monotonically from unity to zero as the frequency increases from zero to the Nyquist frequency. For a digital filter to be stable[22], it is essential that its poles must lie within a unit circle in the z-plane. To solve Equation 3.16 under these constraints, the simplest method is to transform the equation to the p-plane, such that:

$$p = \frac{z - 1}{z + 1} \qquad (3.17)$$

Also $p = u + j\,v$; when z lies on a unit circle, p is given by:

$$p = -j \tan(w\Delta T/2)$$

$$p = u + j\,v = 0 - j \tan(w\Delta T/2)$$

In the p-plane, the poles of Equation 3.16 are the roots of the following equation:

$$\left(\frac{jp}{v_c}\right)^{2N} + 1 = 0$$

or

$$(-1)^N \left(\frac{p}{v_c}\right)^{2N} + 1 = 0 \qquad (3.18)$$

where: $v_c = \tan(w_c \Delta T/2)$

If N is an even number,

$$p_m = v_c e^{j\{(2m+1)/2N\}\pi} \quad : \quad m = 0,1,2,3, \ldots 2N-1 \qquad (3.19)$$

and if N is an odd number,

$$p_m = v_c e^{j(m\pi/N)} \quad : \quad m = 0,1,2,3, \ldots N-1 \qquad (3.20)$$

For even values of N, the real and imaginary parts of p_m are given by:

$$u_m = v_c \cos\left(\frac{2m+1}{2N}\right)\pi \qquad (3.21.a)$$

$$v_m = v_c \sin\left(\frac{2m+1}{2N}\right)\pi \quad : \quad m = 0,1,2,3, \ldots. \; 2N-1 \qquad (3.21.b)$$

For odd values of N, the real and imaginary parts of p_m are given by:

$$u_m = v_c \cos\left(\frac{m\pi}{2N}\right) \qquad (3.22.a)$$

$$v_m = v_c \sin\left(\frac{m\pi}{2N}\right) \quad : \quad m = 0,1,2,3, \ldots. \; N-1 \qquad (3.22.b)$$

Equations 3.21 and 3.22 describe circles of radius v_c and centre at the origin in the p-plane. A reverse transformation to the z-plane provides the locus for the poles. From Equation 3.17, z is given by:

$$z = x + j\,y = \frac{1 + p}{1 - p}$$

$$= \frac{1 + (u + j\,v)}{1 - (u + j\,v)}$$

The real and imaginary parts of z are given by:

$$x = \frac{1 - (u^2 + v^2)}{(1 - u)^2 + v^2} \qquad (3.23)$$

$$y = \frac{2v}{(1 - u)^2 + v^2} \qquad (3.24)$$

Since $u^2 + v^2 = v_c^2$, x and y can be expressed as:

$$x = \frac{1 - v_c^2}{1 - 2u + v_c^2} \qquad (3.25)$$

$$y = \frac{2v}{1 - 2u + v_c^2} \qquad (3.26)$$

It can be shown from Equations 3.25 and 3.26 that:

$$y^2 + \left[x - \frac{1 + v_c^2}{1 - v_c^2} \right]^2 = \frac{4v_c^2}{(1 - v_c^2)^2} \qquad (3.27)$$

This is an equation for a circle whose radius is $\frac{2v_c}{1 - v_c^2}$

and whose centre lies at $\left[\frac{1 + v_c^2}{1 - v_c^2} , 0 \right]$. Substituting the values of u_m , v_m and v_c in Equations 3.25 and 3.26, the real and imaginary parts of the mth pole are given by:

For even values of N,

$$x_m = \frac{1 - \tan^2\left(\frac{w_c \Delta T}{2}\right)}{1 - 2 \tan\left(\frac{w_c \Delta T}{2}\right) \cos\left(\frac{2m+1}{2N}\right)\pi + \tan^2\left(\frac{w_c \Delta T}{2}\right)} \qquad (3.28)$$

$$y_m = \frac{2 \tan\left(\frac{w_c \Delta T}{2}\right) \sin\left(\frac{2m+1}{2N}\right)\pi}{1 - 2 \tan\left(\frac{w_c \Delta T}{2}\right) \cos\left(\frac{2m+1}{2N}\right)\pi + \tan^2\left(\frac{w_c \Delta T}{2}\right)} \qquad (3.29)$$

For odd values of N,

$$x_m = \frac{1 - \tan^2\left(\frac{w_c \Delta T}{2}\right)}{1 - 2 \tan\left(\frac{w_c \Delta T}{2}\right) \cos\left(\frac{m\pi}{2N}\right) + \tan^2\left(\frac{w_c \Delta T}{2}\right)} \qquad (3.30)$$

$$y_m = \frac{2 \tan\left(\frac{w_c \Delta T}{2}\right) \sin\left(\frac{m\pi}{2N}\right)}{1 - 2 \tan\left(\frac{w_c \Delta T}{2}\right) \cos\left(\frac{m\pi}{2N}\right) + \tan^2\left(\frac{w_c \Delta T}{2}\right)} \qquad (3.31)$$

An Nth order Butterworth filter has N zeros which are all situated at $z = -1$

3.3.2 Block diagram representation of Butterworth filters

Equations for designing lowpass Butterworth filters have been developed in the last section. From these equations a procedure for calculating the coefficients of second order lowpass Butterworth filters is developed in this section. A technique to represent the filters in block diagram form is then described.

A Butterworth filter can be constructed either in the direct or serial form[1]. It is easy to determine the coefficients for the direct form as the coefficients in the transfer function appear directly in the block diagram used to implement it. This form is, however, not used in practice because the higher order filters of this form are very sensitive to the effects of arithmetic rounding. The recursive filters are, therefore, implemented in the serial form, constructed from the products of second order transfer functions. A simple procedure to construct a block diagram for a second order lowpass Butterworth filter is described in this section.

For specified sampling rates and cut off frequencies poles of the second order Butterworth filter can be calculated using Equations 3.28 and 3.29. The zeros of the filter are at (-1,0). If the poles are denoted by b_1 and b_2 , the factorized form of the transfer function of a second order filter is given by:

$$H(z) = A_g \frac{(1 + z^{-1})(1 + z^{-1})}{(1 - b_1 z^{-1})(1 - b_2 z^{-1})} \qquad (3.32)$$

where: A_g is the reciprocal of the gain of the filter

The transfer function of a second order recursive filter can also be written from Equation 3.9 using the first three

terms of the series.

$$H(z) = A_g \frac{(1 + A_1 z^{-1} + A_2 z^{-2})}{(1 + B_1 z^{-1} + B_2 z^{-2})} \qquad (3.33)$$

The coefficients of the filter obtained by equating the last two equations are:

$$A_1 = 2$$
$$A_2 = 1$$
$$B_1 = \text{Re}\ (-b_1 - b_2)$$
$$B_2 = \text{Re}\ (b_1 b_2) \qquad (3.34)$$

Equation 3.33 can also be represented in the block diagram form shown in Figure 3.1. In this figure z^{-1} represents time delay. The outputs Y_{n-1} and Y_{n-2} are generally assumed to be zero. These can, however, be initialized to some other values if the output signal can be estimated using other techniques.

3.4 Design of Bandpass Filters

The procedure described in Section 3.3 is used for designing lowpass filters. Frequency transformation technique is used for designing highpass, bandpass and bandstop filters[1]. If w_1 and w_2 are the lower and upper cut off frequencies for a bandpass filter, the poles of the filter are determined by replacing w_c by $(w_2 - w_1)$ in

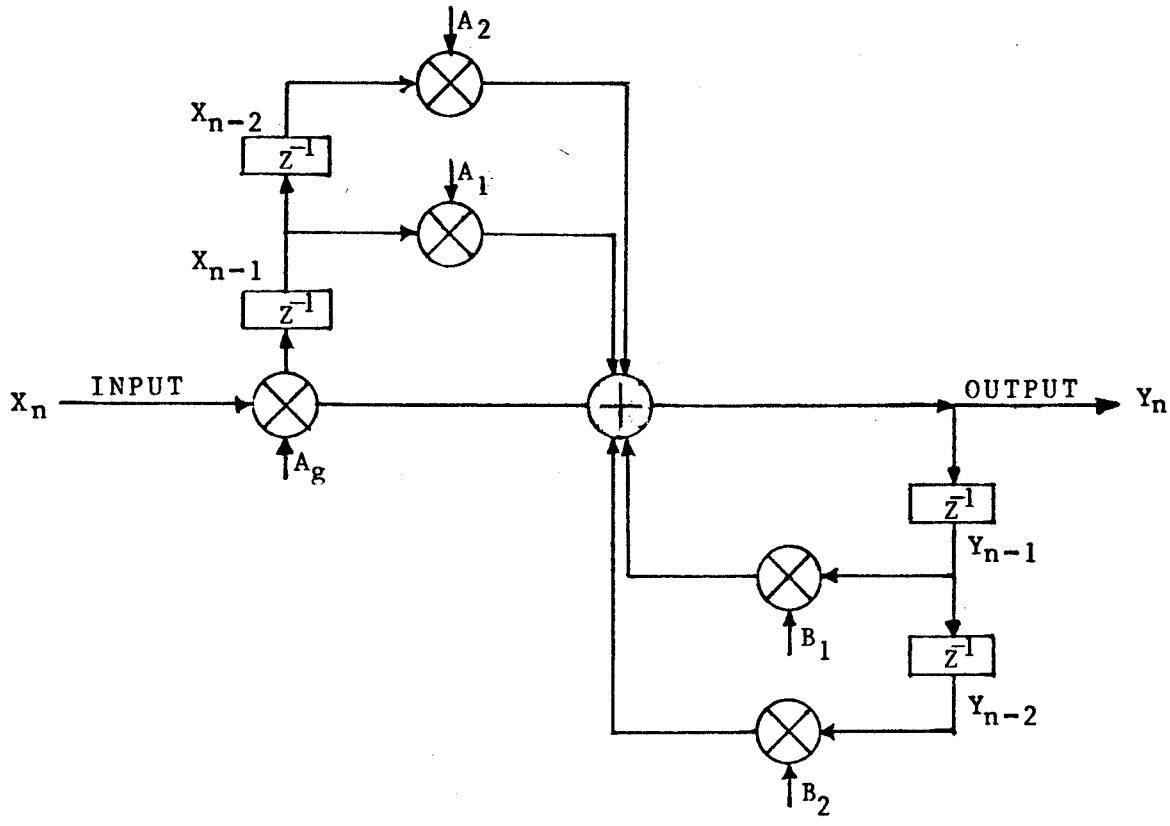

Figure 3.1 Block diagram representing a digital recursive filter

Equations 3.28 and 3.29 and replacing each z^{-1} term in Equation 3.32 by:

$$f(z^{-1}) \triangleq \frac{-z^{-1}(z^{-1} - d)}{(1 - dz^{-1})} \qquad (3.35)$$

where : $$d = \frac{\cos((w_1 + w_2)\Delta T/2)}{\cos((w_2 - w_1)\Delta T/2)}$$

The transfer function for the bandpass filters is similar to Equation 3.33 but the coefficients of the filter are:

$$A_1 = -(a_1 + a_2)$$

$$A_2 = a_1 a_2$$

$$B_1 = \mathrm{Re}\,(-b_1 - b_2)$$

$$B_2 = \mathrm{Re}\,(b_1 b_2)$$

where:

a_1 and a_2 are the zeros of the filter

b_1 and b_2 are the complex poles of the bandpass filter

The block diagram of Figure 3.1 used to represent the lowpass filters is also applicable for bandpass filters. In fact any type of recursive filter (lowpass, highpass, bandpass or bandstop) can be represented in the block diagram shown in Figure 3.1 by assigning suitable values to the coefficients A_1, A_2, B_1 and B_2 . By just changing the

values of the coefficients, the desired type of recursive filter can be obtained without changing the software program. This is the major advantage of using recursive digital filters designed in the manner described above.

3.5 Coefficients of Second Order Butterworth Filters

The procedures for designing second order Butterworth filters have been explained in Sections 3.3 and 3.4. In this section, the parameters of these filters are given. Some test results are also included.

3.5.1 Coefficients of second order lowpass filters

As stated in Section 3.4, the zeros of a second order lowpass filter are at (-1,0) and, therefore, the coefficient A_1 is 2.0 and A_2 is 1.0. Using the selected cut off frequency and selected sampling rate, the poles were calculated using N=2 in Equations 3.28 and 3.29. The coefficients B_1 and B_2 were then calculated using Equation 3.34. For example, the poles were calculated to be $(0.977758 \pm j0.021757)$ when a cut off frequency of 5 Hz and a sampling rate of 1000 Hz were selected. The coefficients B_1 and B_2 were calculated to be -1.955517 and 0.956485. When the cut off frequency was increased to 10 Hz, the complex poles were calculated to be $(0.955537 \pm j0.042568)$ and the coefficients B_1 and B_2 were calculated to be -1.911075 and

0.914864. This procedure was also used to calculate the coefficients of filters for cut off frequencies of 15, 20, 25, 30, 35, 40, 45, 50, 55 and 60 Hz. The poles and the coefficients of these filters are listed in Table 3.1. Filters were also designed for sampling frequencies of 720 and 1440 Hz and the previously selected cut off frequencies. The calculated values of the poles and the filter coefficients for these cases are given in Tables 3.2 and 3.3.

Table 3.1 Coefficients of lowpass Butterworth digital filters - data sampled at 1000 Hz.

F_c	POLES	B_1	B_2	A_g
5	0.977758±j0.021757	-1.955517	0.956485	0.00024202
10	0.955537±j0.042568	-1.911075	0.914864	0.00094724
15	0.933355±j0.062473	-1.866709	0.875054	0.00208613
20	0.911226±j0.081512	-1.822451	0.836976	0.00363126
25	0.889164±j0.099721	-1.778328	0.800557	0.00555723
30	0.867182±j0.117137	-1.734363	0.765725	0.00784048
35	0.845287±j0.133794	-1.690575	0.732412	0.01045920
40	0.823490±j0.149723	-1.646981	0.700553	0.01339318
45	0.801797±j0.164956	-1.603594	0.670088	0.01662373
50	0.780212±j0.179520	-1.560425	0.640959	0.02013354
55	0.758742±j0.193445	-1.517484	0.613110	0.02390662
60	0.737388±j0.206755	-1.474776	0.586489	0.02792819

For all cases $A_1 = 2.000000$ and $A_2 = 1.000000$
F_c is the cut off frequency
A_g is the reciprocal of the gain of the filter

Table 3.2 Coefficients of lowpass Butterworth digital filters - data sampled at 720 Hz

F_c	POLES	B_1	B_2	A_g
5	0.969113±j0.029961	-1.938227	0.940079	0.00046291
10	0.938280±j0.058126	-1.876560	0.883748	0.00179700
15	0.907544±j0.084603	-1.815088	0.830793	0.00392647
20	0.876941±j0.109493	-1.753882	0.781015	0.00678303
25	0.846501±j0.132888	-1.693003	0.734224	0.01030527
30	0.816247±j0.154877	-1.632495	0.690246	0.01443796
35	0.786197±j0.175540	-1.572394	0.648920	0.01913152
40	0.756363±j0.194954	-1.512727	0.610092	0.02434145
45	0.726756±j0.213188	-1.453512	0.573624	0.03002785
50	0.697381±j0.230309	-1.394763	0.539383	0.03615501
55	0.668243±j0.246375	-1.336485	0.507249	0.04269098
60	0.639340±j0.261445	-1.278681	0.477110	0.04960724

Table 3.3 Coefficients of the Butterworth lowpass digital filters - data sampled at 1440 Hz

F_c	POLES	B_1	B_2	A_g
5	0.984553±j0.015212	-1.969106	0.969577	0.00011750
10	0.969113±j0.029961	-1.938227	0.940079	0.00046291
15	0.953687±j0.044261	-1.907374	0.911478	0.00102598
20	0.938280±j0.058126	-1.876560	0.883748	0.00179700
25	0.922897±j0.071569	-1.845794	0.856861	0.00276675
30	0.907544±j0.084603	-1.815088	0.830793	0.00392647
35	0.892224±j0.097240	-1.784448	0.805519	0.00526785
40	0.876941±j0.109493	-1.753882	0.781015	0.00678303
45	0.861699±j0.121372	-1.723399	0.757257	0.00846453
50	0.846501±j0.132888	-1.693003	0.734224	0.01030527
55	0.831350±j0.144053	-1.662700	0.711894	0.01229853
60	0.816247±j0.154877	-1.632495	0.690246	0.01443796

A study of these tables indicates that the values of B coefficients decrease and the value of A_g increases as the bandwidth increases. This means that as the cut off frequency is increased, more weight is given to the input data compared to the weight given to the output data.

3.5.2 Coefficients of second order bandpass filters

The procedure for calculating the coefficients of second order bandpass filters is different from the procedure for designing lowpass filters. As explained in Section 3.4, bandpass filters are designed from their prototype lowpass filters by using the frequency transformation technique. The order of a bandpass filter is twice the order of its prototype lowpass filter. To design second order bandpass filters, first order lowpass filters were, therefore, designed for specified cut off frequencies and sampling rates. The frequency transformation technique was then used to calculate the poles and the parameters of the bandpass filters.

For example, if a bandpass filter with cut off frequencies of 55 and 65 Hz is to be designed, a lowpass filter with cut off frequency of 10 Hz (65 Hz - 55 Hz) is first designed. For a sampling frequency of 1000 Hz, the pole for the first order lowpass filter was calculated to be (0.938981 + j0.000000). Transfer function of this filter was calculated to be:

$$H(z) = \frac{1 + z^{-1}}{1 - b_1 z^{-1}} \quad ; \qquad b_1 = 0.9389810 + j0.000000$$

The coefficient 'd' defined in Equation 3.35 was then calculated to be 0.930235. The transfer function, H(z), of

the bandpass filter was calculated by replacing each z^{-1} term by $-z^{-1}(z^{-1}-d)/(1-dz^{-1})$ in $H(z)$. The desired transfer function was thus calculated to be:

$$H(z) = \frac{1 - z^{-2}}{1 - 1.803709\ z^{-1} + 0.938981\ z^{-2}}$$

In this case A_1 is 0.000000, A_2 is -1.000000, B_1 is -1.803709 and B_2 is 0.938981. The zeros of this filter are at 1,0, -1,0 and the poles are at $0.901854 \pm j0.354457$. Bandpass filters with cut off frequencies of (50,70), (45,75), (40,80), (35,85) and (30,90) Hz were also designed. The coefficients of these filters are given in Table 3.4. Filters for these cut off frequencies and sampling rates of 720 and 1440 Hz were also designed. Their parameters are given in Tables 3.5 and 3.6.

Table 3.4 Coefficients of the Butterworth bandpass digital filters - data sampled at 1000 Hz

*F_1	F_2	POLES	B_1	B_2	A_g
55	65	0.901854±j0.354457	-1.803709	0.938981	0.071992
50	70	0.876400±j0.336730	-1.752800	0.881465	0.072520
45	75	0.853162±j0.314909	-1.706324	0.827053	0.097836
40	80	0.831923±j0.288627	-1.663847	0.775402	0.119170
35	85	0.812499±j0.257016	-1.624997	0.726212	0.139541
30	90	0.794726±j0.218242	-1.589452	0.679219	0.160850

*For all cases A_1 = 0.000000 and A_2 = -1.000000
F_1 and F_2 are the lower and upper cut off frequencies

Table 3.5 Coefficients of the Butterworth bandpass digital filters - data sampled at 720 Hz

F_1	F_2	POLES	B_1	B_2	A_g
55	65	0.830538±j0.475843	-1.661077	0.916220	0.041919
50	70	0.799306±j0.447218	-1.598613	0.838894	0.080782
45	75	0.771753±j0.414050	-1.543507	0.767040	0.117220
40	80	0.747411±j0.375800	-1.494822	0.699849	0.151780
35	85	0.725896±j0.331244	-1.451791	0.636647	0.184900
30	90	0.706891±j0.277802	-1.413782	0.576869	0.214100

Table 3.6 Coefficients of the Butterworth bandpass digital filters - data sampled at 1440 Hz

F_1	F_2	POLES	B_1	B_2	A_g
55	65	0.945496±j0.251536	-1.890993	0.957234	0.052380
50	70	0.926345±j0.241050	-1.852690	0.916220	0.064431
45	75	0.908378±j0.227303	-1.816756	0.876817	0.076758
40	80	0.891510±j0.210009	-1.783021	0.838894	0.088951
35	85	0.875667±j0.188534	-1.751334	0.802337	0.102701
30	90	0.860779±j0.161554	-1.721558	0.767040	0.117640

A perusal of Tables 3.4, 3.5 and 3.6 reveals that the values of B coefficients decrease and the value of A_g increases as the bandwidth of the filter increases. As in the case of lowpass filters, increasing the cut off frequency results in the bandpass filters giving more weight to the input data compared to output data.

3.6 Response of Second Order Butterworth Filters

The filters designed in Section 3.5 were tested by checking their frequency response and by simulating response to the data generated in a computer program.

Figure 3.2 shows the frequency response of a second order bandpass recursive filter whose cut off frequencies are 55 and 65 Hz and the data is sampled at 1000 Hz. It is evident from this figure that the gain of the filter is maximum at 60 Hz and decreases monotonically with the increase and decrease of frequency of the input signal.

The response of a bandpass filter which has cut off frequencies of 55 and 65 Hz was also tested with a simulated sinusoidal input. A computer program was written to implement the second order bandpass filter of the form of Equation 3.36. Another computer program was written to simulate the input data by sampling a sinusoidal signal at the rate of 1000 Hz. This data was used as input to the

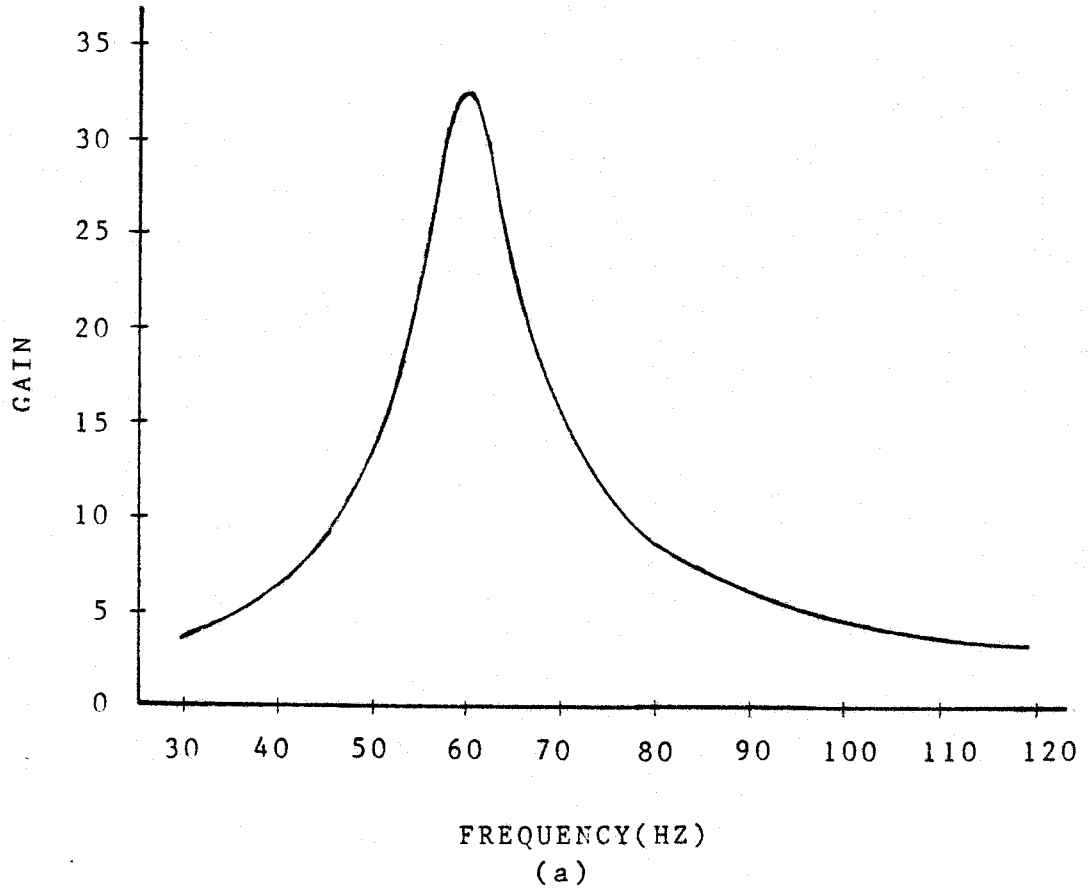

(a)

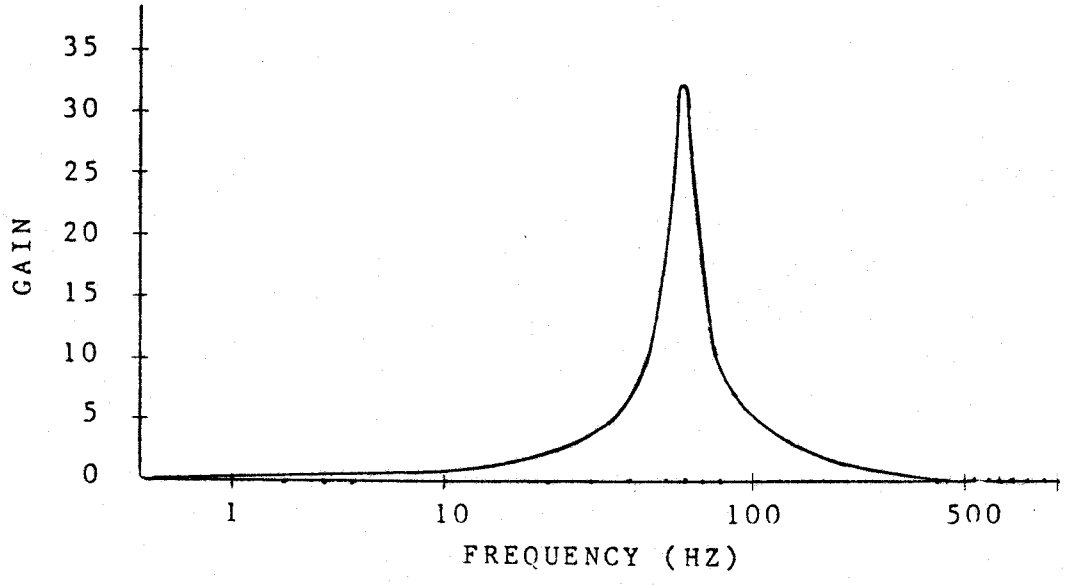

(b)

Figure 3.2 Frequency response of a second order bandpass (55-65) Hz recursive filter - data sampled at 1000 Hz, (a) Flat scale (b) Semilog scale

filter whose output was calculated. Figure 3.3 is the block diagram which represents the described procedure.

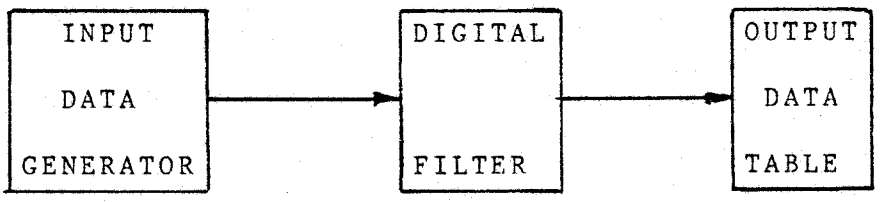

Figure 3.3 Block diagram representing a digital filter, input data generator and output data table

$$Y_n = 0.07199203(X_n - X_{n-2}) + 1.803709Y_{n-1} - 0.938981Y_{n-2} \quad (3.36)$$

Figure 3.4 shows the manner in which the output of the filter builds up when the input is suddenly switched on. It is obvious that the build up process is slow and takes approximately three cycles to reach a steady value. This is because, when the filter is switched on, the outputs Y_{n-1} and Y_{n-2} in the feedback loop are zero. As the process continues, the values of the output increase slowly. As already discussed, a recusive filter remembers the past information. A consequence of this characteristic is that spikes in the input signal will affect the output of the filter for a long time.

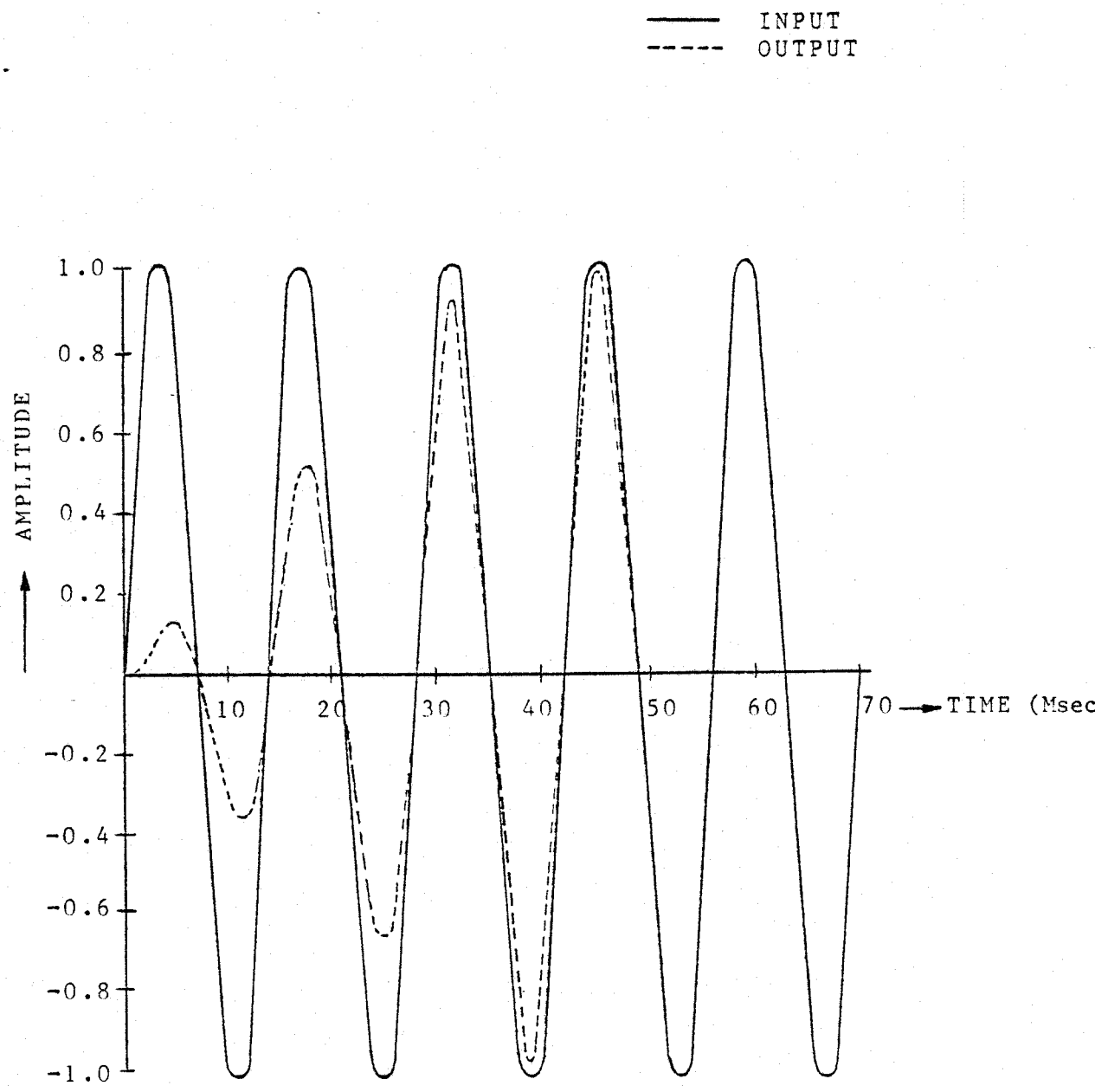

Figure 3.4 Second order bandpass recursive filter (55-65) Hz implemented on a digital computer

Figure 3.5 shows the frequency response of the bandpass filter with cut off frequencies of 40 and 80 Hz and a sampling rate of 1000 Hz. Figure 3.6 shows the response of this filter when a simulated sinusoidal input is suddenly switched on. As expected the frequency response of the filter is not as sharp as the frequency response of (55,65) Hz filter. However, the filter output builds up more rapidly. This is because the input data is weighted more heavily than the output data. A consequence of this property is that the effect of spikes or irregularities will be observed in the output for short durations only.

Figure 3.7 gives the frequency response of a lowpass filter with a cut off frequency of 5 Hz and a sampling rate of 1000 Hz.

From these studies, it is obvious that the filter attenuates the components of the undesired frequencies to a greater extent if the bandwidth of the filter is small but its response is slow. On the other hand, if the bandwidth is large, the filter passes some undesired frequencies but its response would be a bit faster. A compromise between the desired frequency response and the time delay is usually necessary.

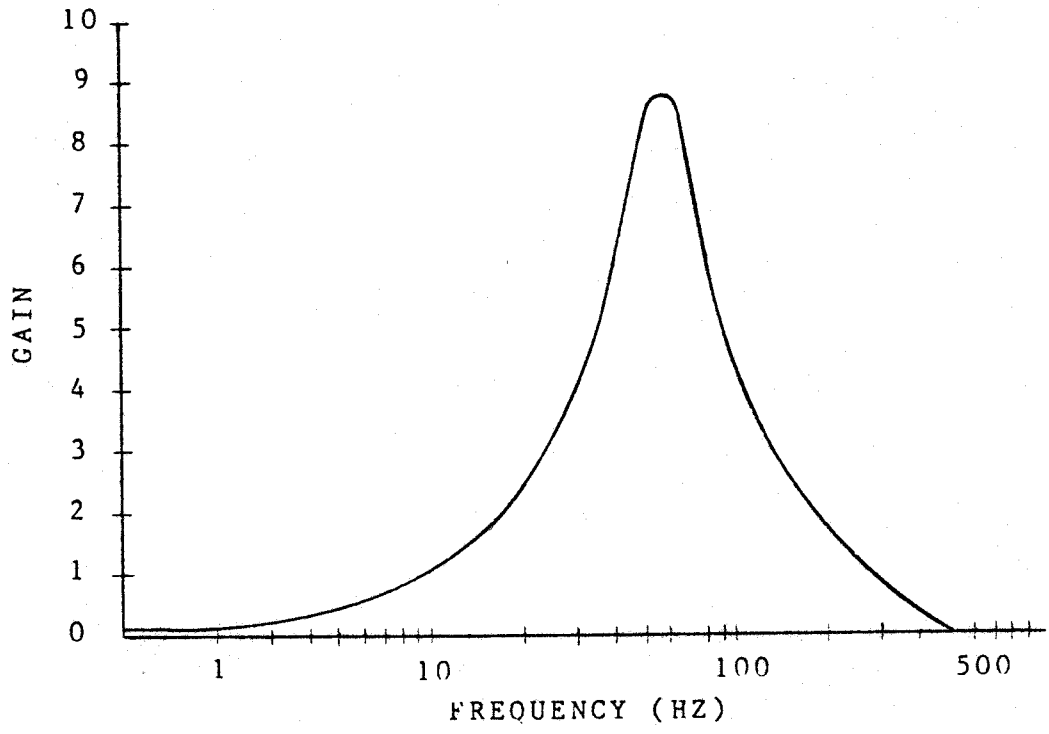

Figure 3.5 Frequency response of a second order bandpass (40-80) Hz recursive filter - data sampled at 1000 Hz

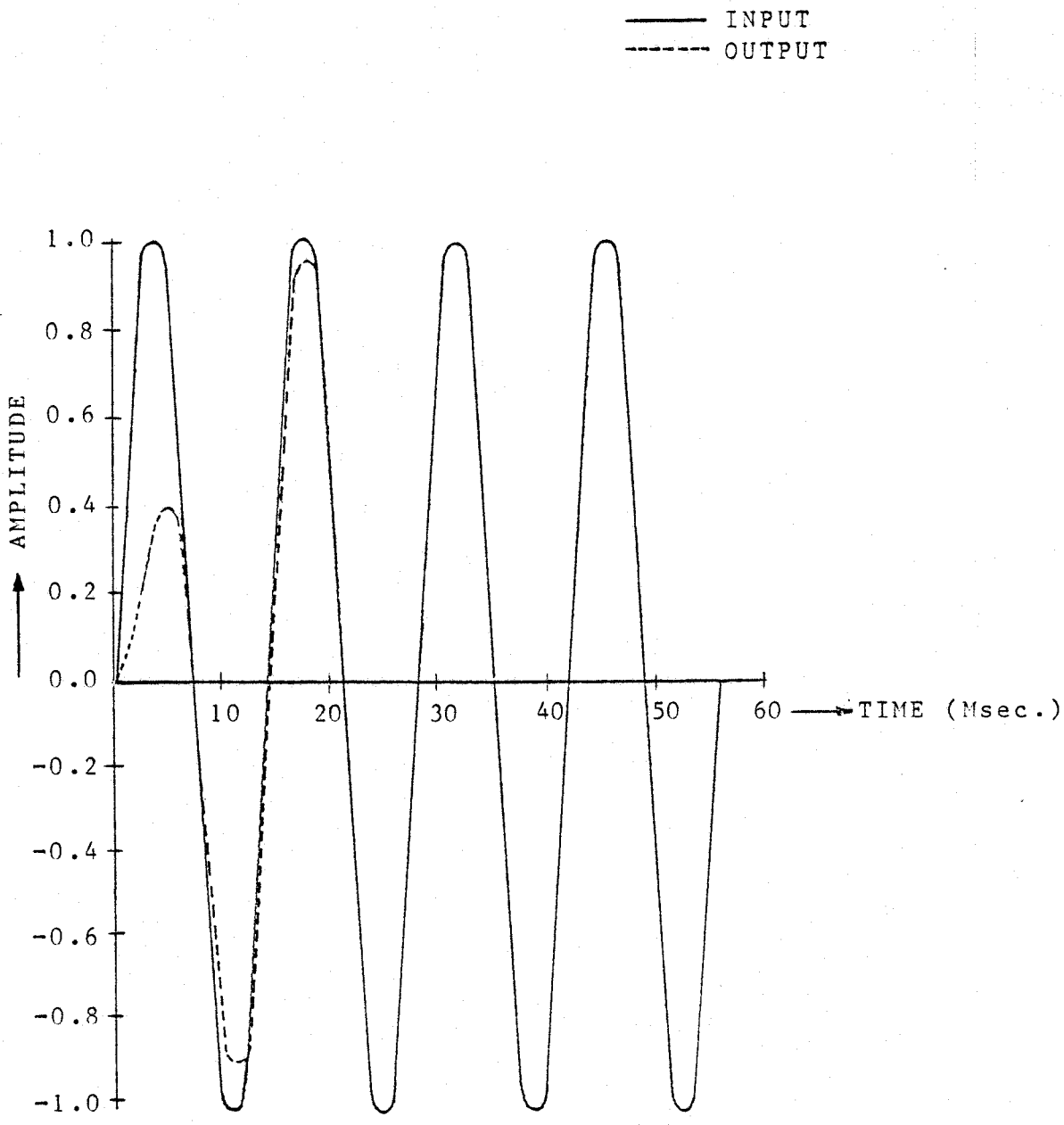

Figure 3.6 Second order bandpass recursive filter (40-80) Hz implemented on a digital computer

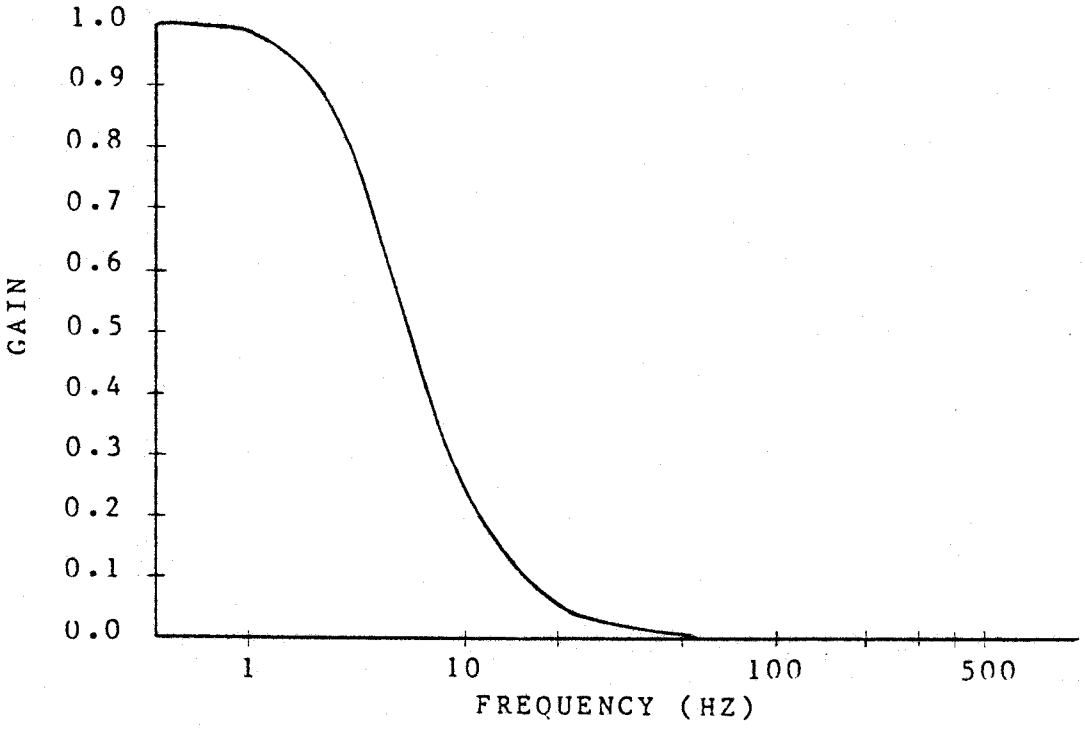

Figure 3.7 Frequency response of a second order lowpass recursive filter (0-5) Hz - data sampled at 1000 Hz

3.7 Summary

The theory of digital recursive filters in general and Butterworth filters in particular has been described. The procedure for determining the poles and zeros of lowpass Butterworth filters is then outlined. A frequency transformation technique which converts a lowpass filter design to a bandpass filter design is also given.

Numerical examples showing the procedure for calculating poles, zeros and coefficients of second order lowpass and bandpass filters have been given. Coefficients of some second order lowpass and bandpass filters have also been listed. Frequency response of some of the designed filters and response to suddenly applied inputs have been given for some of the designed filters.

4. RECURSIVE FILTERS APPLIED TO IMPEDANCE MEASUREMENT

In Chapter 3, it was demonstrated that the output of recursive filters builds up slowly. This shortcoming would be serious in many power system protection applications. For example protection of EHV lines requires the relays to operate with minimum possible delay. In digital protection of transmission lines both voltages and currents are used to calculate the apparent impedance as seen from the relay location. If both voltage and current signals are processed by similar recursive filters, the speed of the filter response may affect the computation of impedances for short periods only. It was, therefore, decided to use second order (55,65) Hz bandpass recursive filters for processing voltages and currents and then use the filter outputs to calculate the apparent impedances assuming that the filtered signals are sinusoids of nominal frequency. The results of the studies are reported in this chapter. These results have been compared with those obtained by using the one cycle Fourier and the 6X9 least error squares algorithms.

4.1 Fault Data Simulation for Testing Digital Filters

To test the suitability of recursive filters for distance protection of transmission lines, fault data was generated using the power system model shown in Figure 4.1.

In this model the transmission line was represented by a series R-L model. The parameters of this system are given in Appendix E.1.

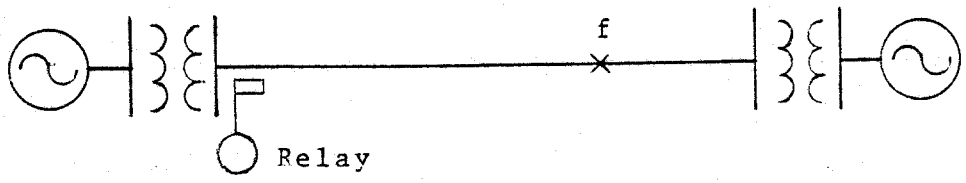

Generator Transmission Line Load

Figure 4.1 Line diagram representing a simple power system

For a fault at location 'f' on the line, fault current flowing at relay location and the voltage at the relay location are given by:

$$I_r = \frac{V_s}{Z_s + Z_L} \sin(wt+\theta_f-\theta) - \frac{V_s}{Z_s + Z_L} \sin(\theta_f-\theta)\, e^{(-R/L)t} \qquad (4.1)$$

$$V_r = \frac{Z_L V_s}{Z_s + Z_L} \sin(wt+\theta_f-\theta+\theta_L) - K_1\, e^{(-R/L)t} \qquad (4.2)$$

where:

$$K_1 = \frac{Z_L V_s}{Z_s + Z_L} \frac{\sin(\theta-\theta_L)\, \sin(\theta_f-\theta)}{\sin(\theta)}$$

θ_L is the line angle at the fundamental frequency

θ_{L3} and θ_{L5} are the line angles at third and fifth harmonics

θ_f is the fault incidence angle

θ is the reference angle for the fundamental frequency component and θ_3 and θ_5 are the reference angles at the third and fifth harmonics

Z_L is the line impedance to the fault point in p.u. at the fundamental frequency and Z_{L3} and Z_{L5} are line impedances at the third and fifth harmonics

Z_s is the source impedance in p.u.

V_s is the source voltage in p.u.

V_r is the voltage at the relay location

I_r is the current at the relay location

Transmission lines are distributed parameter elements of a power system. Fault currents and voltages, therefore, contain high frequency components. For off line testing of the filters, it was decided to add third and fifth harmonic components to Equations 4.1 and 4.2. The augumented equations are as follows:

$$I_r = \frac{V_s}{Z_s + Z_L} \sin(wt+\theta_f-\theta) - \frac{V_s}{Z_s + Z_L} \sin(\theta_f-\theta)\, e^{(-R/L)t} \qquad (4.3)$$

$$+0.3\,\frac{V_s}{Z_s + Z_L} \sin(3wt+\theta_f-\theta_3) + 0.1\,\frac{V_s}{Z_s + Z_L} \sin(5wt+\theta_f-\theta_5)$$

$$V_r = \frac{Z_L V_s}{Z + Z} \sin(wt+\theta_f-\theta+\theta_L) - K_1\, e^{(-R/L)t} \qquad (4.4)$$

$$+0.3\frac{Z_{L3} V_s}{Z_s + Z_L}\sin(3wt+\theta_f-\theta_3+\theta_{L3}) +0.1\frac{Z_{L5}\, V_s}{Z_s + Z_L}\sin(5wt+\theta_f-\theta_5+\theta_{L5})$$

In these equations all the parameters except distance to the fault and fault incidence angle are known for each application.

A computer program was written to generate fault data by varying the distance and the fault incidence angle for an X/R ratio of 10. The data of the simulated faults was stored in data files for use in testing the filters.

4.2 Calculating Transmission Line Impedances

Fault data generated in Section 4.1, was used to test the performance of second order (55,65) Hz bandpass recursive filters. The generated voltages and currents were used as inputs to the filters. The outputs of the filters were then used to calculate the peak values and phase angles of the 60 Hz currents and voltages using the Mann and Morrison and the three sample least error squares sine wave algorithms. From the calculated peak values and phase angles of the voltages and currents, impedances as seen from the relay location were computed. The results obtained by these approaches are presented in this section.

4.2.1 Second order bandpass filters with Mann and Morrison algorithm

The fault currents and voltages were applied to the bandpass filters with lower and upper cut off frequencies of 55 and 65 Hz. It was observed that the filters effectively attenuate the harmonic and decaying d.c. components. The outputs of the filters were practically pure sinusoids of nominal frequency. Figure 4.2 shows the input and output

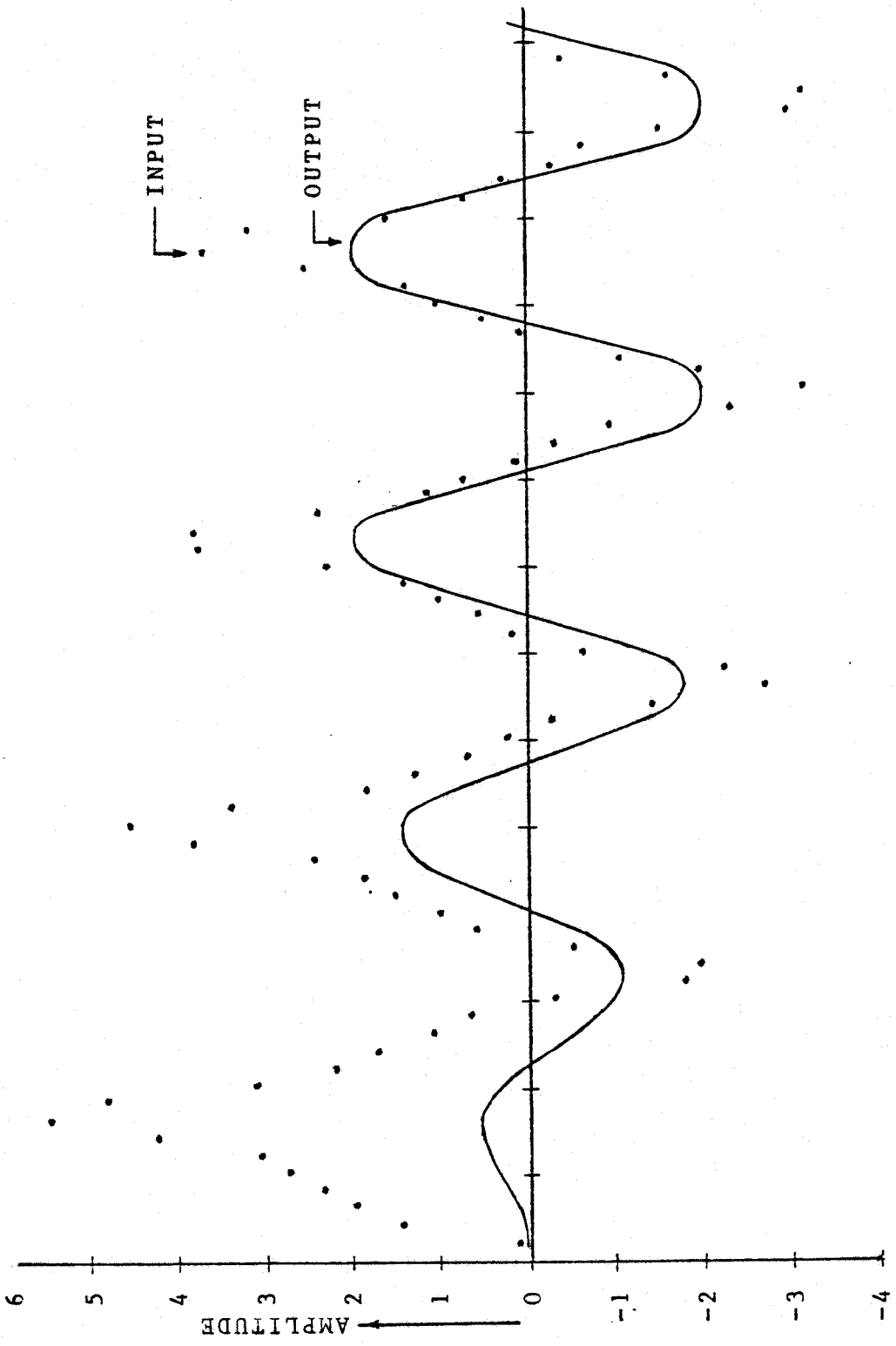

Figure 4.2 Input and output of a second order digital recursive filter (55-65) Hz - data sampled at 1000 Hz

signals of one of the recursive filters.

The Mann and Morrison algorithm[24] was used to calculate the peak values and phase angles of voltages and currents. The following equations were used for this purpose.

$$I_p^2 = i^2 + (i'/w)^2 \qquad \theta = \tan^{-1}(wi/i') \qquad (4.5)$$

where:

i is the instantaneous value of current signal assumed to be a pure sinusoid and i' is its first derivative

$$i' = \frac{1}{2h}(i_{+1} - i_{-1})$$

h is the sampling interval

From the peak values and phase angles of the currents and voltages, line impedances and their phase angles as seen from the relay location were calculated. The calculated impedances and their phase angles when the fault incidence was at zero degrees, are plotted in Figure 4.3. It is observed from the figure that the calculated impedances and their phase angles are not sufficiently accurate during the first one and a half cycles after the occurrence of the fault. This is because the outputs of the filters are initially low and it takes almost one and a half cycles for the output signals to build up and overcome the initial conditions. After the initial one and a half cycle (at 60 Hz) interval, the calculated values are quite accurate.

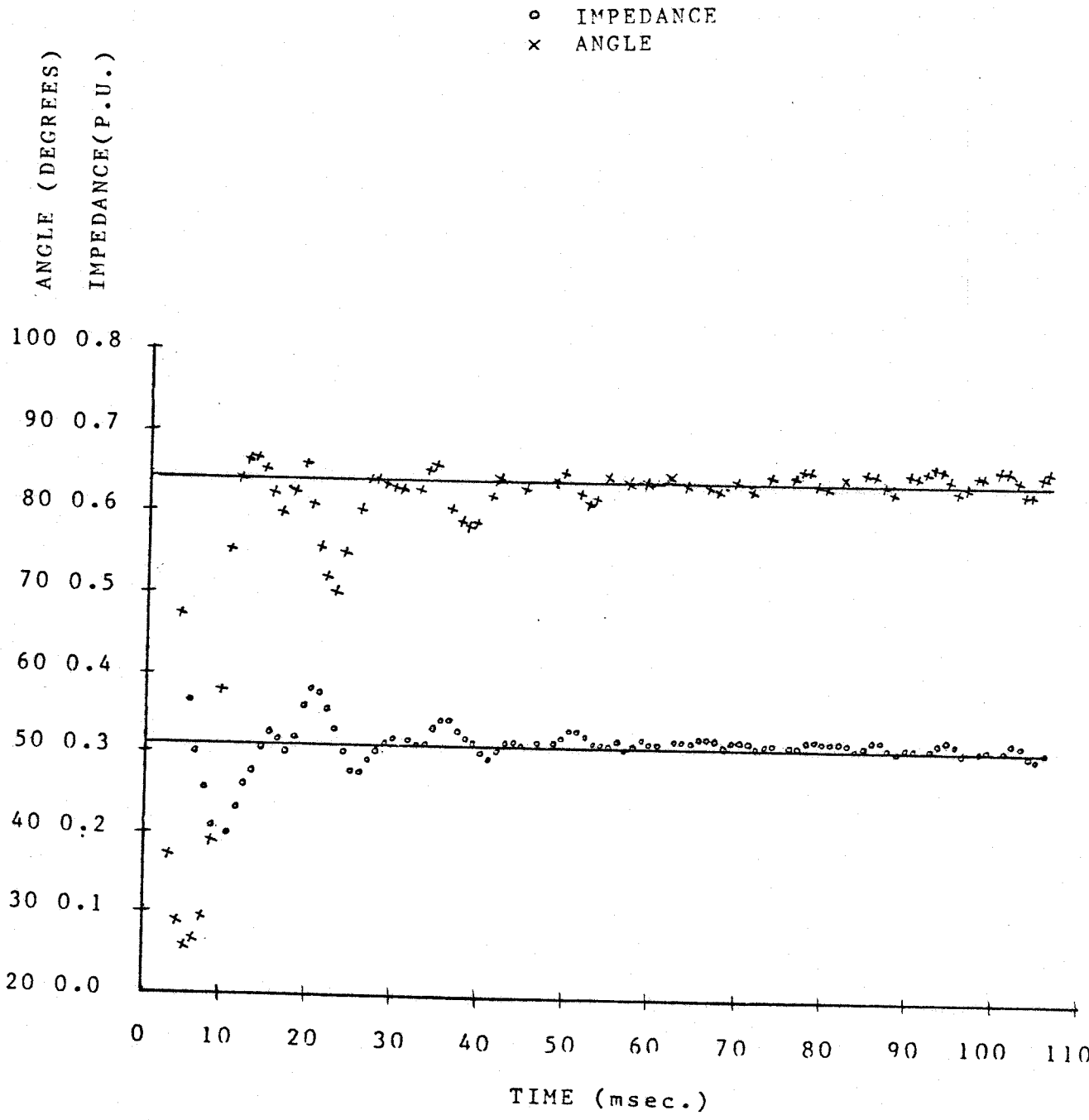

Figure 4.3 Bandpass R-Filter (55-65) Hz with Mann and Morrison algorithm - fault incidence at zero degrees

Typical numerical values for this case are listed in Table 4.1.

The values of line impedances and their phase angles were also calculated for fault incidence at 30, 60 and 90 degrees. These are shown in Figures C.1, C.2 and C.3 given in Appendix C. It is observed from these figures that in all these cases the calculated values are not sufficiently accurate for the initial one and a half cycle duration. It is also observed that the scatter for the calculated impedances and their phase angles is large when the fault incidence is at 90 degrees.

4.2.2 Second order bandpass filters with least error squares pure sine wave algorithm

As observed in Section 4.2.1, the calculated impedances and their phase angles are not sufficiently accurate for approximately one and a half cycles immediately after the inception of a fault. It was, therefore, decided to calculate the line impedances and their phase angles using the three point least error squares pure sine wave algorithm and check if it would improve the results. The model is derived in Appendix C. For 1000 Hz sampling rate, the equations for obtaining the two orthogonal outputs are:

Table 4.1 Impedances and their phase angles calculated using the Mann and Morrison algorithm and the outputs of bandpass recursive filters. Fault was incidence at zero degrees.

SAMPLE NO.	CALCULATED	
	IMPEDANCES P.U.	ANGLES DEGREES
24	0.302	69.927
25	0.279	74.090
26	0.277	80.542
27	0.293	84.082
28	0.307	84.266
29	0.314	83.573
30	0.317	83.101
31	0.319	82.730
32	0.318	82.045
33	0.312	82.725
34	0.316	85.295
35	0.334	85.962
36	0.346	83.459
37	0.343	80.586
38	0.333	79.012
39	0.323	78.623
40	0.315	78.544
..	.....	.....
..	.....	.....
..	.....	.....
57	0.315	82.106
58	0.310	82.734
59	0.311	84.377
60	0.319	84.738

$$V_c = 1.3582527(V_{+1} - V_{-1}) \quad (4.6)$$

$$V_s = 0.340690(V_{-1} + V_{+1}) + 0.366430V_0 \quad (4.7)$$

From these equations the peak value and phase angle of the signal are calculated as follows:

$$V_p^2 = V_c^2 + V_s^2 \quad (4.8)$$

$$\theta = \tan^{-1}(V_s / V_c) \quad (4.9)$$

Using these equations, the impedances and their phase angles were calculated using the simulated data. Figure 4.4 represents the calculated line impedances and their phase angles when the fault incidence was at zero degrees. It is observed that the values are not sufficiently accurate for the initial one and a half cycles in this case also and there is no improvement in the results as compared to the results of Section 4.2.1. Typical numerical values calculated in this case are listed in Table 4.2. For fault incidence at 30, 60 and 90 degrees, the line impedances and their phase angles were also calculated and are plotted in Figures C.4, C.5 and C.6 (Appendix C). Figure C.6 shows that the calculated values for a fault incidence at 90 degrees are slightly better than the results obtained by using the Mann and Morrison algorithm.

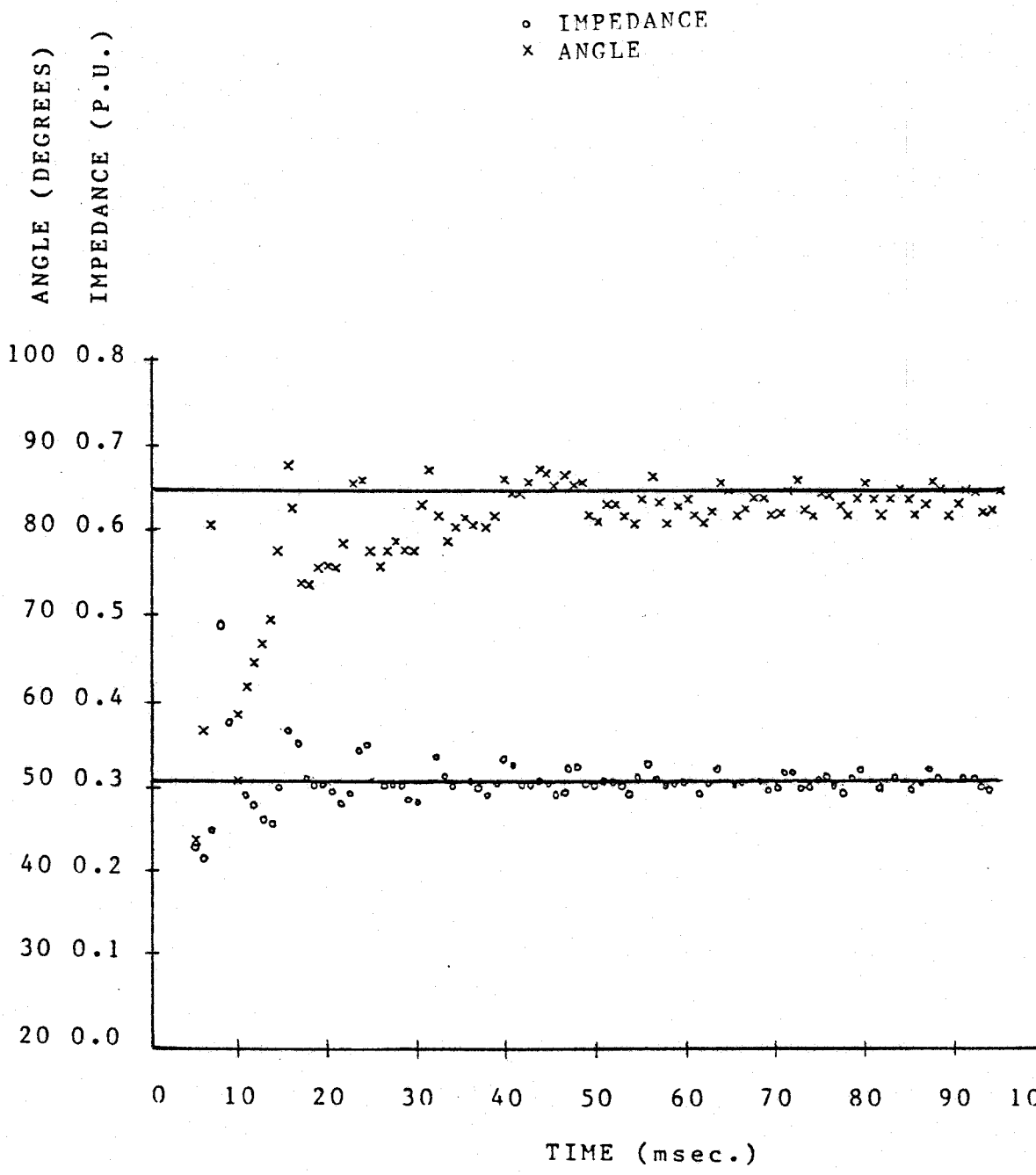

Figure 4.4 Bandpass R-Filter (55-65) Hz with least error squares pure sine wave algorithm - fault incidence at zero degrees

Table 4.2 Impedances and their phase angles calculated using the three sample least error squares pure sine wave algorithm and the outputs of band-pass recursive filters. Fault was incidence at zero degrees.

SAMPLE NO.	CALCULATED	
	IMPEDANCES P.U.	ANGLES DEGREES
24	0.299	85.978
25	0.347	86.097
26	0.354	78.538
27	0.319	76.299
28	0.307	78.565
29	0.309	79.078
30	0.306	78.221
31	0.292	78.673
32	0.288	83.695
33	0.319	87.095
34	0.341	82.547
35	0.320	79.087
36	0.306	80.927
37	0.310	82.053
38	0.313	81.053
39	0.305	79.926
40	0.294	82.371
..	.....	.....
..	.....	.....
..	.....	.....
57	0.297	84.154
58	0.316	86.580
59	0.330	83.407
60	0.314	81.225

4.3 One Cycle Fourier and the 6X9 Least Error Squares Algorithms

Impedances and their phase angles were also calculated from the raw (unfiltered) data using one cycle Fourier[33] and the 6X9 least error squares[36] algorithms. The results were compared with those obtained by using the bandpass filters. This section briefly presents and discusses these results.

4.3.1 One cycle Fourier algorithm

The impedances and their phase angles calculated using one cycle Fourier algorithm (Equations 2.19, 2.20 of Chapter 2) are plotted in Figure 4.5. This algorithm starts providing outputs after one cycle of fault data has been received. The output of this algorithm contains some decaying d.c. and higher harmonic components. As a consequence of this, the calculated values have a fairly large scatter in Figure 4.5. Typical numerical values for calculated impedances and their phase angles are listed in Table 4.3.

4.3.2 The 6X9 least error squares algorithm

The line impedances and their phase angles calculated using the 6X9 least error squares algorithm (for details see Appendix C), are plotted in Figure 4.6. The filter starts providing output after nine samples of fault data have been

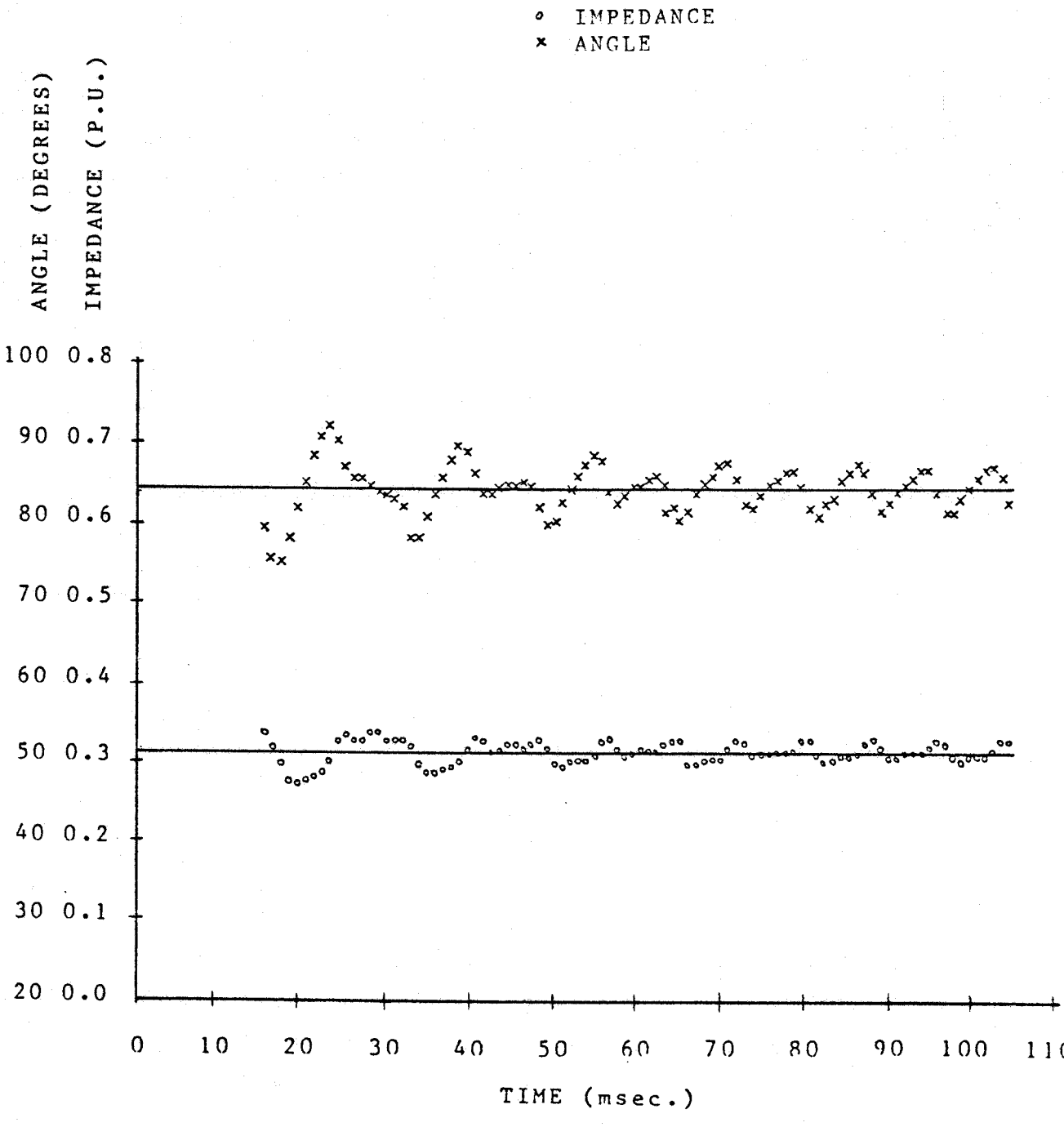

Figure 4.5 One cycle Fourier algorithm - fault incidence at 15 degrees

Table 4.3 Impedances and their phase angles calculated using the one cycle Fourier algorithm. The fault incidence was at 15 degrees.

SAMPLE NO.	CALCULATED	
	IMPEDANCES P.U.	ANGLES DEGREES
16	0.335	79.371
17	0.318	75.450
18	0.293	75.078
19	0.274	78.026
20	0.272	81.852
21	0.276	85.081
22	0.280	88.086
23	0.286	90.825
24	0.304	92.015
25	0.326	90.113
26	0.332	86.804
27	0.324	85.496
28	0.325	85.470
29	0.333	84.726
30	0.333	83.787
31	0.326	83.376
32	0.323	82.956
..	.....	.....
..	.....	.....
..	.....	.....
57	0.308	88.398
58	0.324	86.943
59	0.328	83.734
60	0.314	82.393

received. The algorithm was not designed for rejecting the fifth harmonic which, therefore, appears in the output of the algorithm. Because of this reason, the calculated impedances and their phase angles are fairly scattered. Typical numerical values for calculated impedances and their phase angles are listed in Table 4.4.

Figures 4.3 , 4.4 and C.1 to C.6 show that the recursive filters start providing fairly accurate results approximately one and a half cycles after the occurrence of a fault. The one cycle Fourier algorithm provides sufficiently accurate results one cycle after the inception of a fault. The 6X9 least error squares algorithm provides the results after nine samples of fault data have been received but the results are not sufficiently accurate. Impedances and their phase angles calculated from the outputs of the bandpass filters one and a half cycles after the inception of a fault are more accurate than those calculated by the Fourier and the least error squares algorithms.

4.4 The 6X9 Least Error Squares Algorithm with Second Order Lowpass Recursive Filters

It has been shown in Section 4.3 that the 6X9 least error squares algorithm does not attenuate the fifth harmonic component adequately. Consequently the calculated impedances and their phase angles are quite inaccurate. It

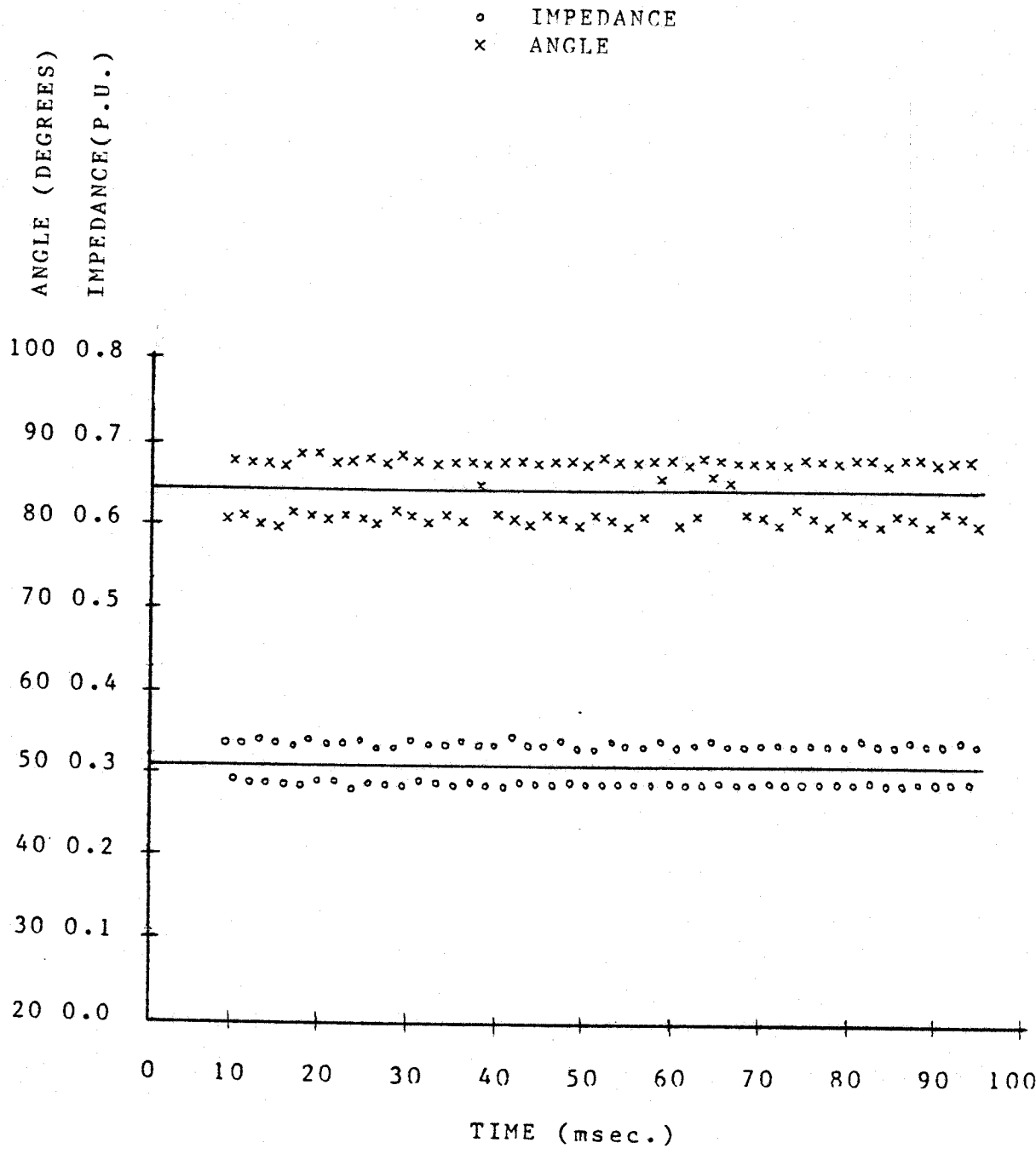

Figure 4.6 6X9 least error squares algorithm - fault incidence at 15 degrees

Table 4.4 Impedances and their phase angles calculated using the 6X9 least error squares algorithm. The fault incidence was at 15 degrees.

SAMPLE NO.	CALCULATED	
	IMPEDANCES P.U.	ANGLES DEGREES
9	0.337	80.603
10	0.291	87.636
11	0.338	81.210
12	0.289	87.606
13	0.341	80.293
14	0.290	87.526
15	0.332	79.884
16	0.286	87.291
17	0.332	81.482
18	0.285	88.268
19	0.340	81.184
20	0.290	88.244
21	0.335	80.407
22	0.290	87.542
23	0.336	81.284
24	0.288	87.786
25	0.341	80.534
..	.....	.....
..	.....	.....
..	.....	.....
57	0.334	80.218
58	0.289	87.451
59	0.335	81.356
60	0.287	87.959

was, therefore, decided to check if the second order lowpass recursive filters can be used to improve these results. The calculated impedances and their phase angles were used as inputs to the lowpass filters which have a cut off frequency of 10 Hz. Figure 4.7 shows the calculated and smoothed apparent impedances and their phase angles for a fault incidence at zero degrees. This figure reveals that the lowpass filters smooth the impedances and their phase angles considerably. Typical numerical values of the calculated and smoothed impedances and their phase angles are given in Table 4.5.

The calculated impedances and their phase angles for fault incidence at 30, 60 and 90 degrees were also smoothed with second order lowpass filters. These are plotted in Figures C.7, C.8 and C.9. Figure C.10 shows the calculated and smoothed R and X for a fault incidence at 120 degrees. The figure shows that the smoothed R and X are also quite accurate. Typical numerical values for this case are listed in Table 4.6.

4.5 Conclusions

It has been shown that the output of recursive filters builds up slowly when the input is suddenly applied. Transmission line distance type relays are generally required to operate in one cycle or less time if the fault

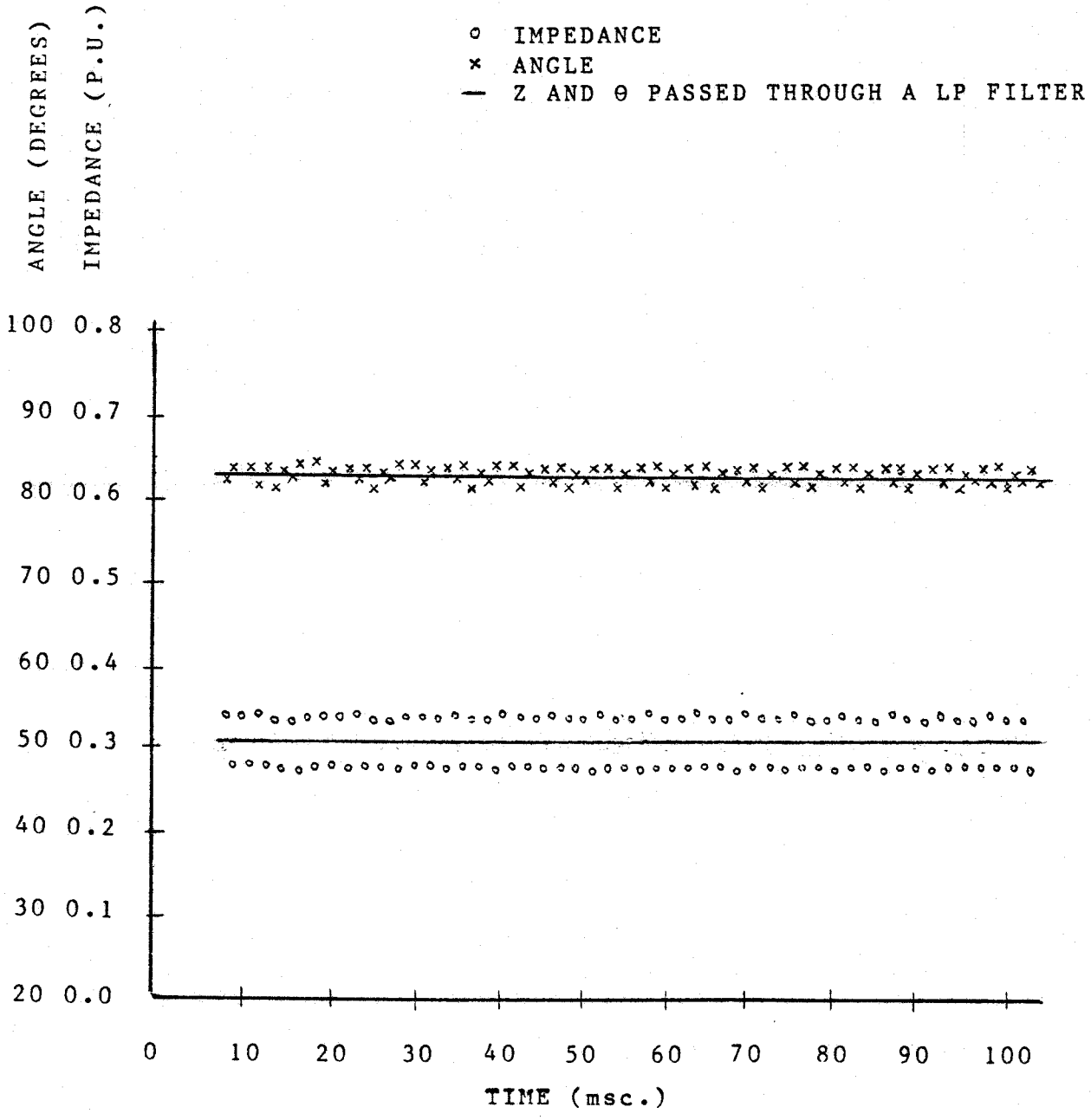

Figure 4.7 6X9 least error squares algorithm with 10 Hz lowpass recursive filter - fault incidence at zero degrees

Table 4.5 Impedances and their phase angles calculated using the 6X9 least error squares algorithm and the impedances after smoothing by 10 Hz lowpass recursive filters. The fault incidence was at zero degrees.

SAMPLE NO.	CALCULATED		SMOOTHED	
	IMPEDANCES P.U.	ANGLES DEGREES	IMPEDANCES P.U.	ANGLES DEGREES
11	0.345	83.841	0.316	84.188
12	0.283	84.988	0.316	84.186
13	0.349	83.133	0.316	84.184
14	0.285	84.995	0.316	84.181
15	0.341	82.433	0.316	84.175
16	0.282	84.360	0.316	84.165
17	0.339	83.854	0.316	84.152
18	0.279	85.509	0.316	84.142
19	0.346	83.973	0.316	84.136
20	0.285	85.773	0.316	84.136
21	0.344	83.171	0.315	84.138
22	0.285	84.788	0.315	84.140
23	0.343	83.844	0.315	84.142
24	0.282	85.130	0.315	84.144
25	0.348	83.361	0.315	84.147
26	0.285	85.204	0.315	84.150
27	0.341	82.631	0.315	84.151
..	.....	.....	.....	.....
..	.....	.....	.....	.....
..	.....	.....	.....	.....
57	0.342	82.905	0.313	84.183
58	0.284	84.634	0.313	84.184
59	0.342	83.848	0.313	84.182
60	0.281	85.267	0.313	84.182

Table 4.6 Resistances and reactances calculated using the 6X9 least error squares algorithm and resistances and reactances after smoothing by 10 Hz lowpass recursive filters. Fault incidence was at 120 degrees.

SAMPLE NO.	CALCULATED		SMOOTHED	
	RESISTANCES P.U.	REACTANCES P.U.	RESISTANCES P.U.	REACTANCES P.U.
11	0.0008	0.3023	0.0302	0.3104
12	0.0629	0.3152	0.0301	0.3104
13	0.0031	0.3023	0.0301	0.3104
14	0.0582	0.3182	0.0301	0.3103
15	0.0032	0.3010	0.0301	0.3103
16	0.0646	0.3210	0.0301	0.3102
17	0.0034	0.3009	0.0301	0.3102
18	0.0636	0.3120	0.0301	0.3102
19	0.0034	0.2994	0.0302	0.3101
20	0.0564	0.3162	0.0303	0.3100
21	0.0094	0.2998	0.0303	0.3099
22	0.0619	0.3216	0.0303	0.3098
23	0.0015	0.3019	0.0304	0.3097
24	0.0672	0.3144	0.0305	0.3097
25	0.0032	0.3015	0.0305	0.3096
26	0.0577	0.3177	0.0306	0.3095
27	0.0026	0.3007	0.0306	0.3095
..	.....	.....	.....	.....
..	.....	.....	.....	.....
..	.....	.....	.....	.....
57	0.0017	0.3002	0.0318	0.3086
58	0.0628	0.3214	0.0318	0.3086
59	0.0022	0.3015	0.0318	0.3086
60	0.0633	0.3007	0.0318	0.3086

is in the first zone. Recursive filters are, therefore, not suitable for use in first zone relays. These filters are, however, useful when limited computer memory is available and lower relay speeds can be tolerated, such as second, third or reverse zone relays.

Due to the presence of a large fifth harmonic component, the impedances calculated using the 6X9 least error squares filters are also not very accurate. Processing the calculated impedances by lowpass recursive filters improve the quality of the results considerably. Lowpass recursive filters effectively cope with the adverse effects of the presence of higher order harmonics in the fault currents and voltages.

5. EXPONENTIAL AND GENERAL EXPONENTIAL SMOOTHING

Procedures for designing lowpass and bandpass Butterworth recursive filters have been presented in Chapter 3. Coefficients of second order lowpass and bandpass Butterworth filters calculated using these procedures are also reported in that chapter. Power system voltages and currents were processed using the second order bandpass recursive filters (55-65 Hz). The outputs of these filters were then used to calculate apparent impedances and their phase angles. The results of these studies are reported in Chapter 4. It was observed that the calculated impedances and their phase angles are not sufficiently accurate during the initial one and a half cycles after the inception of a fault. It was, therefore, decided to investigate if the results could be improved by using smoothing techniques, such as single exponential smoothing. The suitability of general exponential smoothing technique[7] was also investigated.

Exponential and general exponential smoothing techniques are briefly described in this chapter. The suitability of these techniques for computing apparent impedances from the system fault data is also discussed.

5.1 Exponential Smoothing

A common method of smoothing is to calculate the output by averaging the past observations. This technique becomes cumbersome when output is to be revised each time a new sample of the input data is obtained. To avoid this problem, exponential smoothing technique[7] is generally used. This technique consists of calculating the weighted moving averages; the heaviest weight is assigned to the most recent data. By a suitable selection of the smoothing constant, the technique can be applied to provide weighted averages of all the past observations. If the process is repeated after each successive observation of the incoming data, the smoothing function can be defined as:

$$S_n = a\, X_n + (1-a)\, S_{n-1} \qquad (5.1)$$

where:

S_n is the nth (recent) output of the process

S_{n-1} is the (n-1)th output of the process

X_n is the nth data input

a is the smoothing constant

To examine the effect of past observations on the output, Equation 5.1 can be expanded and expressed in terms of previous observations. For this purpose S_{n-1} can be

expressed as follows:

$$S_{n-1} = a\ X_{n-1} + (1-a)\ S_{n-2} \qquad (5.2)$$

The following equation is obtained by substituting Equation 5.2 into Equation 5.1.

$$S_n = a\ X_n + (1-a)\{a\ X_{n-1} + (1-a)\ S_{n-2}\} \qquad (5.3)$$

In this equation S_{n-2} can be replaced by a function of X_{n-2} and S_{n-3} leading to Equation 5.4.

$$S_n = a\ X_n + a(1-a)X_{n-1} + (1-a)^2\{a\ X_{n-2} + (1-a)S_{n-3}\} \qquad (5.4)$$

The general form of the single exponential smoothing process for the past N observations obtained by the procedure described above is given as:

$$S_n = \{a \sum_{N=0}^{n-1} (1-a)^N X_{n-N}\} + (1-a)^n X_0 \qquad (5.5)$$

The value of the smoothing constant 'a' is selected to be in the range 0.0 - 1.0. The weight given to previous observations, therefore, decreases geometrically with age. For a selected value of the smoothing constant, the number of previous observations (N) effectively taken into account for smoothing is given by N=(2/a)-1. For small values of smoothing constants, the number of past observations

affecting the output is large and the output responds slowly to the changes in the recent inputs. For large values of the smoothing constants, the number of past observations affecting the output is small; the output responds quickly to the changes in the recent input data.

5.1.1 Implementation of single exponential smoothing

An ideal algorithm with good filtering properties will provide results which will be free from noise and the calculated impedances and their phase angles will be invariant. The impedances and their phase angles calculated by using recursive bandpass filters and reported in Chapter 4, are considerably scattered; the scatter is large during the first one and a half cycles after the inception of a fault. The impedances and their phase angles can be considered to be step functions superimposed with noise. These values were, therefore, processed using single exponential smoothing represented by Equation 5.1.

Impedances and their phase angles calculated using recursive filters and the Mann and Morrison algorithm when the fault incidence angle was zero degrees have been depicted in Figure 4.3. The voltages and currents in this case were filtered using (55-65 Hz) second order bandpass recursive filters. The impedances and their phase angles calculated in Chapter 4 and depicted in Figure 4.3 were

smoothed using the single exponential smoothing process and a smoothing constant of 0.300. The smoothing process was started one cycle after the inception of the fault. The smoothed impedances and their phase angles are plotted in Figure 5.1. This figure reveals that during the first half cycle after the commencement of the smoothing process, the effect of smoothing on the calculated values is negligible. For the later smoothed values, the scatter is reduced considerably.

Mean value and standard deviation for the unsmoothed and the smoothed impedances and their phase angles were also calculated and are listed in Table 5.1. It is observed from this table that the standard deviation for the smoothed values is less than the standard deviation for the unsmoothed values. This shows that the scatter for the calculated impedances is considerably reduced by the use of the single exponential smoothing process.

Table 5.1 Mean value and standard deviation of the unsmoothed and smoothed impedances and their phase angles - data processed by recursive filters and the Mann and Morrison algorithm

	IMPEDANCES		PHASE ANGLES	
	UNSMOOTHED	SMOOTHED	UNSMOOTHED	SMOOTHED
MEAN VALUE	0.32170	0.32137	84.12864	84.11808
STANDARD DEVIATION	0.01474	0.00912	3.28470	2.43729

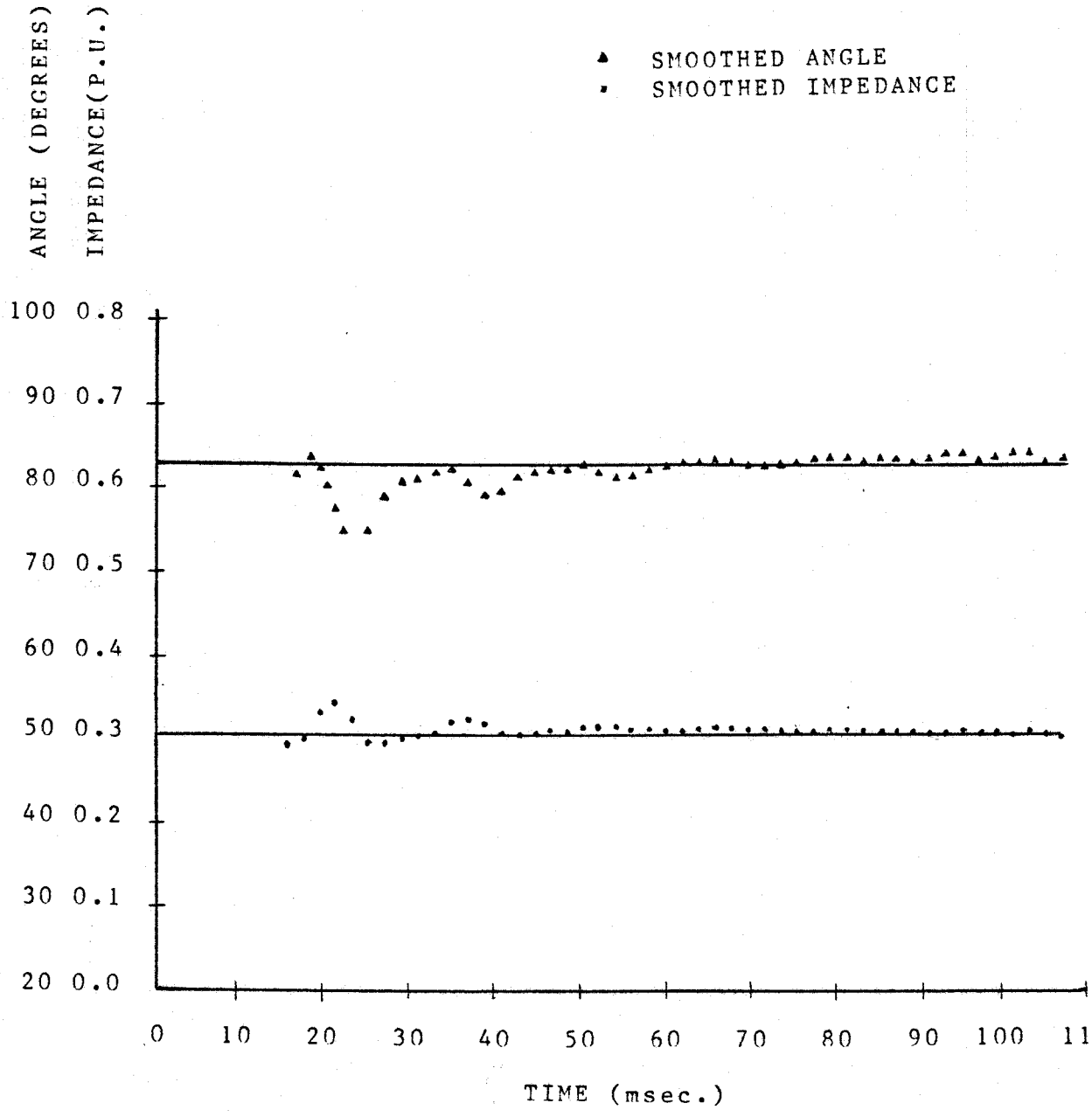

Figure 5.1 Bandpass R-Filter (55-65 Hz) + Mann and Morrison Algorithm + Single Exponential Smoothing (a=0.3) - fault incidence at zero degrees

The impedances and their phase angles were also calculated using recursive filters and the Mann and Morrison algorithm for fault incidence angles of 30, 60 and 90 electrical degrees. The results are plotted in Figures C.1, C.2 and C.3. These impedances and their phase angles were also smoothed using single exponential smoothing process described above. The smoothed impedances and their phase angles are plotted in Figures D.1, D.2 and D.3. The conclusions drawn from Figure 5.1 are reaffirmed by the results depicted in Figures D.1, D.2 and D.3.

The impedances and their phase angles, which were calculated from the voltages and currents processed by second order (55-65 Hz) bandpass recursive filters and the least error squares sine wave model, are shown in Figure 4.4. The fault incidence angle in this case was zero electrical degrees. The calculated values depicted in Figure 4.4 were also smoothed using single exponential smoothing process described earlier in this section. The smoothed impedances and their phase angles are plotted in Figure 5.2. This figure reveals that smoothed values are less scattered but the improvement in the values during the first half cycle after the commencement of the smoothing process is negligible. After this period, the scatter is considerably reduced. Mean value and standard deviation for the unsmoothed and the smoothed impedances and their phase angles were also calculated for this case and are listed in

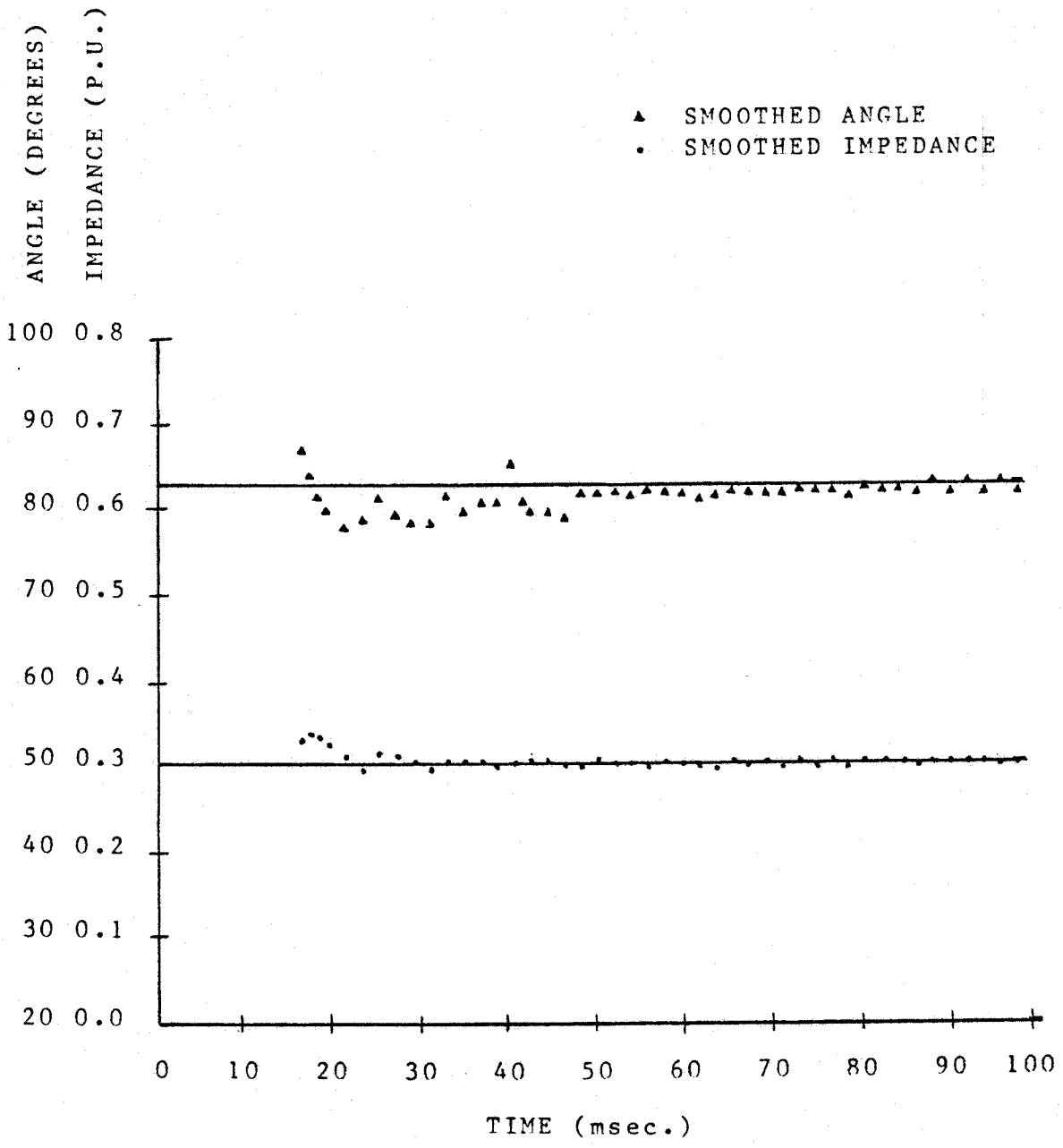

Figure 5.2 Bandpass R-Filter (55-65 Hz) + Least Error Squares Pure Sine Wave Model + Single Exponential Smoothing (a=0.3) - fault incidence at zero degrees

Table 5.2. It is observed from this table that the standard deviation for the smoothed values is less than the standard deviation for the unsmoothed values. This reaffirms that the use of the single exponential smoothing process considerably reduces the scatter of the calculated impedances.

Table 5.2 Mean value and standard deviation of the unsmoothed and smoothed impedances and their phase angles - data processed by recursive filters and the least error squares sine wave model

	IMPEDANCES		PHASE ANGLES	
	UNSMOOTHED	SMOOTHED	UNSMOOTHED	SMOOTHED
MEAN VALUE	0.31555	0.31703	83.84975	83.98075
STANDARD DEVIATION	0.01365	0.00870	2.85923	1.89225

The impedances and their phase angles were also calculated using recursive filters and the least error squares sine wave model when the fault incidence angle was 30, 60 and 90 degrees. The results are plotted in Figures C.4, C.5 and C.6. The calculated impedances and their phase angles were smoothed using single exponential smoothing and the smoothed values are plotted in Figures D.4, D.5 and D.6. The conclusions drawn from Figures 5.1 and 5.2 are reaffirmed by the results depicted in Figures D.4, D.5 and D.6.

5.2 General Exponential Smoothing

Power system voltages and currents during faults can be considered to be composed of sine and cosine functions of various frequencies. Generally, the fault currents also contain decaying d.c. components. The objective of many relaying and instrumentation devices is to extract the information pertaining to the fundamental frequency voltages and currents only and use it in decision making. For this purpose general exponential smoothing[7] can be applied for processing the fault data. This section briefly outlines the general exponential smoothing technique and its application for calculating line impedances and their phase angles.

In general exponential smoothing, the smoothing coefficients are revised each time a new set of samples of the input data becomes available. The initial conditions are also predicted frequently to improve the results. Equation 5.6, whose derivation is given in Appendix D, can be used to estimate the coefficients at a specified time.

$$A_{in} = [L'] A_{i(n-1)} + h \{X_n - S_{n-1}\} \qquad (5.6)$$

where:

A_{in} is the ith coefficient at the time nth sample is received

$[L']$ is the transpose of the transition matrix

h is the smoothing vector

S_{n-1} is the (n-1)th output

The values of different terms in the state transition matrix 'L' and the smoothing vector 'h' depend on the type of model used to represent the input, value of the smoothing constant and the inter-sampling interval. Numerical values for the state transition matrix and the smoothing vector for different types of models are given in Reference 7.

5.2.1 Fault data model

As already mentioned, power system voltages and currents during faults may be represented by the following equation:

$$V(t) = K_0 e^{-t/T} + \sum_{m=1}^{M} K_m \sin(mwt + \theta_m) \qquad (5.7)$$

where:

K_0 is the magnitude of the d.c. offset at t=0 seconds

T is the time constant of the system

K_m is the magnitude of the mth harmonic

θ_m is the phase angle of the mth harmonic

The term $e^{-t/T}$ can be expanded using the Taylor series expansion and the sinusoidal terms can be expanded using the

trigonometric equation:

$$\sin(mwt+\theta_m) = \cos(\theta_m)\ \sin(mwt) + \sin(\theta_m)\ \cos(mwt)$$

To simplify the calculations, the harmonic terms in Equation 5.7 were assumed to be negligible. Representing the exponential by the first two terms of the Taylor series expansion and using the fundamental frequency components, Equation 5.7 reduces to:

$$V(t)=K_0 - K_0 t/T + K_1 \sin(\theta_1)\cos(wt) + K_1 \cos(\theta_1)\sin(wt) \quad (5.8)$$

This equation reduces to Equation 5.9 if the following substitutions are made.

$$A_1 = K_0$$
$$A_2 = - K_0 / T$$
$$A_3 = K_1 \sin(\theta_1)$$
$$A_4 = K_1 \cos(\theta_1)$$

$$V(t)=A_1 + A_2 t + A_3 \sin(wt) + A_4 \cos(wt) \quad (5.9)$$

This equation represents voltages and currents during power system faults if the effects of system capacitances are neglected. The coefficients A_1 through A_4 can be calculated using Equation 5.6. The values of these coefficients are revised each time a new set of samples is obtained.

5.2.2 Implementation of general exponential smoothing

A computer program was written to implement the general exponential smoothing explained in the preceding paragraph. Model represented by Equation 5.9 was used to calculate the real and imaginary components of the fundamental frequency current and voltage phasors. These values were then used to calculate the apparent line impedances and their phase angles. Fault data generated in Chapter 4 was used as input. The impedances and their phase angles calculated by this procedure are plotted in Figure 5.3. This figure shows that the scatter for the calculated impedances and their phase angles is large at the start of the process. The values are not sufficiently accurate for approximately one and a half cycles after the inception of a fault. This is because the coefficients $A_{i(n-1)}$ and output S_{n-1} in Equation 5.6 are not known when the process is started. These values are generally initialized to zero. It takes almost one and a half cycles for the coefficients to overcome the initial conditions and stabilize to give sufficiently accurate results.

From the above discussion, it is observed that there are two major drawbacks in the general exponential smoothing technique. First drawback is that the output builds up slowly during the first one and a half cycles after the process is started. Because of this drawback, general

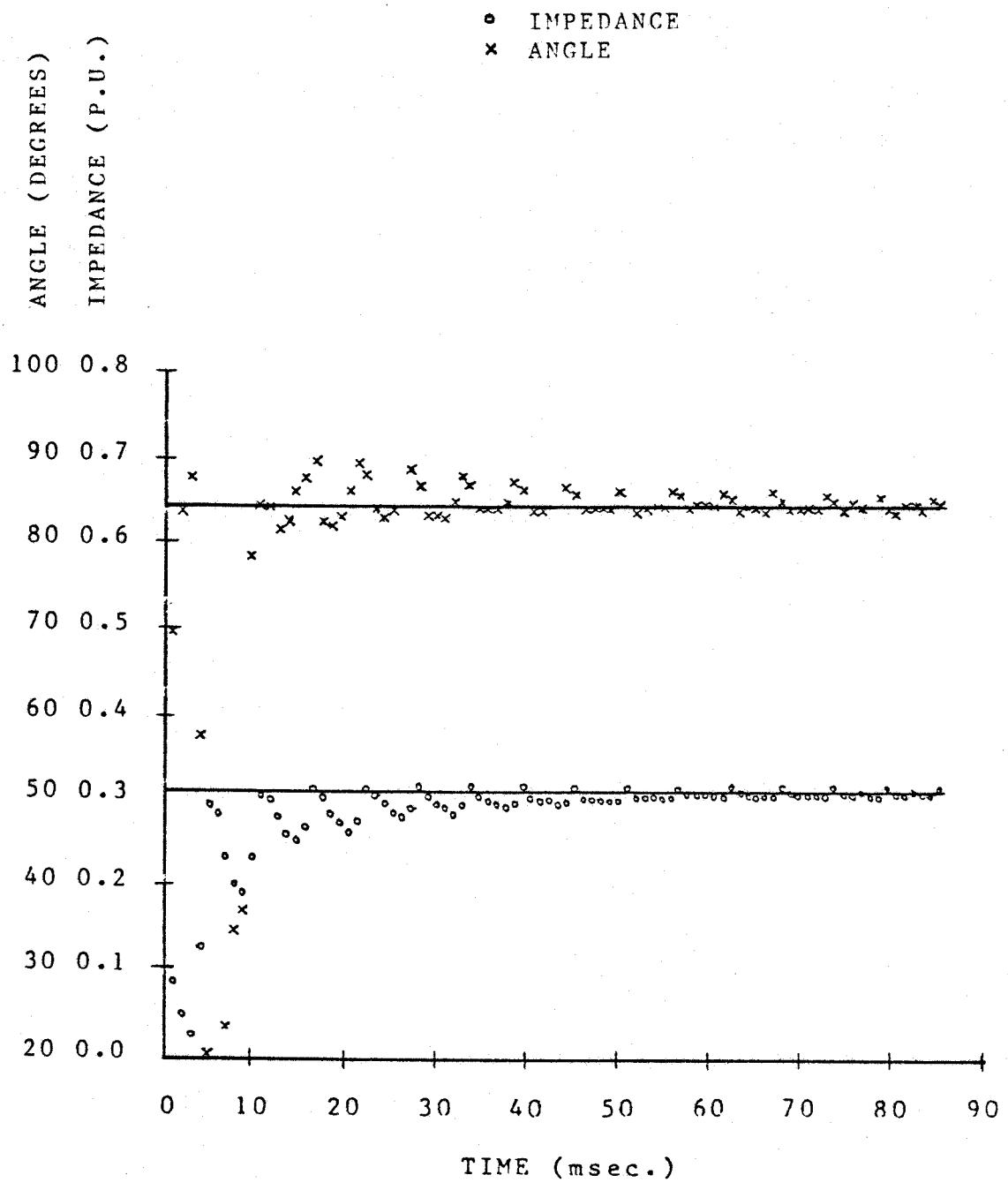

Figure 5.3 General Exponential Smoothing - fault incidence at zero degrees

exponential smoothing technique is not suitable in situations where initial conditions cannot be predicted and where rapid and accurate response is desired. The second shortcoming is that all the coefficients in the model, selected to represent the input data, have to be revised each time a new set of input data is obtained. As a consequence of this, the computation time is large.

These drawbacks cannot be tolerated in power system protection applications. General exponential smoothing technique is, therefore, not suitable for application to digital protection of power system components. Further study on the subject was, therefore, abandoned.

5.3 Conclusion

The general exponential smoothing is a recursive process like digital recursive filters. It seems that this technique cannot be applied for power system protection where rapid relay response is desired. A comparison reveals that the results obtained by this technique are not better than those obtained by the use of recursive filters discussed in Chapter 4. Moreover, the general exponential smoothing technique requires more computation time because the coefficients have to be calculated in the real time mode and have to be revised each time a new set of samples is obtained.

Single exponential smoothing can be applied to improve the results (impedances and their phase angles or R and X) calculated by various relaying algorithms. This technique requires one addition, one subtraction and one multiplication. The improvement in the results obtained in this manner is substantial while the additional computational requirements are minimal.

6. POLYPHASE DIGITAL DISTANCE RELAY

Various kinds of distance relays have been briefly described in Chapter 2. The previously published relaying algorithms have also been presented in that chapter. Procedures for designing digital recursive filters have been presented in Chapter 3 and the performance of a few designed filters has been reported in Chapter 4. In Chapter 5, exponential and general exponential smoothing techniques have been presented. To select the design for a generic polyphase distance relay system for digital processor implementation, past developments of polyphase distance relays are reviewed in this chapter. The selected design was implemented on PDP 11/60 mini-computer and its performance tested in the laboratory. The implementation and some test results are also presented.

It is well known that 10 types of shunt faults can be experienced in a three phase power system:

(i) Single line to ground faults - three possibilities (phase A to ground fault, phase B to ground fault and phase C to ground fault)

(ii) Two phase faults - six possibilities (phase A to phase B fault, phase B to phase C fault,

phase C to phase A fault, phases A and B to ground fault, phases B and C to ground fault and phases C and A to ground fault)

(iii) Three phase fault - one possibility (three phase fault with or without ground)

Electro-mechanical and solid state distance relay systems presently used on EHV transmission lines consist of six or seven impedance measuring units. A similar approach has been used in digital impedance relays developed so far. This approach required that the impedance measuring algorithm be executed six times after each new set of voltage and current samples is received. This increases the computation burden considerably. To reduce this burden two distinct approaches can be used. One, a switching type logic can be used to select the faulted phase/phases and then calculate the apparent impedance of the selected phase/phases only. The second approach is to use a polyphase type distance relay design. A comparison of the two approaches revealed that the polyphase approach would require fewer computations. It was, therefore, decided that a digital polyphase relay be developed.

6.1 Development of Polyphase Distance Relays

Development of polyphase distance relays was first reported by W. K. Sonemann and H. W. Lenser[39]. In the

proposed system two relay units were used; one unit was designed to operate for phase to phase faults and the other unit was designed to operate for three phase faults. It was also shown by the authors that one of these units would operate for two phases to ground faults. The commercial version of the reported system (K-DAR relays) consists of two phase comparators. Bus voltages are compensated for the voltage drops in the transmission line upto the required reach of the relay. Two of the three compensated voltages are then used to decide if the fault is in the protected zone. These voltages are in phase when a fault occurs at the far end of the protected zone; no output is produced in such cases. For faults inside the protected zone, the voltages are shifted such that a command to trip the line breakers is generated. Similarly, for faults outside the protected zone, the sequence of the compensated voltages is reversed. This phase reversal is used to generate a restraint signal. The basic elements used in the K-DAR relays are induction cups whose direction of rotation depend on the sequence of the applied voltages. These relay elements continuously monitor the phase sequence of the compensated voltages at the relay terminals and decide if the system is experiencing a fault or not. As already stated, the two induction cup elements can detect all two phase and three phase faults.

G. D. Rockefeller reported the development of a "Zone Packaged Ground Distance Relay"[35]. This system consists of an amplitude comparator which responds to all single phase to ground faults. A system consisting of the K-DAR phase to phase and three phase relays and a zone packaged ground distance relay would be normally adequate for detecting all shunt faults on a protected line.

The concept of polyphase relays progressively became more popular during the late sixties and early seventies. References 4,9,19,28,29 and 39 discuss the key developments in this area. Like the K-DAR concept, Reference 4 describes a solid-state polyphase distance relay which operates for all shunt faults except the three phase faults. In a similar approach the authors of Reference 9 designed a polyphase distance relay which uses the principle of phase coincidence. This relay operates for all single phase to ground and two phases to ground faults. The relay does not operate for phase to phase and three phase faults. Reference 29 describes a single polyphase distance relay which responds to all types of faults.

In the AEP digital relay development project[32], symmetrical components approach was used in designing a polyphase digital distance relay. The relay responds to all types of shunt faults. It is a useful concept except that the computation burden is large when the relay is

implemented on a digital processor for on line application.

It is obvious that a digital relay which requires fewer arithmetic operations and simple logic will require less computation effort and time. Arithmetic operations required for digital implementation of the polyphase distance relays listed above were, therefore, checked and are listed in Table 6.1. A review of this table reveals that a combination of the solid state polyphase relay of Reference 4 and the K-DAR three phase relay would be less demanding computationally. This combination of the relay units was, therefore, selected for implementing on a digital processor. These relays are inherently directional in character and their operating characteristics, when plotted on the R-X plane, are circular - similar to that shown in Figure 2.1.

6.2 Principles of the Selected Polyphase Distance Relays

The principles of the polyphase relay units[4,39] selected in Section 6.1 are briefly presented in this section. The relay performance for single phase to ground, phase to phase, two phases to ground and three phase faults is also examined.

Table 6.1 Arithmetic operations required for digital implementation of the polyphase distance relays

REFERENCE NO.	AND NAME	A	B	C	D	E	GENERAL REMARKS
37	K-DAR ϕ-ϕ UNIT	4	4	2	-	1	OPERATES FOR ϕ-ϕ FAULTS
37	K-DAR 3-ϕ UNIT	-	5	2	-	1	OPERATES FOR 3-ϕ FAULTS
35	ZONE PACKAGED GROUND DISTANCE RELAY	12	19	8	2	3	OPERATES FOR SINGLE LINE TO GROUND FAULTS
29	POLYPHASE DISTANCE RELAY	14	6	8	-	4	OPERATES FOR ALL TYPES OF FAULTS
4	A STATIC POLYPHASE DISTANCE RELAY	13	6	6	-	3	OPERATES FOR ALL EXCEPT THREE PHASE FAULTS
9	POLYPHASE GROUND DISTANCE RELAYING (PHASE COINCIDENCE)	13	6	6	-	3	OPERATES FOR ALL EXCEPT ϕ-ϕ AND THREE PHASE FAULTS
32	DISTANCE RELAYING WITH SYMMETRICAL COMPONENTS	49	5	38	5	2	OPERATES FOR ALL TYPES OF FAULTS

A is the number of additions
B is the number of subtractions
C is the number of multiplications
D is the number of divisions
E is the number of comparisons

6.2.1 Unbalanced faults

As stated in the last section, one impedance measuring unit can detect single phase to ground, phase to phase and two phases to ground faults. The operating principle of such a relay can be explained as follows:

Consider the three compensated line to line voltages as defined in Equations 6.1, 6.2 and 6.3:

$$V_x = V_a - (I_a + K3I_0)Z_r \tag{6.1}$$

$$V_y = V_b - (I_b + K3I_0)Z_r \tag{6.2}$$

$$V_z = V_c - (I_c + K3I_0)Z_r \tag{6.3}$$

Where:

V_x, V_y and V_z are the three compensated voltages at the relay location

V_a, V_b and V_c are the three phase voltages at the relay location

I_a, I_b and I_c are the three line currents at the relay location

I_0 is the zero sequence component of the fault current

Z_r is the impedance of the line from the relay location to the set reach

$$K = \frac{Z_{0L} - Z_{1L}}{3Z_{0L}}$$

Z_{1L} and Z_{0L} are the positive and zero sequence impedances of the transmission line from the relay location to the end of the protected zone

It has been shown in Reference 4 that a phase comparison of V_x and V_y can detect all types of faults except the phase C to ground, phases A and B to ground and three phase faults. The comparator operates if V_y leads V_x. It is also shown in that reference that a phase comparison of V_y and V_z can detect all faults except the phase A to ground, phases B and C to ground and three phase faults. In this case the comparator operates if V_z leads V_y. Two phase comparators, one using V_x and V_y and the other using V_y and V_z, can, therefore, detect all types of shunt faults except three phase faults.

The performance of the relay described above was examined for faults inside and outside the protected zone. For this purpose a single transmission line protected by the selected polyphase relay was considered. The line interconnects two power systems as shown in Figure 6.1. The relay reach and the fault locations considered in the study are also shown in the figure. Parameters of the selected system are given in Appendix E.

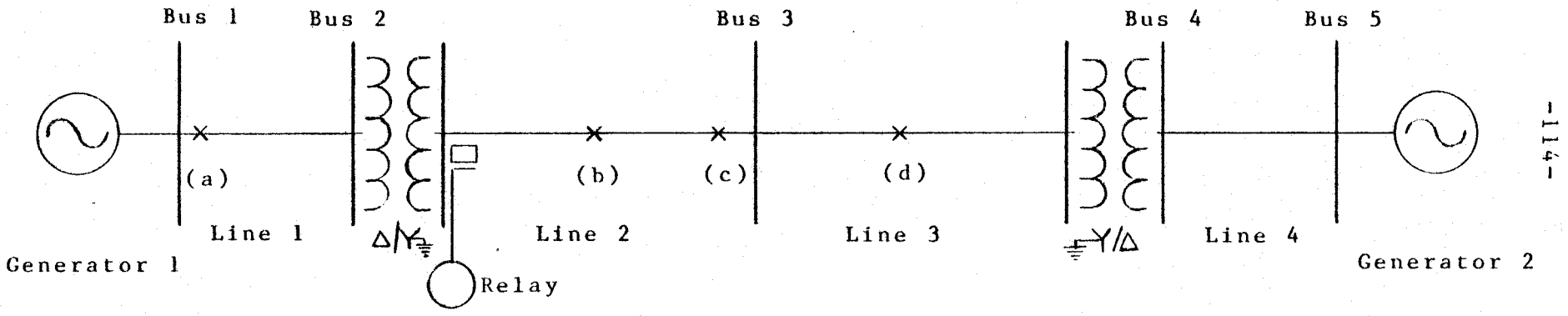

(a) Fault behind the relay
(b) Fault within the set reach point
(c) Fault at the set reach point
(d) Fault beyond the set reach point

Figure 6.1 Power system model used to calculate the relay inputs for drawing phasor diagrams

During a fault the sequence voltages at the relay location can be expressed by Equations 6.4 through 6.6 if the fault resistance is neglected.

$$V_{a1} = E_a - I_{a1} Z_{1s} \tag{6.4}$$

$$V_{a2} = - I_{a2} Z_{2s} \tag{6.5}$$

$$V_{a0} = - I_{a0} Z_{0s} \tag{6.6}$$

where:

E_a is the source voltage

Z_{1s}, Z_{2s} and Z_{0s} are the equivalent positive, negative and zero sequence impedances of the power system behind the relay

The compensated positive sequence voltage at the relay location is given by:

$$V_{x1} = V_{a1} - I_{a1} Z_r \tag{6.7}$$

Substituting for V_{a1} from Equation 6.4 provides the following equation:

$$V_{x1} = E_a - (Z_{1s} + Z_r) I_{a1} \tag{6.8}$$

Similarly, the compensated negative and zero sequence

voltages at the relay location can be expressed as:

$$V_{x2} = -(Z_{2s} + Z_r) I_{a2} \tag{6.9}$$

$$V_{x0} = -\{Z_{0s} + (K+1) Z_r\} I_{a0} \tag{6.10}$$

In Equations 6.8 through 6.10, all the parameters except I_{a1}, I_{a2} and I_{a0} are known. The values of these currents depend upon the type and location of the fault. To illustrate the relay performance during different types of faults, the values of these currents were calculated for each type of fault at the selected locations. The sequence voltages V_{x1}, V_{x2} and V_{x0} were then computed. From these voltages, the compensated voltages at the relay location were determined using the following equations.

$$V_x = V_{x1} + V_{x2} + V_{x0} \tag{6.11}$$

$$V_y = a^2 V_{x1} + a V_{x2} + V_{x0} \tag{6.12}$$

$$V_z = a V_{x1} + a^2 V_{x2} + V_{x0} \tag{6.13}$$

where: $a = 1 \angle 120^{\circ}$

The performance of the selected relay for single phase to ground, phase to phase and two phases to ground faults on the selected system is illustrated in the following subsections.

6.2.1.1 Single phase to ground faults

It can be shown that for a phase A to ground fault[41]:

$$I_{a1} = \frac{E_a}{Z_1 + Z_2 + Z_0} \tag{6.14}$$

$$I_{a2} = I_{a0} = I_{a1} = I_a/3 \tag{6.15}$$

where: $Z_1 = Z_{1s} + Z_{1L}$, $Z_2 = Z_{2s} + Z_{2L}$, $Z_0 = Z_{0s} + Z_{0L}$

Substituting for I_{a1}, I_{a2} and I_{a0} in Equations 6.8, 6.9 and 6.10, the compensated sequence voltages at the relay location are given by:

$$V_{x1} = E_a - \frac{(Z_{1s} + Z_r)}{Z_1 + Z_2 + Z_0} E_a$$

$$= \frac{(Z_1 + Z_2 + Z_0 - Z_{1s} - Z_r)}{Z_1 + Z_2 + Z_0} E_a \tag{6.16}$$

$$V_{x2} = - \frac{(Z_{2s} + Z_r)}{Z_1 + Z_2 + Z_0} E_a \tag{6.17}$$

$$V_{x0} = - \frac{Z_{0s} + (K+1)Z_r}{Z_1 + Z_2 + Z_0} E_a \tag{6.18}$$

Using these equations V_{x1}, V_{x2} and V_{x0} were calculated for

the selected faults. From these sequence voltages, compensated voltages V_x, V_y and V_z were determined. Four fault locations were considered; one selected location was on the bus side of the relay, the second location was in the protected zone of the relay, the third location was at the end of the protected zone and the fourth selected location was beyond the set reach of the relay. The calculated compensated voltages for these faults are listed in Table 6.2. Phasor diagrams for the compensated voltages at the relay location are depicted in Figure 6.2. This figure reveals that the voltage V_y leads the voltage V_x when the fault is in the protected zone of the relay. For faults at the other three locations, the voltage V_y lags the voltage V_x and the relay, therefore, does not operate.

Figure 6.3 shows that the comparator using the compensated voltages V_x and V_y operates for phase B to ground faults in the protected zone only. Similarly Figure 6.4 shows that the comparator does not operate for phase C to ground faults.

Similarly it can be shown that the phase comparator using the compensated voltages V_y and V_z will operate for phase B to ground and phase C to ground faults. It can also be shown that this comparator will not operate for phase A to ground faults.

Table 6.2 Compensated voltages at the relay location for various types of faults occurring at different locations on a transmission line

FAULT TYPE	COMPENSATED VOLTAGES						LOCATION OF FAULT
	V_x		V_y		V_z		
	MAG	ANG	MAG	ANG	MAG	ANG	
A-G	0.54	175.45	1.27	-138.04	1.29	136.98	WITHIN REACH
	0.00	0.00	1.17	-132.42	1.17	132.27	AT THE S.P.
	0.33	-2.03	1.11	-128.71	1.11	128.82	BEYOND S.P.
	1.90	-4.64	0.88	-93.74	0.85	93.88	BEHIND RELAY
B-C	1.00	0.00	0.60	138.99	0.67	-144.23	WITHIN REACH
	1.00	0.00	0.50	180.09	0.50	180.09	AT THE S.P.
	1.00	0.00	0.58	-153.14	0.55	151.74	BEYOND S.P.
	1.00	0.00	1.53	-115.72	1.42	103.71	BEHIND RELAY
B-C-G	1.36	-0.44	0.51	47.68	0.48	-58.92	WITHIN REACH
	1.22	-0.06	0.00	0.00	0.00	0.00	AT THE S.P.
	1.15	0.05	0.32	-125.66	0.31	120.22	BEYOND S.P.
	0.64	0.93	1.78	-132.41	1.69	121.17	BEHIND RELAY
THREE PHASE FAULT	0.46	173.32	0.57	-126.83	0.57	113.29	WITHIN REACH
	0.00	0.00	0.71	-124.70	0.71	115.42	AT THE S.P.
	0.30	-3.24	0.80	-123.30	0.80	116.82	BEYOND S.P.
	1.61	-6.78	0.57	-126.83	0.57	113.29	BEHIND RELAY

Fault within reach is at 50 percent of the first zone
Set point is at 90 percent of the first zone
Fault beyond set point is at 145 percent of the first zone
Fault behind the relay is at -50 percent of the first zone

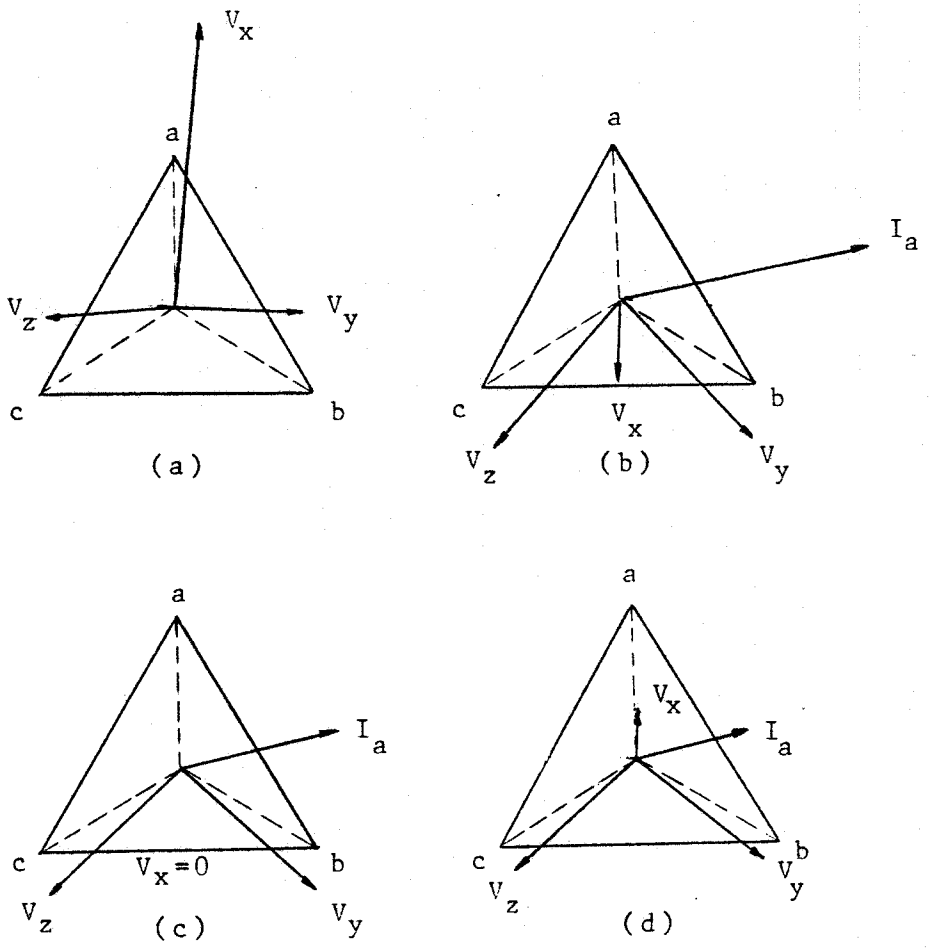

Figure 6.2 Phasor diagrams of the relay inputs during a phase A to ground fault occurring

(a) behind the relay
(b) within the set reach point
(c) at the set reach point
(d) beyond the set reach point

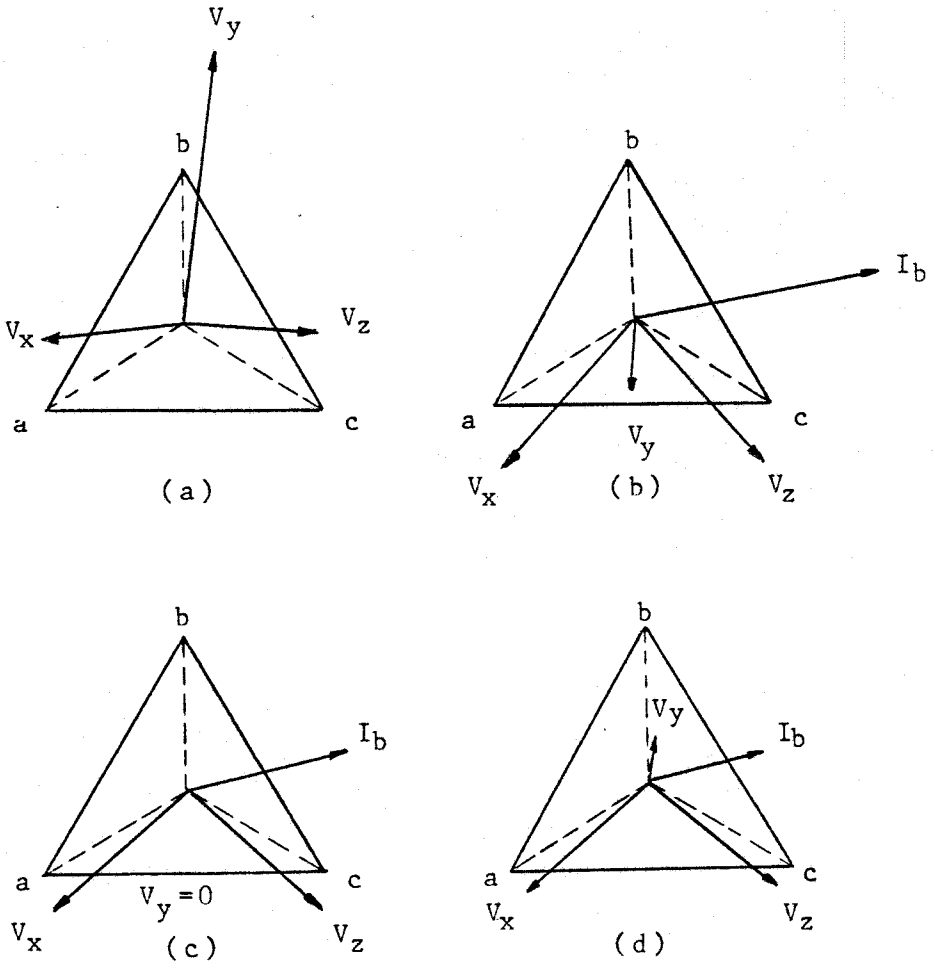

Figure 6.3 Phasor diagrams of the relay inputs during a phase B to ground fault occurring

(a) behind the relay
(b) within the set reach point
(c) at the set reach point
(d) beyond the set reach point

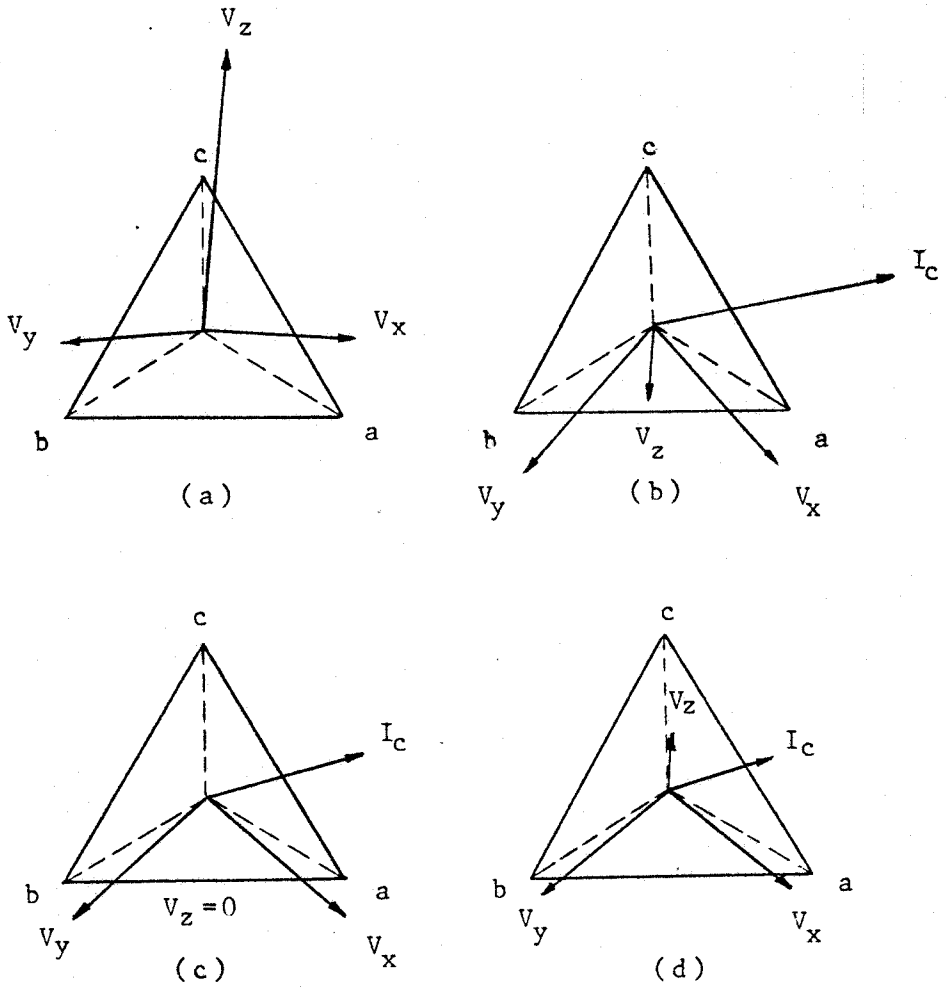

Figure 6.4 Phasor diagrams of the relay inputs during a phase C to ground fault occurring

(a) behind the relay
(b) within the set reach point
(c) at the set reach point
(d) beyond the set reach point

6.2.1.2 Two phase faults

For a phase B to phase C fault, the positive and negative sequence currents are given by[41]:

$$I_{a1} = \frac{E_a}{Z_1 + Z_2} \tag{6.19}$$

$$I_{a2} = - I_{a1} \tag{6.20}$$

By substituting for I_{a1} and I_{a2} in Equations 6.8 and 6.9, the compensated sequence voltages at the relay location are obtained as follows:

$$V_{x1} = E_a - \frac{Z_{1s} + Z_r}{Z_1 + Z_2} E_a$$

$$= \frac{Z_1 + Z_2 - Z_{1s} - Z_r}{Z_1 + Z_2} E_a \tag{6.21}$$

$$V_{x2} = \frac{Z_{2s} + Z_r}{Z_1 + Z_2} E_a \tag{6.22}$$

V_{x1} and V_{x2} were calculated for phase B to phase C faults at the four selected locations. From these sequence voltages, compensated voltages V_x, V_y and V_z were determined. The calculated voltages are listed in Table 6.2. Phasor diagrams showing the compensated voltages at the relay

location are depicted in Figure 6.5. An examination of this figure reveals that the voltage V_y leads the voltage V_x only when a phase B to phase C fault is in the protected zone of the relay. For faults at the other three locations, the voltage V_y lags the voltage V_x and the relay, therefore, does not operate.

Figure 6.6 shows that the voltage V_y leads the voltage V_x when a phase C to phase A fault occurs in the protected zone of the relay. Similarly Figure 6.7 shows that voltage V_y leads the voltage V_x when a phase A to phase B fault occurs in the relay's protected zone. Figures 6.6 and 6.7 also show that the voltage V_y lags voltage V_x for faults outside the relay's protected zone.

Similarly it can be shown that V_z would lead V_y when a two phase fault is experienced in the protected zone of the relay. Should the fault be outside the relay's zone, V_z would lag V_y.

6.2.1.3 Two phases to ground faults

Positive, negative and zero sequence currents during a

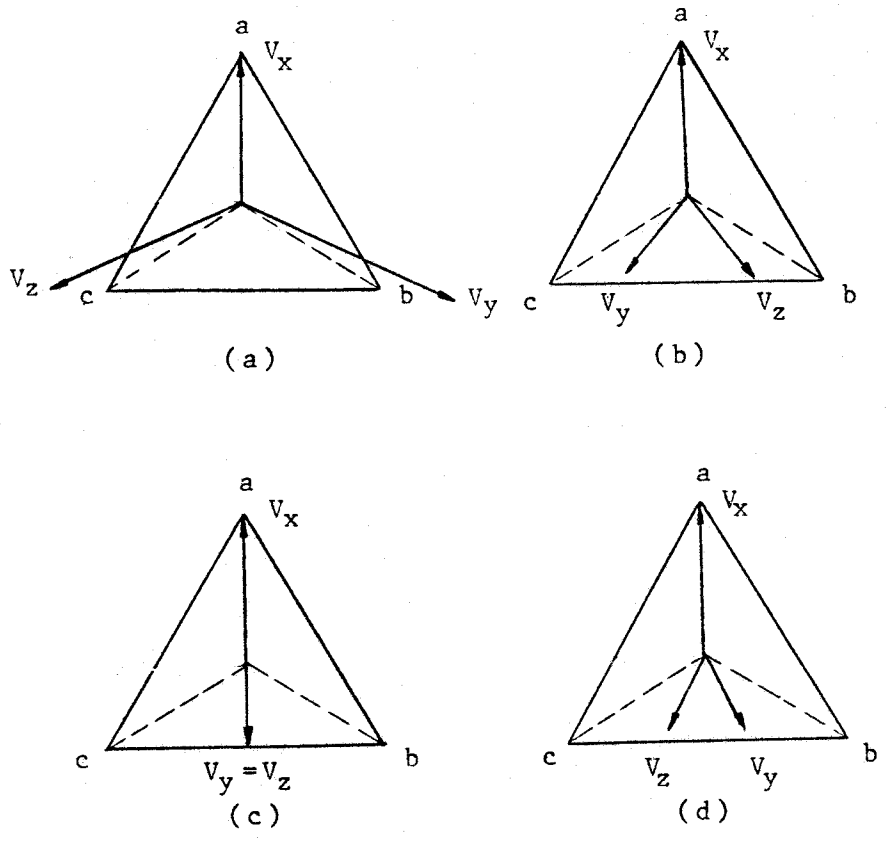

Figure 6.5 Phasor diagrams of the relay inputs during a double line (B-C) fault occurring

(a) behind the relay
(b) within the set reach point
(c) at the set reach point
(d) beyond the set reach point

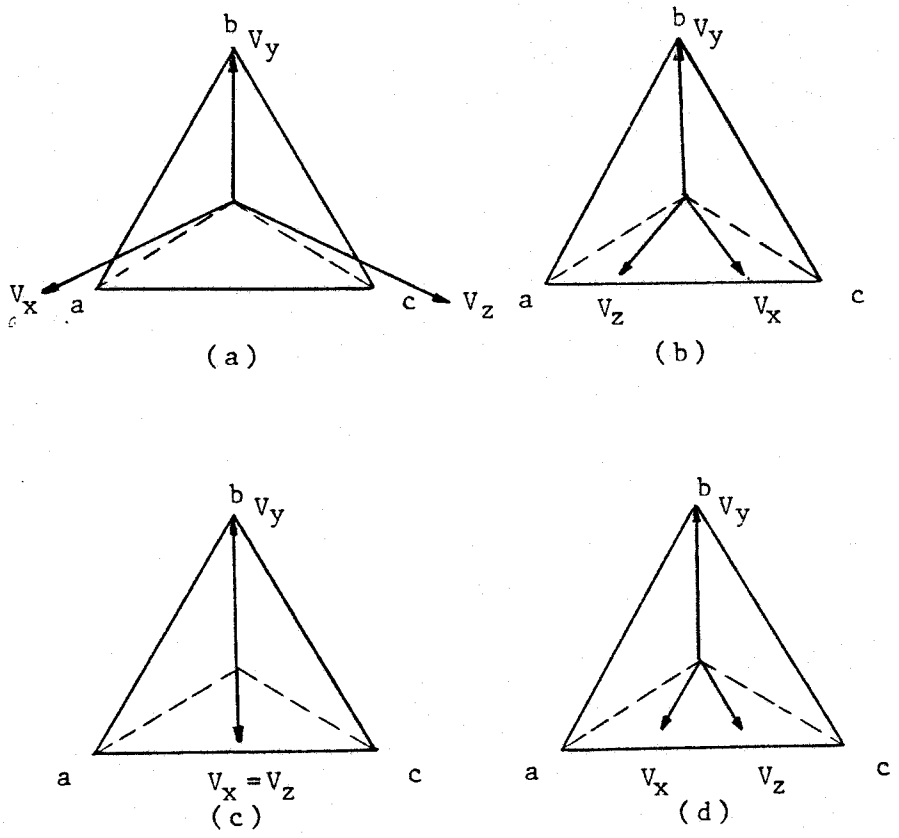

Figure 6.6 Phasor diagrams of the relay inputs during a double line (C-A) fault occurring

(a) behind the relay
(b) within the set reach point
(c) at the set reach point
(d) beyond the set reach point

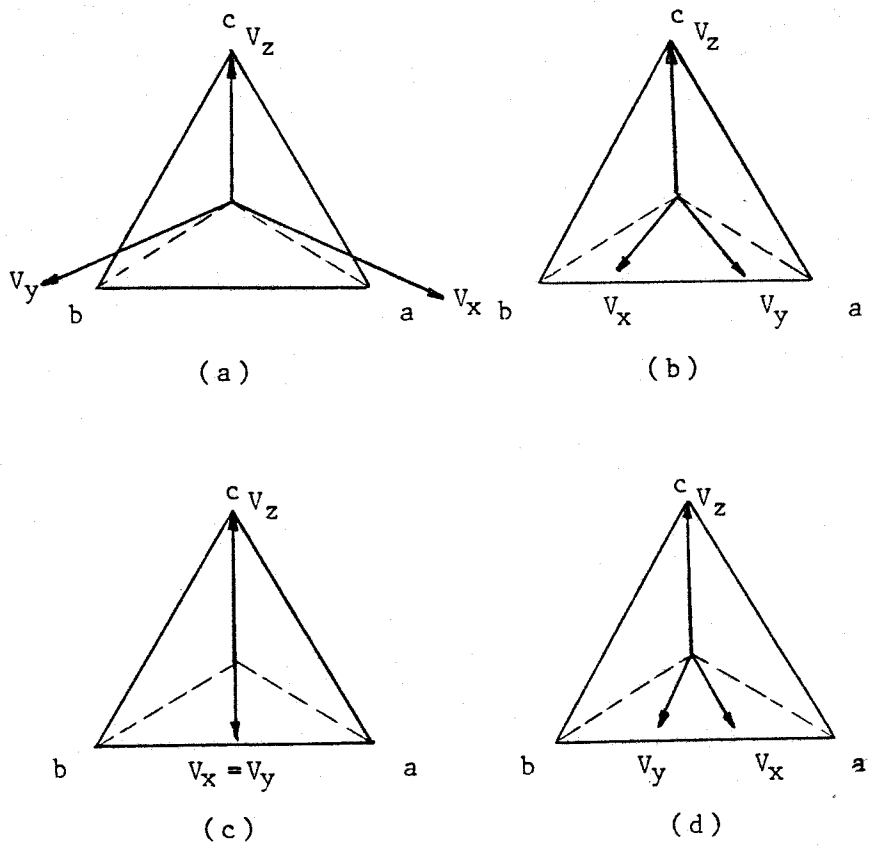

Figure 6.7 Phasor diagrams of the relay inputs during a double line (A-B) fault occurring

(a) behind the relay
(b) within the set reach point
(c) at the set reach point
(d) beyond the set reach point

phase B and phase C to ground fault are given by[41]:

$$I_{a1} = \frac{E_a}{Z_1 + \frac{Z_0 Z_2}{Z_0 + Z_2}} \tag{6.23}$$

$$I_{a2} = -I_{a1} \frac{Z_0}{Z_0 + Z_2} \tag{6.24}$$

$$I_{a0} = -I_{a1} \frac{Z_2}{Z_0 + Z_2} \tag{6.25}$$

Substituting for I_{a1}, I_{a2} and I_{a0} in Equations 6.8, 6.9 and 6.10, the compensated sequence voltages at the relay location are given by:

$$V_{x1} = E_a - \frac{(Z_{1s} + Z_r)(Z_0 + Z_2)}{Z_1(Z_0 + Z_2) + Z_0 Z_2} E_a$$

$$= \left[1 - \frac{(Z_{1s} + Z_r)(Z_0 + Z_2)}{Z_1(Z_0 + Z_2) + Z_0 Z_2}\right] E_a \tag{6.26}$$

$$V_{x2} = \frac{Z_0(Z_{2s} + Z_r)}{Z_1(Z_0 + Z_2) + Z_0 Z_2} E_a \tag{6.27}$$

$$V_{x0} = \frac{Z_2\{Z_{0s} + (K+1)Z_r\}}{Z_1(Z_0 + Z_2) + Z_0 Z_2} E_a \tag{6.28}$$

Sequence voltages V_{x1}, V_{x2} and V_{x0} were calculated for phase B and phase C to ground faults occurring at four selected

locations of the system shown in Figure 6.1. From these values compensated voltages V_x, V_y and V_z were determined and are listed in Table 6.2. Phasor diagrams for the compensated voltages at the relay location are depicted in Figure 6.8. An examination of the figure reveals that the voltage V_y leads the voltage V_x when a phase B and phase C to ground fault occurs in the protected zone of the relay. For faults at the other three locations, the voltage V_y lags the voltage V_x.

Figure 6.9 shows that the voltage V_y leads the voltage V_x when a phase C and phase A to ground fault occurs in the relay's protected zone only. Figure 6.10 shows that the voltage V_y lags the voltage V_x for a phase A and phase B to ground fault inside or outside the protected zone of the relay.

Similarly it can be shown that V_z would lead V_y for phase C and phase A to ground faults and phase A and phase B to ground faults in the protected zone of the relay. For these faults outside the protected zone of the relay, V_z would lag V_y. It can also be shown that V_z would lag V_y for phase B and phase C to ground faults inside or outside the protected zone of the ralay.

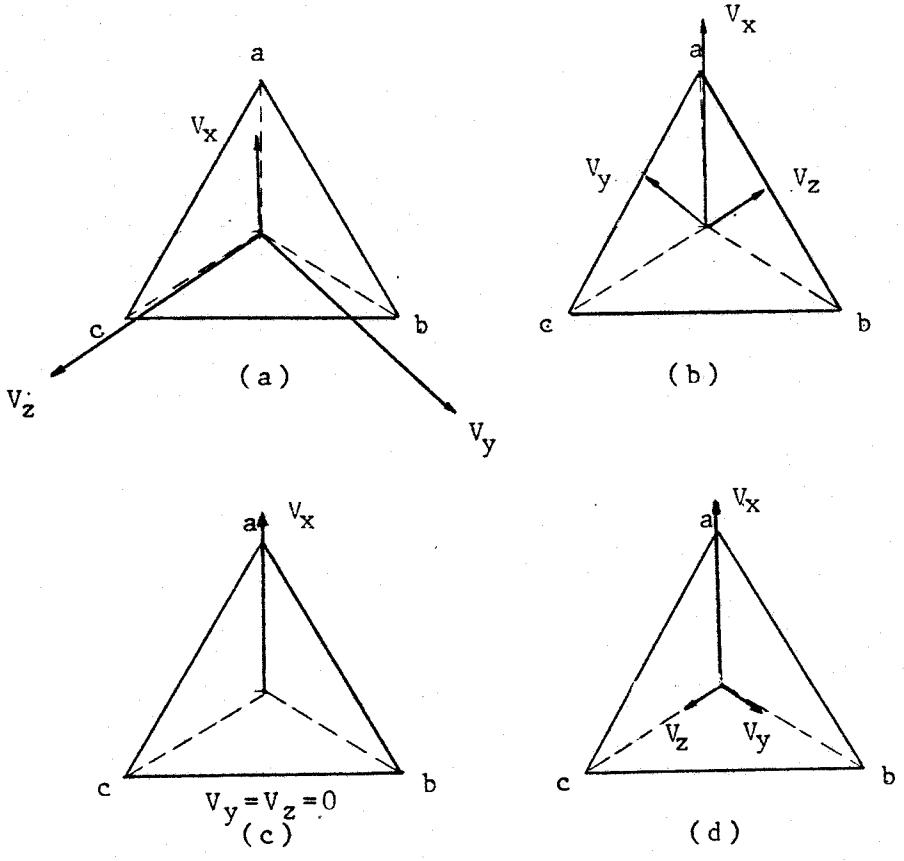

Figure 6.8 Phasor diagrams of the relay inputs during a double line to ground (B-C-G) fault occurring

(a) behind the relay
(b) within the set reach point
(c) at the set reach point
(d) beyond the set reach point

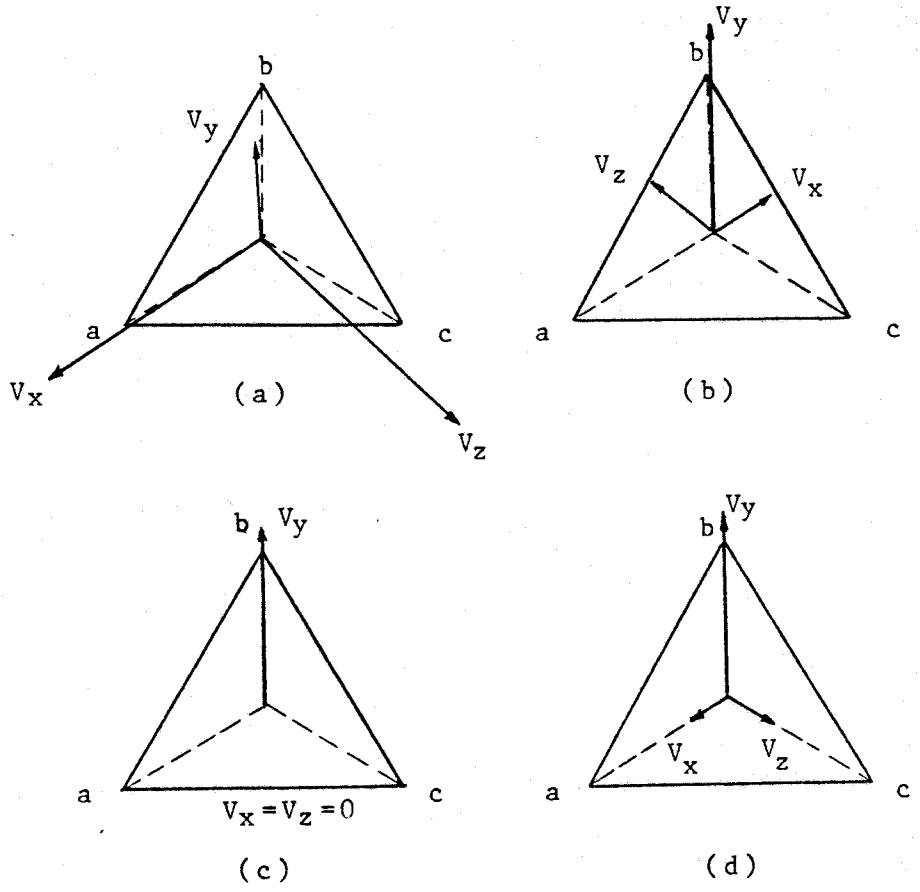

Figure 6.9 Phasor diagrams of the relay inputs during a double line to ground (C-A-G) fault occurring

(a) behind the relay
(b) within the set reach point
(c) at the set reach point
(d) beyond the set reach point

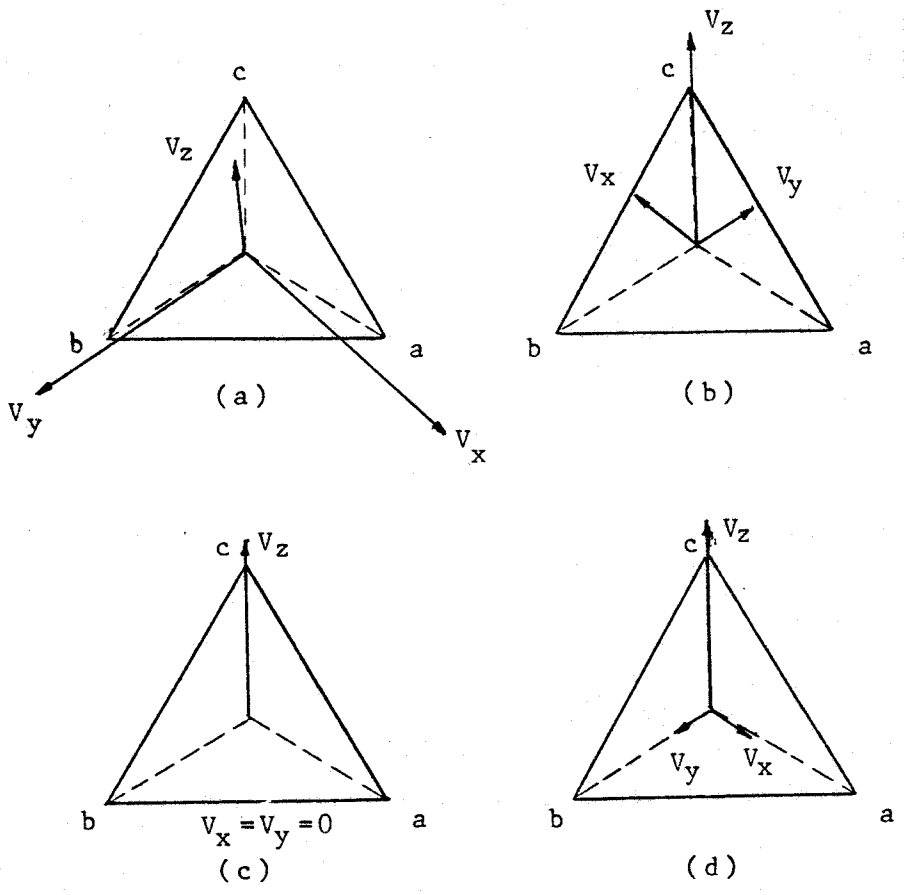

Figure 6.10 Phasor diagrams of the relay inputs during a double line to ground (A-B-G) fault occurring

(a) behind the relay
(b) within the set reach point
(c) at the set reach point
(d) beyond the set reach point

6.2.2 Detecting three phase faults

A three phase K-DAR unit[39] responds to three phase faults. For these faults, the equations for the compensated voltages at the relay location are:

$$V_x = V_a - I_a Z_r \tag{6.29}$$

$$V_y = V_b \tag{6.30}$$

$$V_z = V_c \tag{6.31}$$

From these equations, phase to phase compensated voltages are obtained as follows.

$$V_{xy} = V_x - V_y \tag{6.32}$$

$$V_{yz} = V_y - V_z \tag{6.33}$$

The three phase comparator operates if V_{yz} leads V_{xy}. In this case, the phase sequence of the compensated voltages is XZY when the fault is in the protected zone of the relay. The phase sequence is, however, XYZ if the fault is outside the protected zone of the relay.

It can be shown that for a three phase fault[39]:

$$I_{a1} = I_a = \frac{E_a}{Z_{1s} + Z_{1L}} \tag{6.34}$$

$$V_{a1} = V_a = I_{a1} Z_{1L} \tag{6.35}$$

The compensated positive sequence voltage V_{x1} is given by Equation 6.36 as:

$$V_{x1} = \frac{1}{3} (V_x + a\ V_y + a^2\ V_z) \tag{6.36}$$

This equation reduces to the following form if V_x , V_y and V_z are substituted from Equations 6.29, 6.30 and 6.31 and V_a is substituted from Equation 6.35.

$$V_{x1} = \frac{1}{3} (V_a - I_a Z_r + a\ V_b + a^2\ V_c)$$

$$= V_a - \frac{I_a Z_r}{3}$$

$$= \left[Z_{1L} - \frac{Z_r}{3} \right] I_a \tag{6.37}$$

Substituting for I_a from Equation 6.34; Equation 6.37 leads to:

$$V_{x1} = \frac{Z_{1L} - Z_r/3}{Z_{1s} + Z_{1L}}\ E_a \tag{6.38}$$

Similarly the compensated negative sequence voltage is

given by:

$$V_{x2} = \frac{1}{3}(V_x + a^2 V_y + a V_z)$$

$$= \frac{1}{3}(V_a - I_a Z_r + a^2 V_b + a V_c)$$

$$= - \frac{I_a Z_r}{3} \qquad (6.39)$$

Substituting for I_a in Equation 6.39, negative sequence component of the compensated voltage at the relay location is obtained as follows:

$$V_{x2} = - \frac{E_a Z_r}{3(Z_{1s} + Z_{1L})} \qquad (6.40)$$

Similarly the zero sequence component of the compensated voltage at the relay location is given by:

$$V_{x0} = - \frac{E_a Z_r}{3(Z_{1s} + Z_{1L})} \qquad (6.41)$$

From the sequence voltages, V_x is determined. The phase to phase sequence voltages V_{xy} and V_{yz} are then calculated.

Using this procedure, the compensated voltages V_x, V_y and V_z were calculated for the faults at the four selected locations of the system shown in Figure 6.1. The calculated values are listed in Table 6.2 and the phasor diagrams are depicted in Figure 6.11. This figure reveals

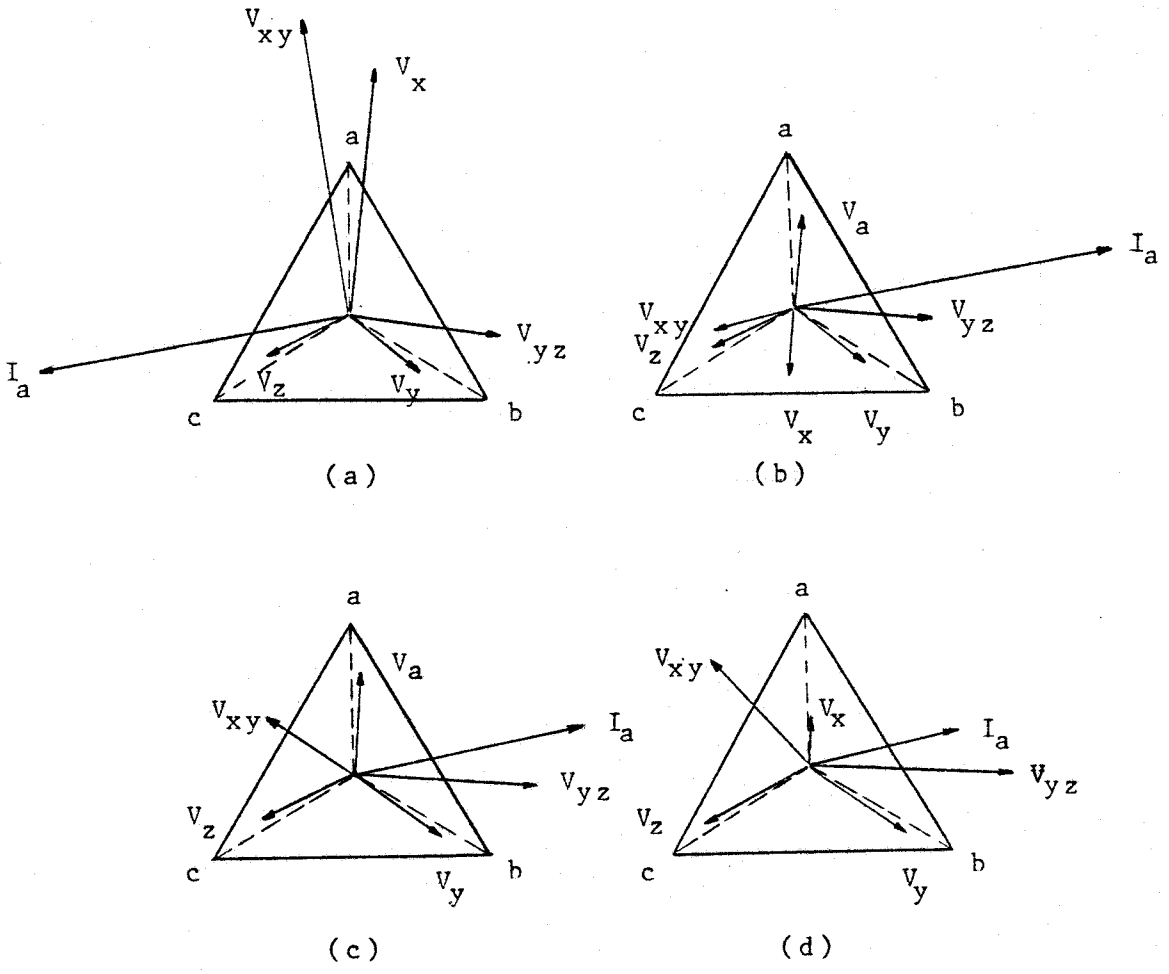

Figure 6.11 Phasor diagrams of the relay inputs during a three phase fault occurring

(a) behind the relay
(b) within the set reach point
(c) at the set reach point
(d) beyond the set reach point

that the voltage V_{yz} leads the voltage V_{xy} when the fault is in the protected zone of the relay. For the faults at the other selected locations V_{yz} lags V_{xy}.

6.2.3 Summary

A system consisting of a solid state polyphase distance relay and a three phase K-DAR unit will detect all types of shunt faults on the protected transmission line. Arithmetic operations required to implement the protection system (excluding the arithmetic operations required for digital filtering) are listed in Table 6.3.

Table 6.3 Arithmetic operations required for digital implementation of the polyphase relay algorithm

	SOLID STATE DISTANCE RELAY	K-DAR THREE PHASE UNIT	TOTAL
ADDITIONS	12	0	12
SUBTRACTIONS	6	5	11
DIVISIONS	0	0	0
MULTIPLICATIONS	4	2	6
BIT SHIFT OPERATIONS	2	-	2

6.3 Implementing the Digital Polyphase Distance Relay

In the last section operation of the polyphase relay during various types of faults was analysed with the aid of phasor diagrams. The relay was programmed on the PDP 11/60 mini-computer and its performance was tested in the real-time mode. Test circuit representing a three phase transmission line was set up in the laboratory for obtaining fault data which was used to test the relay. The relay was also tested by using fault data obtained from the Saskatchewan Power Corporation. The relay software and the test results are briefly presented in this section.

Two approaches can be used in implementing a polyphase relay. The first approach consists of continuously calculating system voltages and currents to determine whether the system is experiencing a fault or not. This approach requires fewer computations for each decision made by the relay but the total computations would be very large because the compensated voltages would have to be calculated on a continuous basis. The second approach which has been implemented in this project, is to include a fault detector in the polyphase relay. The fault detector would supervise the system and initiate the relay algorithm only if there is a fair chance that the system is in an abnormal operating state. Many fault detection approaches have been reported in the literature[3,6,25,32]. The criterion used in this

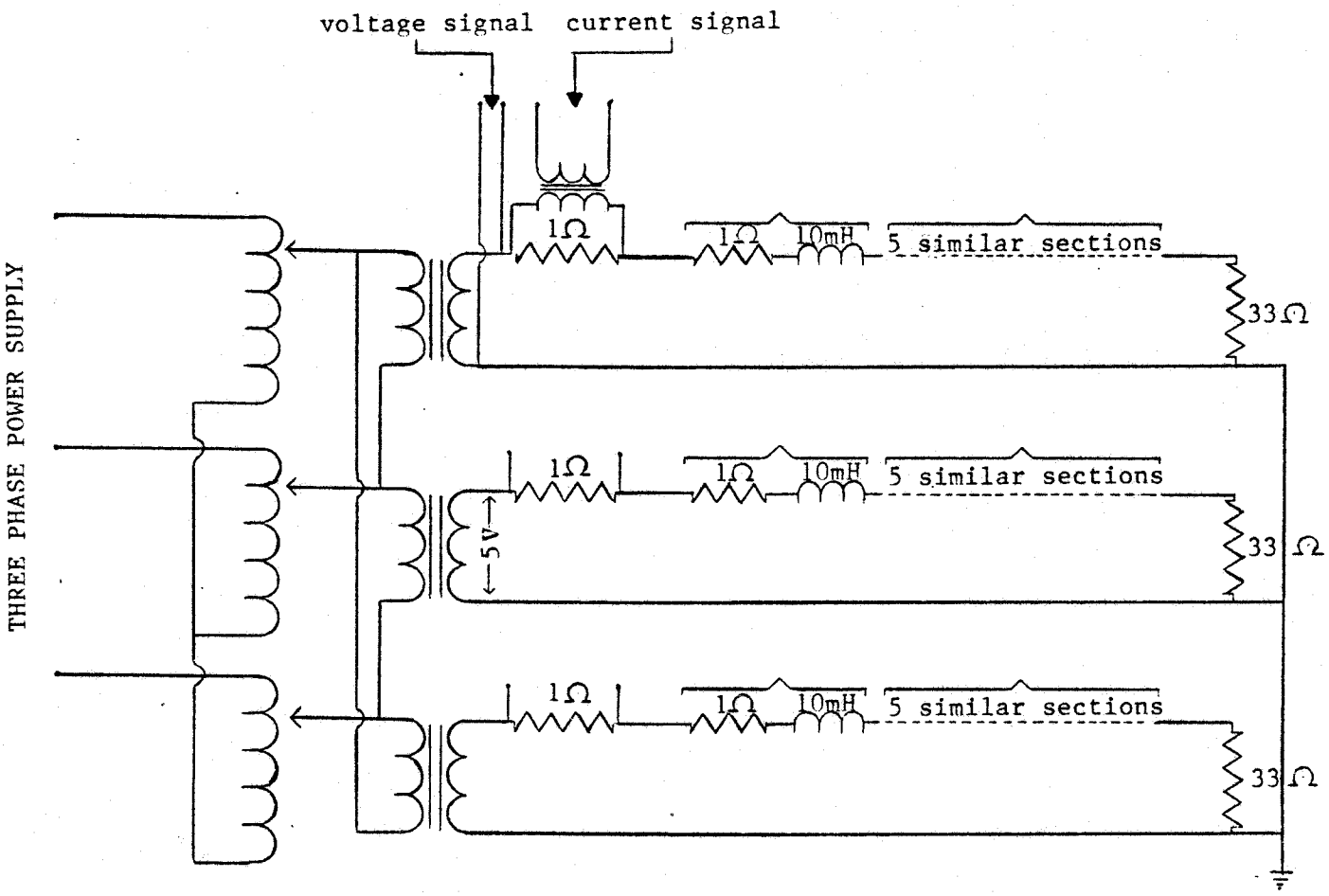

Figure 6.12 The circuit used to supply data to test the polyphase distance relay

project consists of comparing the magnitudes of the line currents with specified threshold values. If the magnitudes of the line currents are less than the threshold, the relay logic is not implemented. The program remains in the fault detection mode in which a few computations are required.

6.3.1 The relay logic

The relay logic consists of subroutines which perform specific tasks such as fault detection, digital filtering, fault analysis and trip routine. The developed software is described in the flowchart given in Figure 6.13. Details of different segments of the software are described in the flowcharts given in Figures 6.14 to 6.22. Major segments of the logic are briefly outlined in this section.

6.3.1.1 Initialization and interrupt routines

The logic starts with the initialization of data buffers, specifying the total number of buffers, number of channels, the starting channel and the data sampling rate. Maximum value of load current (maximum threshold) and a permissible maximum change of current are specified. The change of current is defined as the difference between the values of the recent current samples and the samples taken one cycle earlier. A program counter and a zone indicator are initialized to zero.

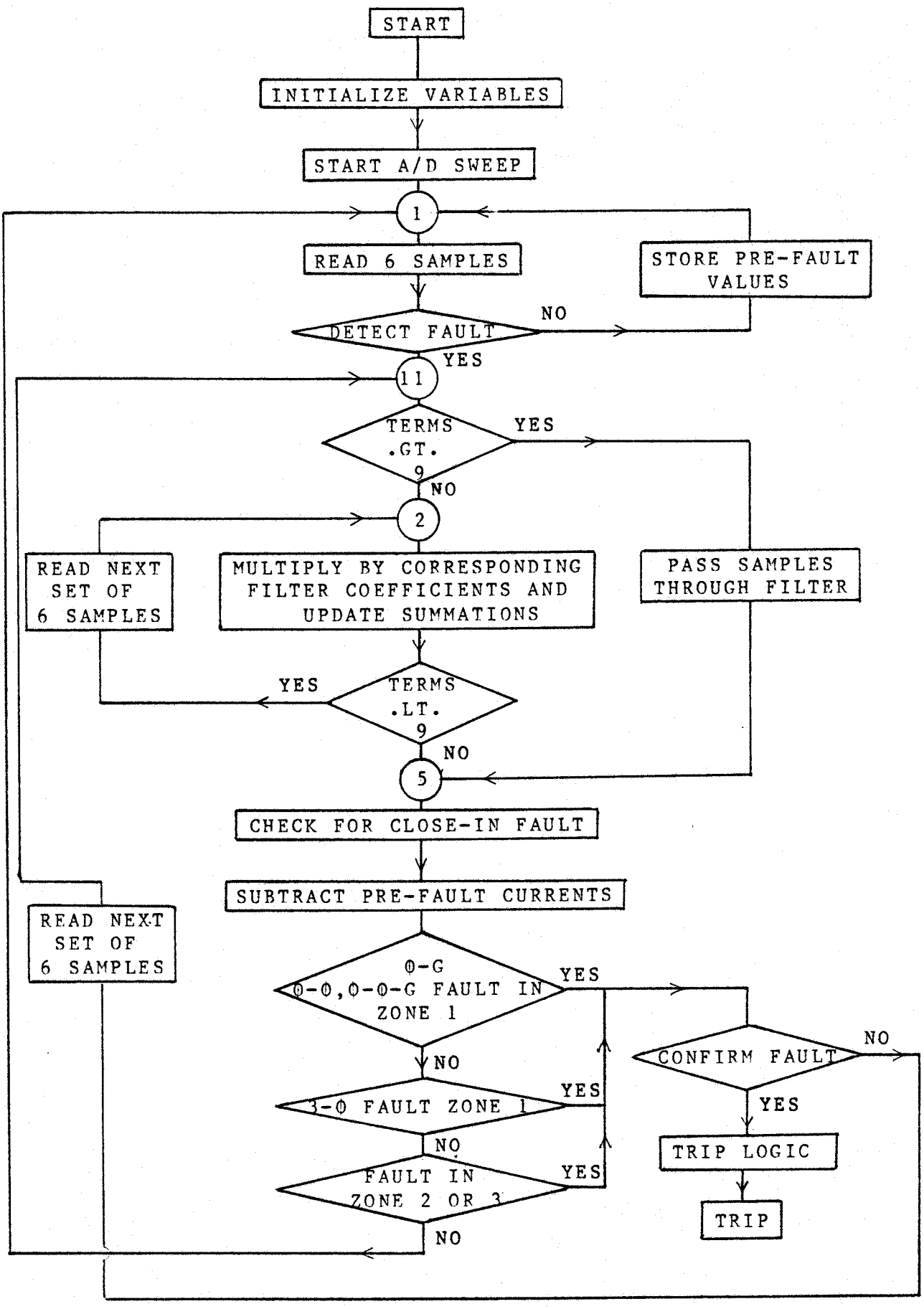

Figure 6.13 Flowchart showing implementation of a Polyphase Digital Relay on a Digital Computer

After the buffers are released and the clock is set, A/D sweep is initiated. Six channels are sampled at 720 Hz; three channels for voltages and three channels for line currents. The acquired data is placed in eight data buffers which are arranged in the form of a ring to enable continuous sampling. Everytime six A/D channels are read, the digitized values of the signals are stored in six circular data arrays. The data buffers are then emptied releasing them to be filled again. In the mean time A/D conversion continues filling the empty buffers.

6.3.1.2 Fault detection routine

After a set of data has been read and stored in the data arrays, the program enters the fault detection routine. The sampled values of the currents and their change from the values observed one cycle earlier are checked. If either value exceeds the threshold, the relay logic is activated otherwise the prefault voltages and currents are stored for future use and the program waits for the next set of data samples to arrive.

6.3.1.3 Storing pre-fault voltages and currents

If neither of the threshold limits specified in subsection 6.3.1.2 is exceeded, the real and imaginary components of the voltages are stored in one cycle long arrays. The recent sample of each variable is considered to be the real component whereas the sample taken one quarter cycle earlier is considered to be the imaginary component. The sampled values of the components of current phasors are multiplied by the impedance representing the first zone of the relay; the resulting phasor components are also stored in one cycle long arrays. The prefault voltages are used for memory action and the prefault IZ_r products are later subtracted from the post-fault IZ_r products.

6.3.1.4 Digital filtering

When the fault detection routine indicates an abnormal operating condition, the fault analysis logic is initiated. The fault voltages and currents contain high frequency and decaying d.c. components. The sampled data is, therefore, processed by digital filters. The 6X9 least error squares digital filters have been used for this purpose. The sampled values of the voltages are multiplied by the first terms of the orthogonal digital filters and stored in separate arrays. The sampled values of the three line currents are also multiplied by the first terms of the

digital filters which provide the IZ_r outputs. (The coefficients of the 6X9 least error squares filters are given in Appendix C and the technique for modifying the filter coefficients is given in Appendix E). After processing the first set of samples, the relay logic waits for the second set of samples to arrive. On receiving the second set of samples, the sampled values are multiplied by the second terms of the orthogonal filters. The products are added to the previous products of the sampled values and digital filter coefficients. The summations are stored in circular arrays. The process continues until processing of nine sets of samples is completed. At this stage the first set of the real and imaginary components of the voltages and IZ_r phasors are available.

When the next set of samples is received, the second estimate of the real and imaginary components of the voltages and IZ_r phasors are calculated. Recent set of samples and the past eight sets of samples are multiplied sequentially with the nine terms of the orthogonal filters. The procedure is repeated every time a new set of samples becomes available. In this manner the data window is advanced one intersampling interval at a time.

6.3.1.5 Load currents

In many cases load currents are comparable to fault currents. It is, therefore, desirable to compensate for the prefault load currents. The stored compensated prefault currents are subtracted from the compensated post-fault currents in this subroutine.

6.3.1.6 Close-in faults

The voltages of the three phases are compared with a threshold value. If one or more voltages are less than the threshold value, the voltages observed one quarter cycle earlier are checked. In case, both the recently observed and one quarter cycle earlier observed voltages are less than the threshold, it is concluded that the fault is close to the relay. Pre-fault voltages are then used to determine the directionality of the fault location.

6.3.1.7 Overall relay logic

The relay software executes the following logic for determining the type and location of a fault:

(i) Program counter and zone indicator are initialized; the program then proceeds to step (ii).

The program counter keeps track of the number of times the fault analysis logic is executed. Similarly, the zone indicator keeps track of the relay zone in which the fault is detected to be. The zone indicator is set to one if a fault is in the first zone of the relay. The indicator is set to two for second zone faults, three for third zone faults and four for faults outside the three zones of protection.

(ii) Digitized values of the voltages and currents are obtained.

(iii) Fault detection routine detects if a fault is being experienced. If yes, the program advances to step (iv); otherwise records the sampled values and reverts to step (ii).

(iv) The voltage and current samples are processed by the digital filters; real and imaginary components of the voltage and current phasors are now available.

(v) The logic checks if the fault is a close-in fault; if yes, prefault voltages are retrieved for generating memory action.

(vi) Pre-fault currents are subtracted from the

post-fault currents.

(vii) The program checks if a single phase to ground, a phase to phase or a two phases to ground fault exists in the first zone of the relay or not. If yes, the zone indicator is set to one and the program proceeds to step (xiii); otherwise it continues to step (viii).

(viii) The program checks if a three phase fault exists in the first zone or not. If yes, the zone indicator is set to one and the program proceeds to step (xiii); otherwise it continues to step (ix).

(ix) The program checks if a single phase to ground, phase to phase and two phases to ground fault exists in the second zone of the relay or not. If yes, the zone indicator is set to two and the program proceeds to step (xiv); otherwise it continues to step (x).

(x) The program checks if a three phase fault exists in the second zone of the relay or not. If yes, the zone indicator is set to two and the program proceeds to step (xiv); otherwise it continues to step (xi).

(xi) The program checks if a single phase to ground, phase to phase or two phases to ground fault exists

in the third zone of the relay or not. If yes, the the zone indicator is set to three and the program proceeds to step (xv); otherwise it continues to step (xii).

(xii) The program checks if a three phase fault exists in the third zone of the relay or not. If yes, the zone indicator is set to three and the program proceeds to step (xv); otherwise the zone indicator is set to four and the program proceeds to step (xvi).

(xiii) If the value of the program counter is equal to or more than three, the program proceeds to step (xviii); otherwise it proceeds to step (xvii).

(xiv) If the value of the program counter is equal to or more than 215, the program proceeds to step (xviii); otherwise it proceeds to step (xvii).

(xv) If the value of the program counter is equal to or more than 300, the program proceeds to step (xviii); otherwise it proceeds to step (xvii).

(xvi) If the value of the program counter is equal to or more than 300, the program reverts to step (ii); otherwise it continues to step (xvii).

(xvii) The value of the program counter is incremented and the program waits for the next set of samples to arrive. As soon as the next set of samples arrives, the program goes to step (iv).

(xviii) The program proceeds to the trip routine.

Steps (ii) to (vi) are executed by subroutines which have been described earlier in this section. Steps (vii) to (xvii) form the distance analysis and time delay logic subroutine. The last step, step (xviii) is executed by the trip routine which is described in the next subsection.

6.3.1.8 The trip routine

Once a fault is confirmed to be in a protected zone of the relay, a trip signal is generated. This signal would, in a power system, open the line breaker/breakers. In this application, the program execution is terminated at the generation of a trip signal. The date, the time of day, the value of the program counter and the zone indicator are then printed.

6.3.2 Real time implementation on PDP 11/60

The relay logic described in Section 6.3.1 was programmed on the PDP 11/60 mini-computer which is available

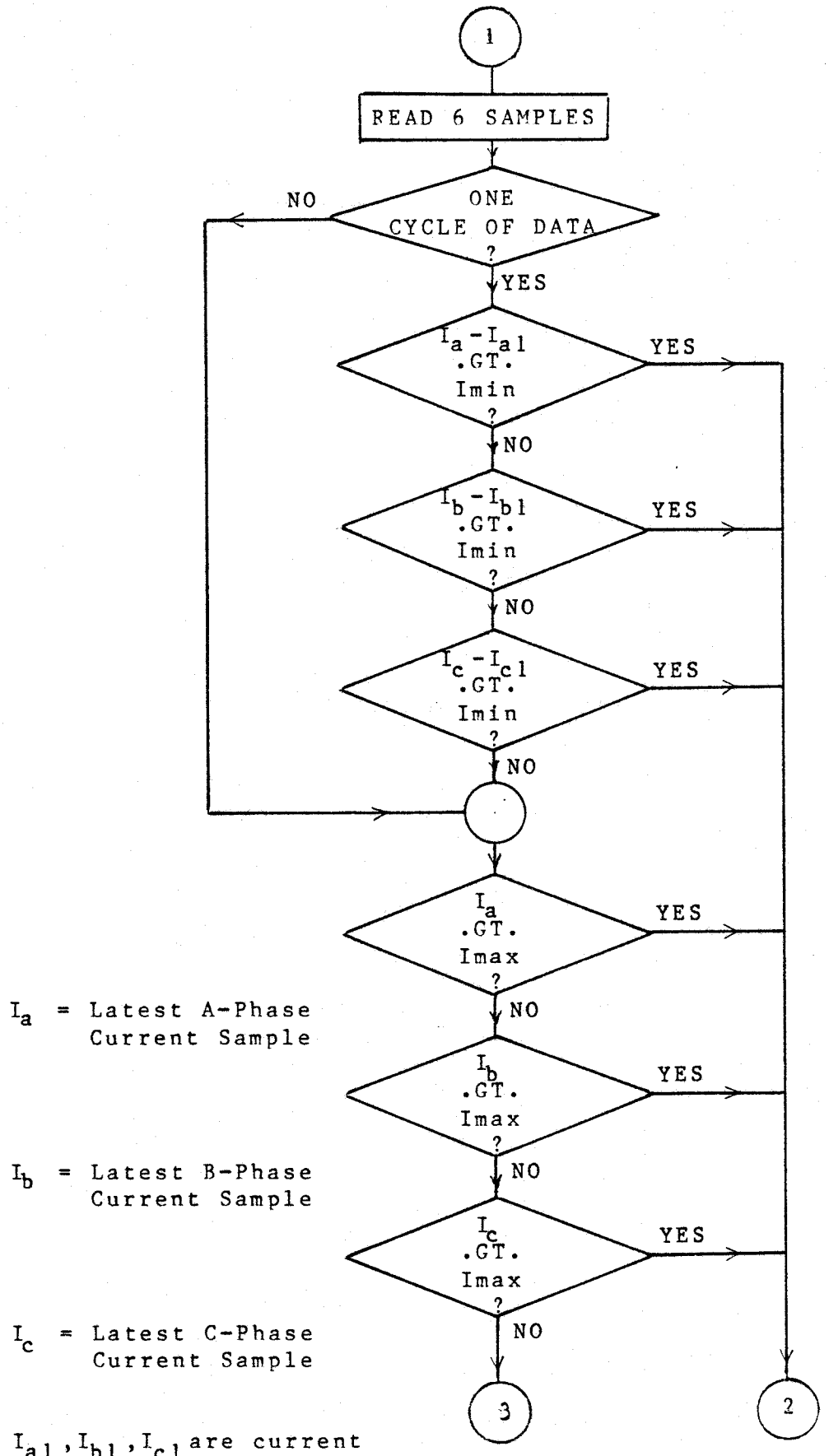

Figure 6.14 The Flowchart used to detect fault

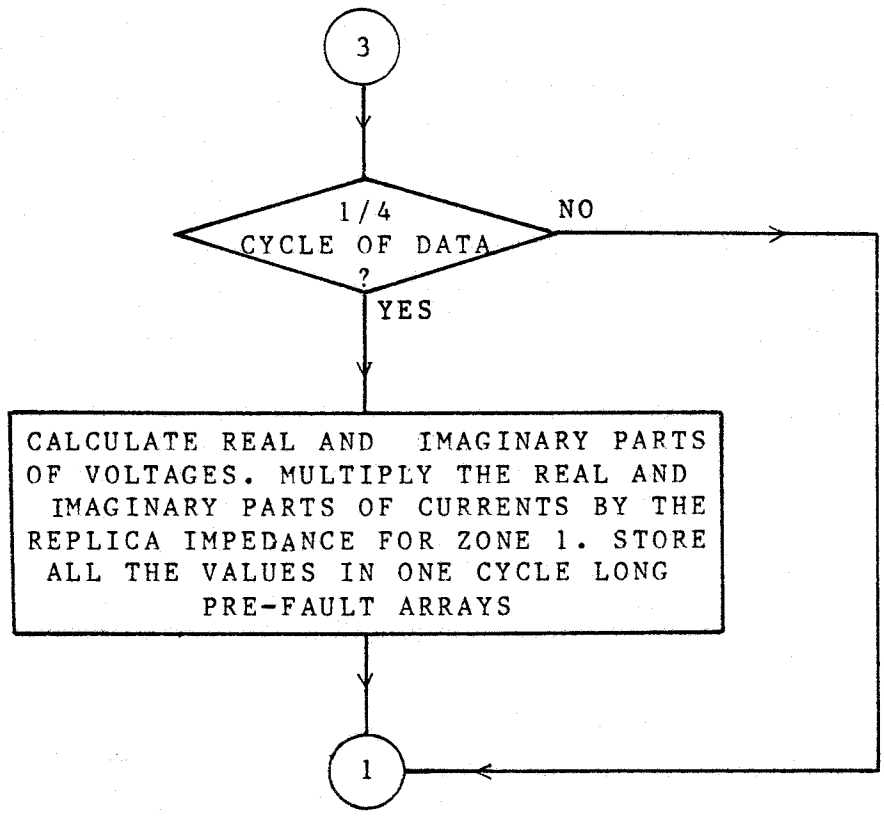

Figure 6.15 The Flowchart used to store pre-fault Voltages and Currents

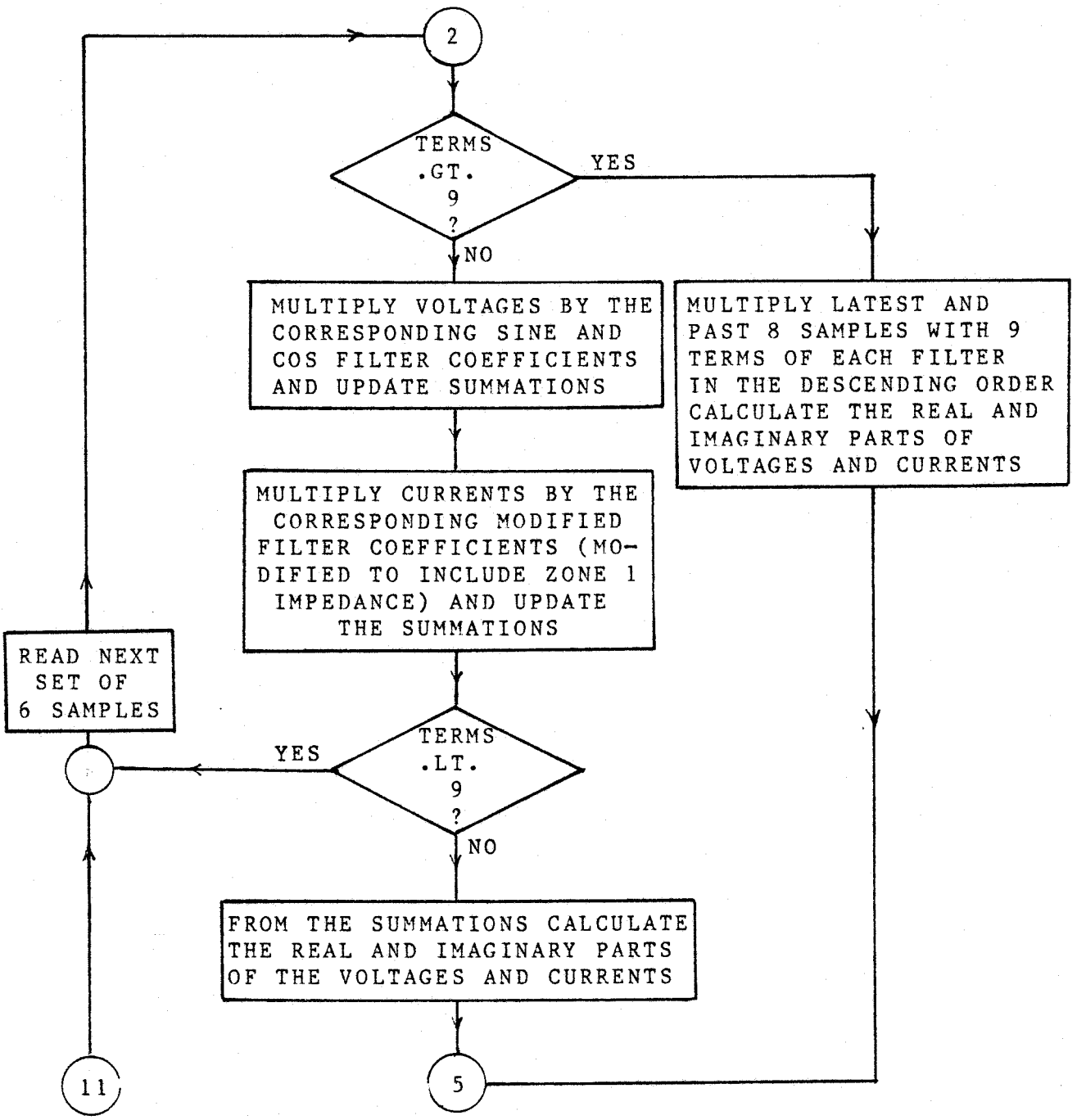

Figure 6.16 The flowchart used to filter the fault voltages and currents

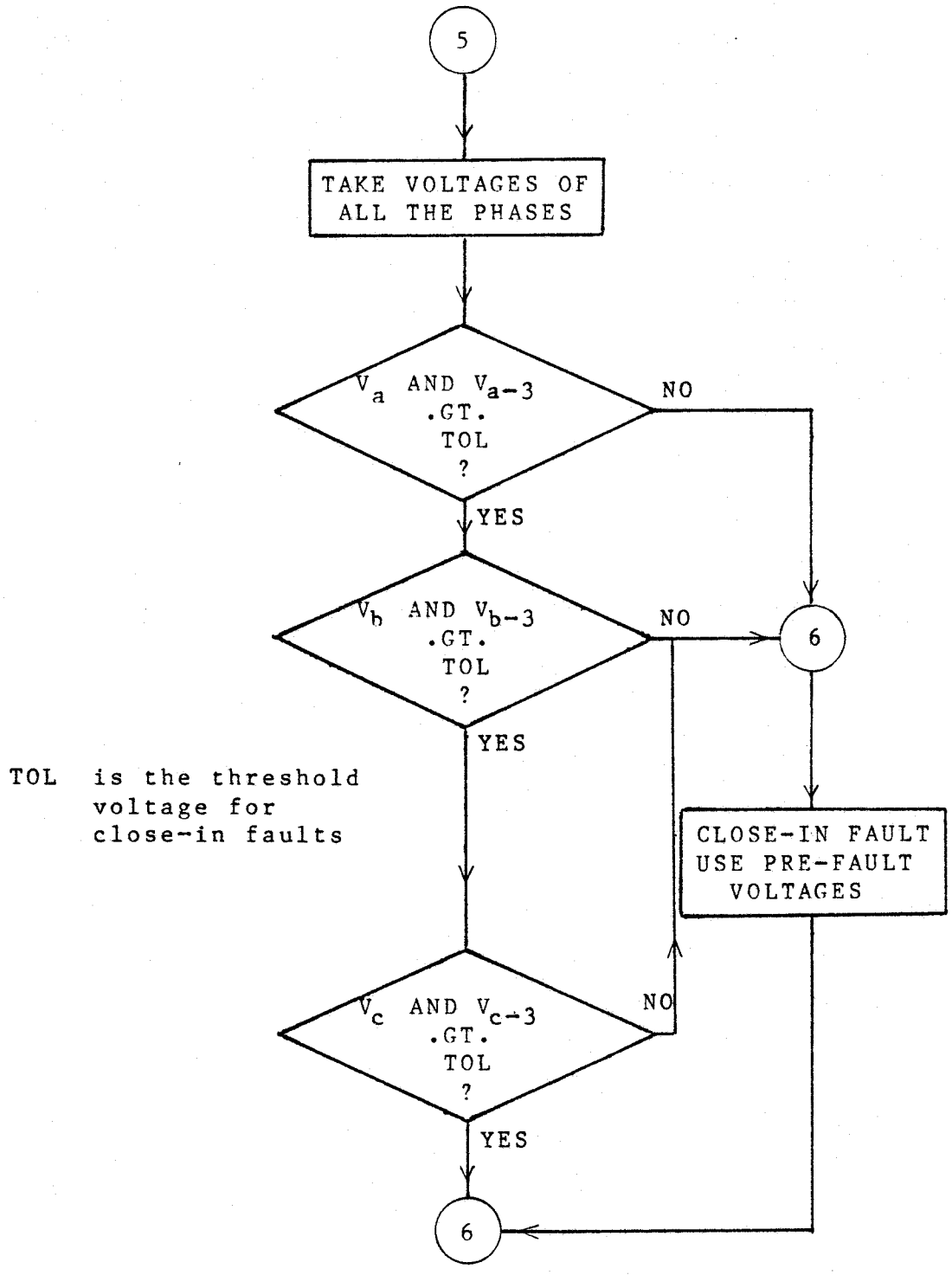

Figure 6.17 Flowchart used to determine whether the fault is close to the relay location

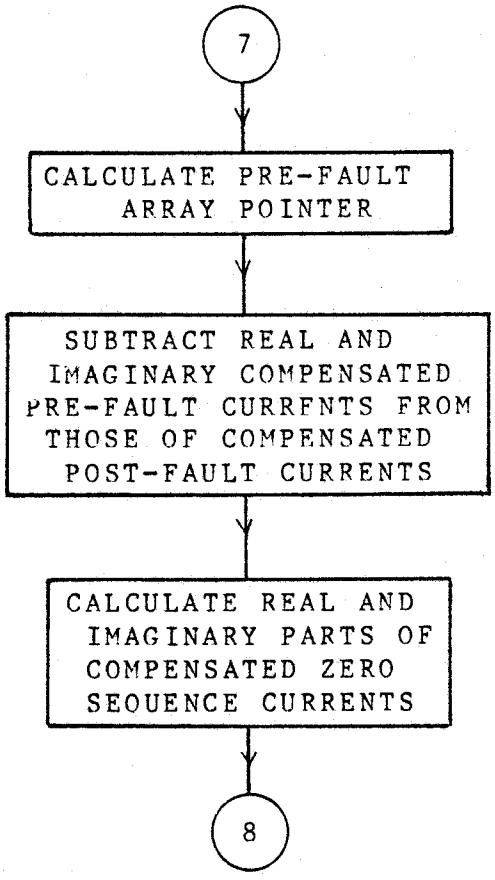

Figure 6.18 Flowchart used to subtract pre-fault currents from post-fault currents and calculate the zero sequence currents

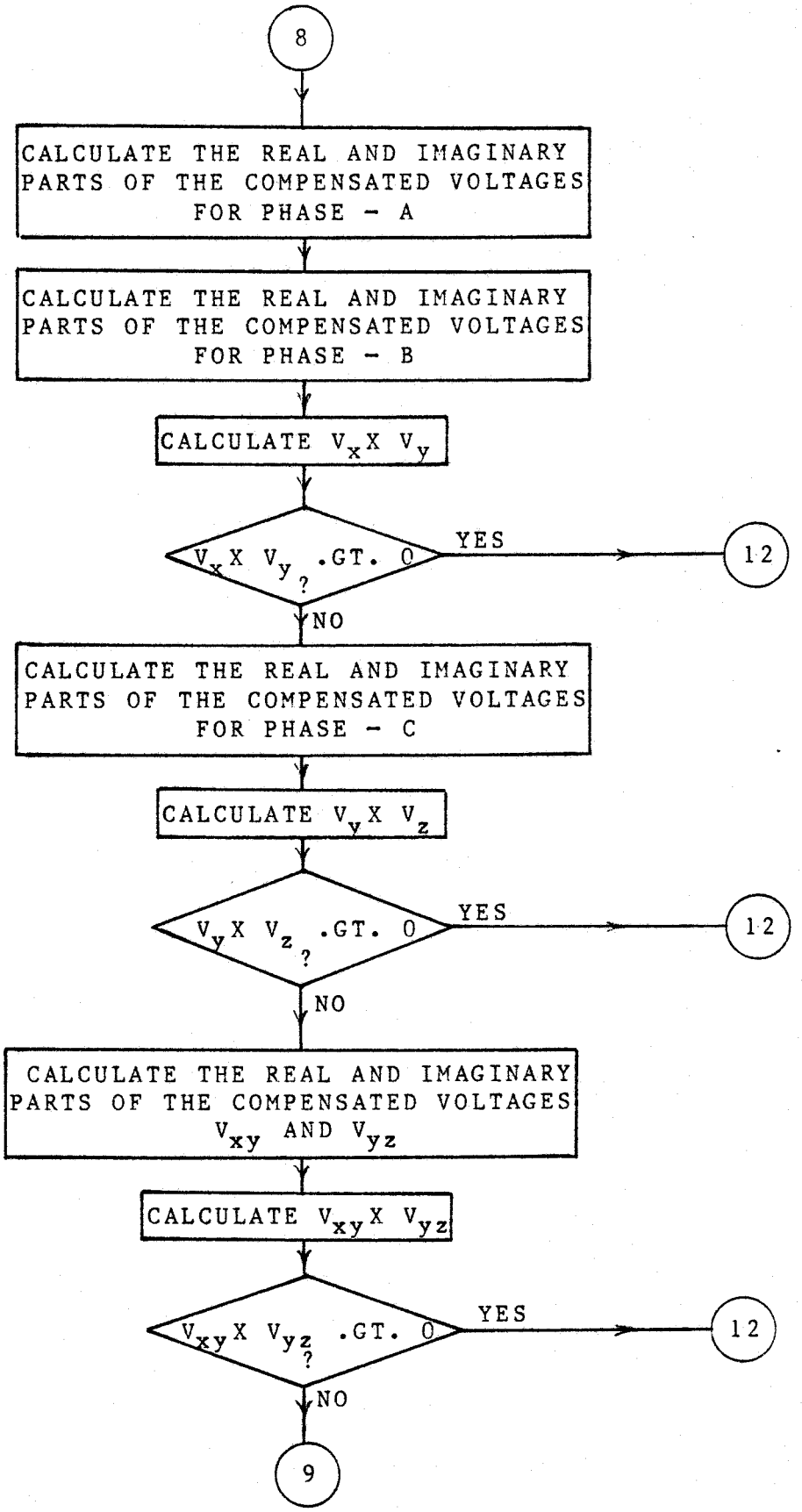

Figure 6.19 The flowchart used to implement the polyphase relay logic for the first zone of protection

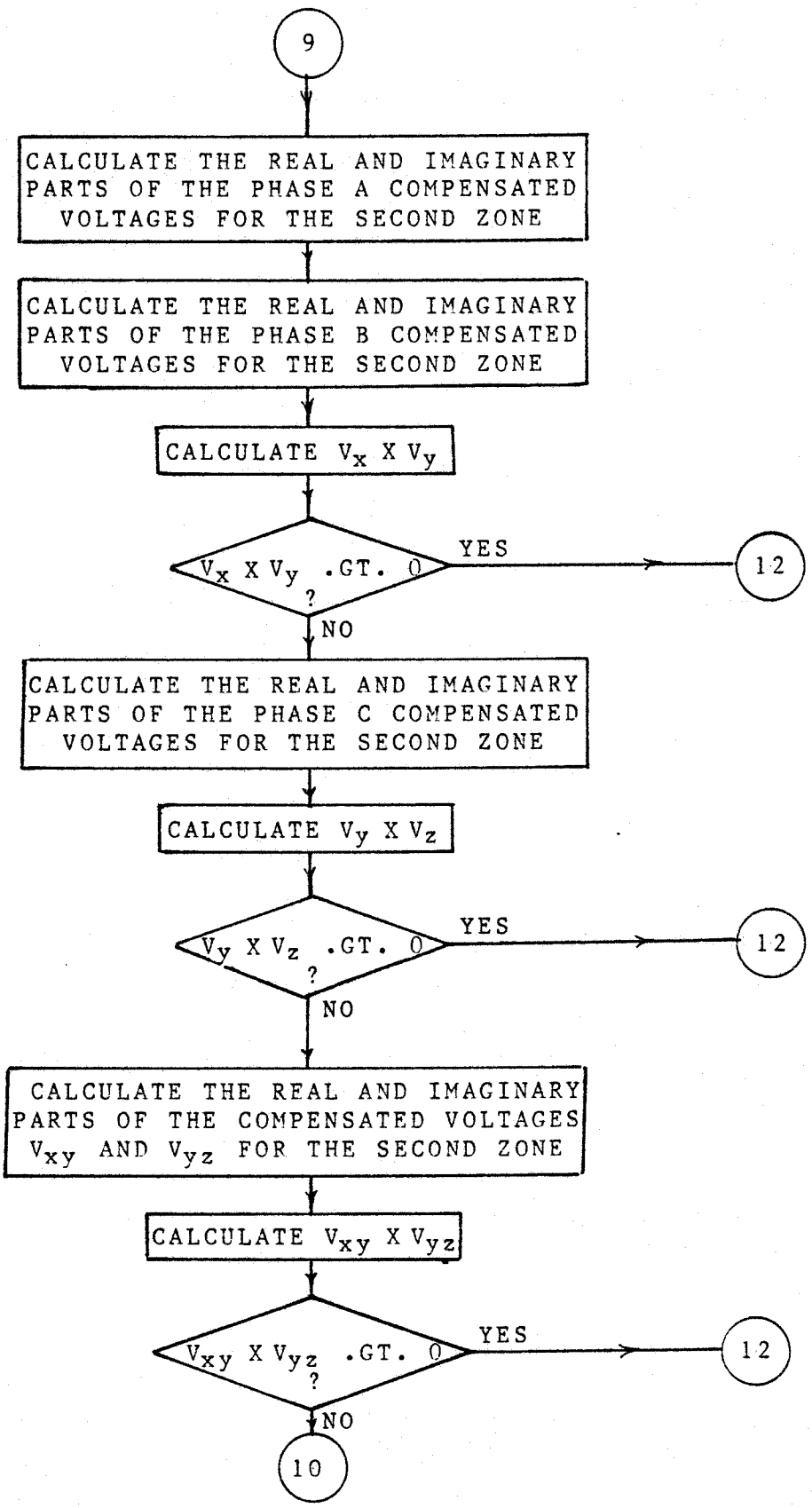

Figure 6.20 The flowchart used to implement the polyphase relay logic for the second zone of protection

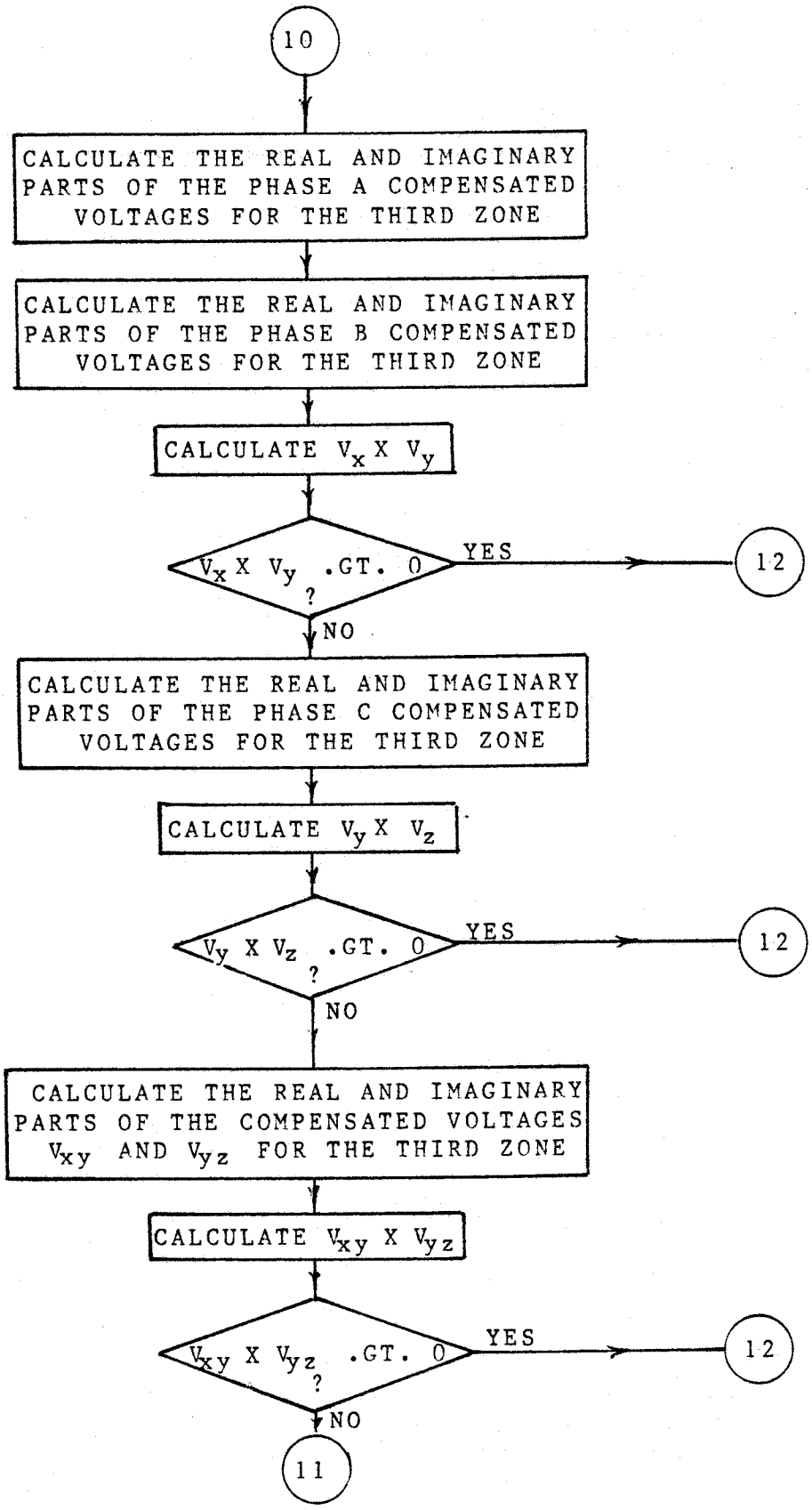

Figure 6.21 The flowchart used to implement the polyphase relay logic for the third zone of protection

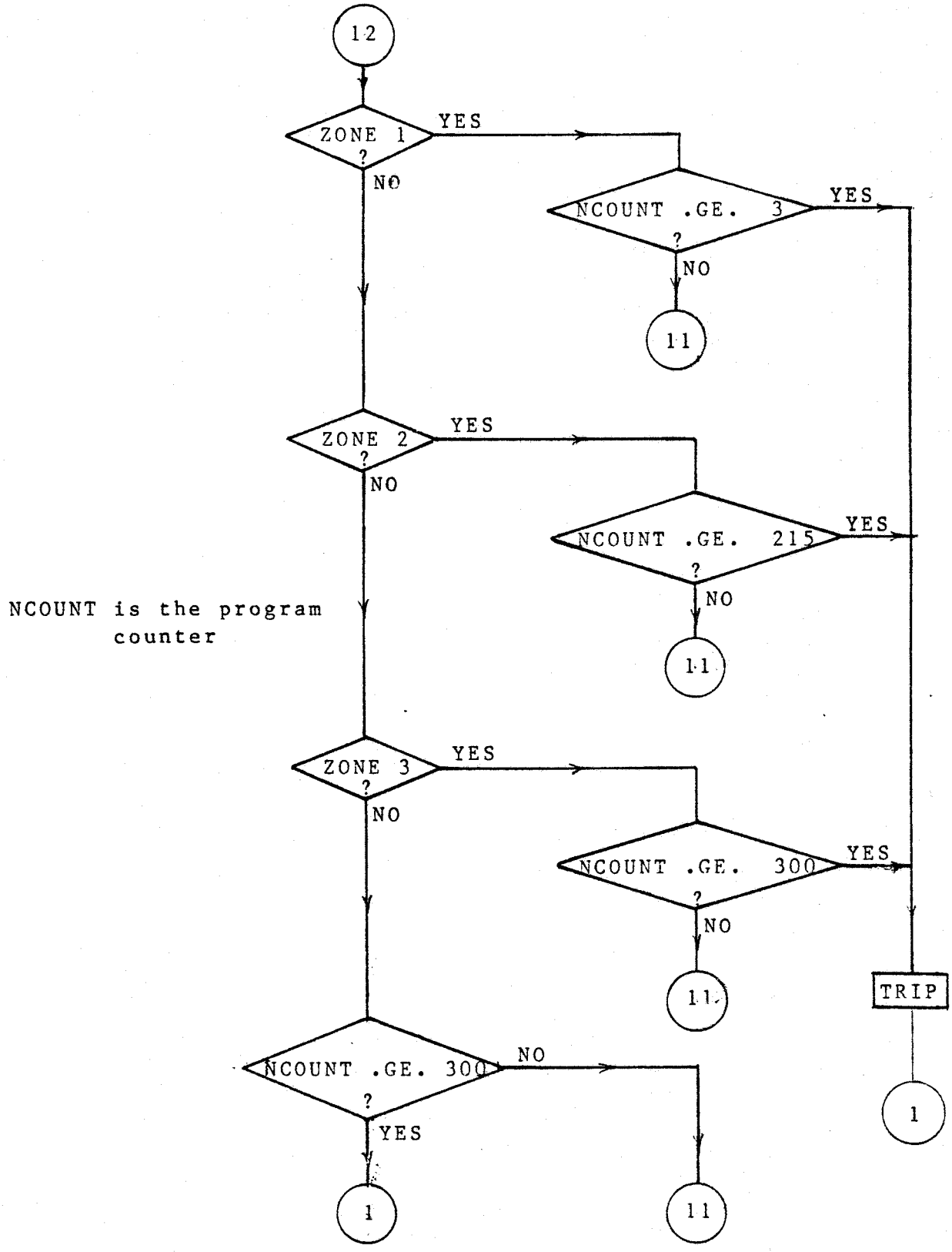

Figure 6.22 The flowchart used to implement the trip logic

in the Department of Electrical Engineering of the University of Saskatchewan, Saskatoon, Canada. The circuit shown in Figure 6.12 was set up. Faults were created at different locations of the simulated transmission line by shorting a line to ground, two lines or all the three lines. Data obtained from each test was processed by the relay software. The digital polyphase relay operated for all single phase to ground, phase to phase, two phases to ground and three phase faults. Some of the test results are listed in Tables 6.4 through 6.11 and are discussed in this section.

Table 6.4 lists the three compensated voltages recorded during a phase A to ground fault. The cross products of the compensated voltages (V_x X V_y; V_y X V_z and V_z X V_x) are also given. A study of this table reveals that the cross products V_x X V_y and V_z X V_x are positive during the fault. This indicates that the phasor V_y leads the phasor V_x which in turn leads the phasor V_z. The software logic, therefore, indicates that the relay is required to operate. The cross products of V_y and V_z are negative which reaffirms the theoretical analysis presented in Section 6.2. Single phase to ground faults were also applied to phases B and C. As in the case of phase A to ground faults, the relay operated during the phase B to ground and phase C to ground faults.

Compensated voltages and their cross products for two phase, two phases to ground and three phase faults are listed in the following tables.

Table 6.5: phase A to phase B fault

Table 6.6: phases C and A to ground fault

Table 6.7: three phase fault

All these faults were in the zone protected by the relay and the results reported in the tables indicate that the relay generated trip decisions correctly.

The relay was also tested with fault data recorded at the Regina South Switching Station of the Saskatchewan Power Corporation. The fault data is presently stored on a magtape, PLDATA. Compensated voltages and their cross products were calculated by the relay software using data from four faults. Table 6.8 lists the compensated voltages and their cross products calculated using the fault data stored in file AP1067A.DAT, line one. Similarly Table 6.9 lists the compensated voltages and their cross products calculated using fault data stored in file AP1093A.DAT, line two. These faults are in the protected zones of the relay which generated the trip command correctly. Data from other two faults was also used to test the software. File AP1067A.DAT, line two, contains voltages and currents during a fault on the bus side of the relay. The four sets of

Table 6.4 Compensated voltages and their cross products at the relay location for a phase A to ground fault - data obtained from the test circuit

SAMPLE NO.	COMPENSATED VOLTAGES						CROSS PRODUCTS		
	V_x		V_y		V_z				
	REAL	IMAG.	REAL	IMAG.	REAL	IMAG.	$V_x \times V_y$	$V_y \times V_z$	$V_z \times V_x$
9	1719	-1469	1979	-1528	856	-1901	28097	-245575	201189
10	2204	-331	2465	-174	1680	-1132	43412	-249817	193835
11	2086	912	2261	1196	2037	-55	43264	-256362	197584
12	1438	1871	1490	2239	1884	1025	43078	-269124	205256
13	430	2349	333	2695	1234	1827	37476	-271761	211509
14	-704	2199	-919	2416	249	2156	32141	-258523	206667
15	-1669	1468	-1943	1522	-822	1906	31309	-245319	197515
16	-2188	348	-2451	193	-1675	1142	43236	-247682	191511
17	-2165	-888	-2322	-1174	-2097	75	47888	-263911	202822
18	-1508	-1877	-1547	-2250	-1936	-1024	48870	-277366	209137
19	-410	-2398	-316	-2732	-1223	-1864	36142	-275385	217002

Table 6.5 Compensated voltages and their cross products at the relay location for a phase A to phase B fault - data obtained from the test circuit

SAMPLE NO.	COMPENSATED VOLTAGES						CROSS PRODUCTS		
	V_x		V_y		V_z				
	REAL	IMAG.	REAL	IMAG.	REAL	IMAG.	$V_x \times V_y$	$V_y \times V_z$	$V_z \times V_x$
9	3988	-9783	-779	-11029	897	-8230	516116	163183	240406
10	7266	-5336	3448	-8277	3899	-5557	417533	131143	195798
11	8871	280	6906	-3522	6037	-1584	331827	103241	157458
12	7899	6040	8392	2417	6429	2994	315953	95835	151846
13	4944	10164	7701	7769	5175	6796	398675	121286	190066
14	749	11437	4983	10851	2584	8644	488701	150387	230795
15	-3922	9708	770	11006	-879	8198	506477	159889	236234
16	-7271	5346	-3494	8291	-3929	5571	416020	131071	195283
17	-8904	-269	-6930	3500	-6067	1578	330367	102955	156962
18	-7941	-6051	-8410	-2449	-6449	-3016	314464	956899	150805

*

The cross products in Table 6.4 and the compensated voltages in Table 6.5 have been divided by 10 and the cross products in Table 6.5 have been divided by 10000.

Table 6.6 Compensated voltages and their cross products at the relay location for a phase C to phase A to ground fault - data obtained from the test circuit

SAMPLE NO.	COMPENSATED VOLTAGES						CROSS PRODUCTS		
	V_x		V_y		V_z				
	REAL	IMAG.	REAL	IMAG.	REAL	IMAG.	$V_x \times V_y$	$V_y \times V_z$	$V_z \times V_x$
9	7781	-1414	5849	40	5542	4162	859188	2411797	-4022681
10	7286	3117	4833	3631	2604	6813	1138904	2348003	-4153041
11	4736	6791	2427	6212	-1137	7649	1295965	2563770	-4395910
12	996	8610	-564	7128	-4505	6402	1195926	2850591	-4517300
13	-2988	8092	-3408	6111	-6680	3446	932303	2907841	-4376351
14	-6106	5407	-5260	3435	-6947	-472	746811	2635621	-4045714
15	-7701	1345	-5796	-81	-5527	-4168	842718	2371348	-3954244
16	-7166	-3129	-4741	-3649	-2548	-6800	1131371	2294389	-4076005
17	-4751	-6756	-2424	-6206	1135	-7645	1310863	2558468	-4400423
18	-1164	-8522	422	-7070	4393	-6346	1200953	2825683	-4484004

Table 6.7 Compensated voltages and their vector products at the relay location for a three phase fault - data obtained from the test circuit

SAMPLE NO.	COMPENSATED VOLTAGES						CROSS PRODUCTS
	V_x		V_y		V_z		
	REAL	IMAG.	REAL	IMAG.	REAL	IMAG.	$V_{xy} \times V_{yz}$
9	-387	-1763	-11628	-9223	5294	-364	112673
10	4212	-15298	-11729	-13538	463	2509	112691
11	7820	-8768	-8826	-14042	-4217	4789	111468
12	9066	187	-3428	-10758	-8068	5881	112354
13	7986	8908	2673	-4710	-9773	5293	110852
14	4718	15169	8089	2425	-8797	3144	111679
15	251	17505	11373	9189	-5603	336	111794
16	-4069	15131	11713	13394	-549	-2655	111049
17	-7547	8665	9105	13868	4468	-4981	112020
18	-8934	-202	3682	10659	8354	-6002	113689

* The cross products in Tables 6.6 and 6.7 have been divided by 10 and 100 respectively.

Table 6.8 Compensated voltages and their cross products at the relay location for a phase C to ground fault - data obtained from the Saskatchewan Power Corporation (file AP1067A.DAT, line one)

SAMPLE NO.	COMPENSATED VOLTAGES						CROSS PRODUCTS		
	V_x		V_y		V_z				
	REAL	IMAG.	REAL	IMAG.	REAL	IMAG.	$V_x \times V_y$	$V_y \times V_z$	$V_z \times V_x$
9	-1238	-2710	-2285	-2091	-2097	-2570	-360583	148754	250282
10	266	-2833	-971	-2765	-548	-3155	-348859	154917	239412
11	1651	-2216	562	-2709	1081	-2890	-322746	130572	237477
12	2588	-1022	1932	-1925	2403	-1880	-300844	99402	241031
13	2873	427	2833	-677	3129	-416	-315850	94210	253360
14	2395	1769	2994	754	3041	1155	-349108	116583	261246
15	1276	2623	2343	1989	2151	2414	-360922	137807	256345
16	-158	2780	1093	2699	715	3037	-346774	139094	246920
17	-1618	2191	-528	2695	-999	2853	-320354	118496	242842
18	-2619	990	-1983	1933	-2432	1892	-309923	94804	254901
19	-2906	-470	-2898	648	-3192	396	-325055	92097	265698
20	-2399	-1806	-3013	-816	-3077	-1201	-348332	110691	267579
21	-1248	-2649	-2307	-2053	-2129	-2470	-355061	132748	255833
22	233	-2783	-1004	-2728	-613	-3073	-343335	141471	242355
23	1623	-2179	546	-2689	1027	-2852	-317521	120391	239239

Table 6.9 Compensated voltages and their cross products at the relay location for a phases A and B to ground fault - data obtained from Saskatchewan Power Corporation (file AP1093A.DAT, line two)

SAMPLE NO.	COMPENSATED VOLTAGES						CROSS PRODUCTS		
	V_x		V_y		V_z				
	REAL	IMAG.	REAL	IMAG.	REAL	IMAG.	$V_x \times V_y$	$V_y \times V_z$	$V_z \times V_x$
9	-619	1180	301	2591	68	1470	-196056	26740	99062
10	-323	-36	134	1359	109	508	-43523	-69717	18662
11	60	-1166	-70	-212	135	-407	-9553	5763	13312
12	415	-1964	-271	-1738	108	-1312	-125557	54432	33242
13	669	-2205	-397	-2667	56	-1746	-266332	84450	104551
14	730	-1825	-428	-2886	-30	-1721	-288965	64879	131307
15	637	-1017	-307	-2389	-70	-1316	-183629	23644	91119
16	331	230	135	-1092	-134	-384	-33075	-95165	9646
17	-28	1301	98	444	-132	561	-14126	11451	-15692
18	-383	2133	309	1959	-96	1427	-141160	63173	34054
19	-659	2439	424	2975	-51	1957	-299733	98345	116591
20	-746	2010	425	3148	17	1897	-32680	75225	145192
21	-632	1087	318	2531	82	1378	-194843	22954	96201

* The cross products in the above tables have been divided by 10

Table 6.10 Compensated voltages and their cross products at the relay location for a phase C to ground fault - data obtained from the Saskatchewan Power Corporation (file AP1067A.DAT, line two)

SAMPLE NO.	COMPENSATED VOLTAGES						CROSS PRODUCTS			
	V_x		V_y		V_z					
	REAL	IMAG.	REAL	IMAG.	REAL	IMAG.	$V_x \times V_y$	$V_y \times V_z$	$V_z \times V_x$	$V_{xy} \times V_{yz}$
9	355	-319	-552	61	175	661	-1547	-3765	-2912	-6255
10	507	-76	-463	-181	-144	695	-1280	-3557	-3418	-6391
11	491	183	-283	-368	-444	550	-1288	-3196	-3519	-6346
12	351	411	-32	-454	-642	252	-1510	-2997	-3551	-6366
13	137	539	250	-428	-648	-112	-1941	-3074	-3347	-6474
14	-117	514	477	-275	-471	-442	-2134	-3141	-2942	-6460
15	-386	360	529	-41	-213	-652	-1744	-3538	-3290	-6523
16	-501	90	482	198	152	-691	-1435	-3637	-3332	-6483
17	-501	195	282	394	452	-530	-1425	-3284	-3550	-6406
18	-367	-422	11	473	635	-232	-1692	-3036	-3540	-6393
19	-126	-532	-256	431	641	122	-1910	-3083	-3258	-6334
20	148	-495	-443	274	500	447	-1788	-3360	-3143	-6260
21	381	-332	-519	51	204	656	-1529	-3514	-3186	-6262
22	500	-68	-475	-171	-144	698	-1182	-3570	-3395	-6235
23	487	197	-295	-362	-456	545	-1186	-3270	-3563	-6237

*

The compensated voltages have been divided by 100 and the cross products have been divided by 100000

Table 6.11 Compensated voltages and their cross products at the relay location for a phase C to ground fault - data obtained from the Saskatchewan Power Corporation (file AP1067A.DAT, line one)

SAMPLE NO.	COMPENSATED VOLTAGES						CROSS PRODUCTS			
	V_x		V_y		V_z					
	REAL	IMAG	REAL	IMAG	REAL	IMAG	$V_x \times V_y$	$V_y \times V_z$	$V_z \times V_x$	$V_{xy} \times V_{yz}$
9	237	-480	-519	88	198	195	-228485	-119260	-141731	-497854
10	446	-292	-495	-183	69	275	-226764	-123509	-143352	-502285
11	537	-41	-337	-397	-78	283	-227357	-126777	-149168	-512353
12	487	225	-93	-508	-206	201	-226547	-123940	-144910	-504406
13	307	448	178	-497	-279	68	-233241	-126605	-146279	-514872
14	43	545	403	-340	-274	-81	-234905	-126275	-146116	-515584
15	-234	492	521	-96	-195	-210	-234265	-128635	-145503	-516617
16	-449	307	497	183	-64	-284	-235542	-129348	-147708	-521091
17	-541	31	337	406	82	-269	-230845	-124558	-143283	-507682
18	-486	-248	89	514	204	-190	-227915	-122300	-143390	-502784
19	-299	-453	-182	490	272	-65	-229715	-121447	-143230	-503224
20	-35	-534	-402	326	267	79	-226743	-119342	-140326	-494641
21	236	-477	-514	89	192	201	-224455	-120911	-139549	-492967
22	443	-293	-490	-178	66	271	-223280	-121036	-139526	-492167
23	532	-34	-334	-394	-78	270	-221353	-121662	-141566	-493299

cross products and the compensated voltages are listed in Table 6.10. This table indicates that operation of the relay is blocked consistantly. File AP1067A.DAT, line one, contains data for a fault beyond the reach of the relay. The compensated voltages and their cross products calculated in this case are listed in Table 6.11. A study of this table reveals that the relay does not generate a trip signal in this case.

6.4 Summary

The development of polyphase distance relays has been outlined in this chapter. A polyphase relay unit comprised of a solid-state relay and a K-DAR three phase relay was found to be less demanding computationally and was, therefore, selected for implementation as a digital relay. Phasor diagrams have been included to illustrate the operation of the relay for various types of in-zone and out of zone faults. A digital version of the relay was developed and the essential details of this development have been reported. Flowcharts have been included to show details of the relay logic. The relay software was tested in both the on-line and off-line modes. The results of these tests have been briefly reproduced. In all the cases the relay operated/blocked correctly.

7. CONCLUSIONS

One of the objectives of this thesis was to design, implement and test a digital processor based generic polyphase distance relay. Before proceeding with the design of the relay, published literature was searched. Previously published literature on digital relaying algorithms and polyphase distance relays was obtained and reviewed. Study of the digital relaying publications showed that the line relaying algorithms proposed in the past use digital non-recursive filters to extract fundamental frequency phasors from sampled voltages and currents. A possible alternative would be to use recursive filters instead of non-recursive filters. Procedures for designing lowpass and bandpass recursive filters were, therefore, examined and are briefly presented in Chapter 3. Coefficients of digital lowpass and bandpass recursive filters for various cut off frequencies and sampling rates were calculated and have been tabulated in that chapter. Also reported are the frequency responses of some of the designed filters and responses of the filters when sinusoidal inputs are suddenly applied. It was observed that the output of a recursive filter builds up slowly after the input is suddenly applied. Because of the slow increase of the output level, the impedances and their phase angles calculated during the first one and a half cycles (at 60 Hz) are not sufficiently accurate. The recursive filters are, therefore, not suitable for

implementing first zone relay elements. These filters are, however, useful when limited computer memory is available and slow relay speeds can be tolerated, such as, second, third or reverse zones of distance relays and overcurrent and directional overcurrent relays.

The studies presented in Chapter 4 demonstrate that impedances calculated from the outputs of the 6X9 least error squares filters are not sufficiently accurate if the power system voltages and currents include fifth and higher harmonics. It is shown in that chapter that the use of lowpass recursive filters can considerably improve the quality of results.

General exponential and single exponential smoothing techniques have been outlined in Chapter 5. It has also been shown that the general exponential technique can be used to process sampled voltages and currents for determining their phasor equivalents. It was observed that the calculated impedances and their phase angles are not sufficiently accurate during the first one and a half cycles after the inception of a fault. This technique is also computationally more expensive than the recursive filters. General exponential smoothing technique cannot be, therefore, used for implementing first zone relay elements. It has also been shown in Chapter 5 that single exponential smoothing is quite suitable for processing the impedances

and their phase angles calculated from voltages and currents processed by bandpass recursive filters. The studies reported in Chapter 5 show considerable stabilization of the impedances computed from voltage and current samples.

The development and design of a generic polyphase digital distance relay has been presented in Chapter 6. Phasor diagrams have been included to illustrate the expected performance of the selected relays during various types of transmission line faults. Flowcharts and brief descriptions of the software routines have been provided to explain the relay logic. The relay was programmed on the PDP 11/60 mini-computer which is available in the Department of Electrical Engineering. A transmission line model was set up and the designed digital relay was used to monitor it in the real time mode. Faults were applied on the line model and the relay response was recorded. The relay was also tested using fault data obtained from the Saskatchewan Power Corporation. In all the tests, the relay operated correctly. Some of the responses of the relay have been outlined and discussed in Chapter 6. It was also observed that the computation time required by the relay is small compared to inter-sampling time of 1.4 milli-seconds when the data is sampled at 720 Hz. It is, therefore, possible to implement a polyphase distance relay on a digital processor whose operating speed is similar to the speed of the PDP 11/60.

In conclusion, the studies presented in this thesis demonstrate that a software based digital polyphase distance relay can be designed and implemented. Digital recursive filters can be used to stabilize the impedances calculated by digital distance relays.

8. REFERENCES

1 Ackroyd, M.H., "Digital Filters", Computers in Medicine Series, London, Butterworths, [1973].

2 Atabekov, G.I., "The Relay Protection of High Voltage Networks", Pergamon Press, London, [1960].

3 Baribeau, M.A., "The Design of a Digital Impedance Relay", An Msc. Engg. Thesis, Deptt. of Elect. Engg. (U of S) Saskatoon, Canada, Sept., [1978].

4 Bhattacharya, D., Basu, S.K., Bose, K.P., Patra, S.P., "A Static Polyphase Distance Relay", IEEE Transactions PAS, 1972, pp. 1183-1191.

5 Bogner, R.E., Constantinides, A.G., "Introduction to Digital Filtering", A Wiley Interscience Publication, London, New York, [1975].

6 Breingan, W.D., Chen, M.M., Gallen, T.F., "Laboratory Investigation of a Digital System for the Protection of Transmission Lines", IEEE Transactions on Power Apparatus and Systems, Vol. PAS-98, No. 2, March/April 1979, pp. 394-368.

7 Brown, R.G., "Smoothing, Forcasting and Prediction of Discrete Time series", Englewood Cliffs, N.J., Prentice Hall, [1963].

8 Carr, J., Jackson, R.V., "Frequency Domain Analysis Applied to Digital Transmission Line Protection", IEEE Transactions on Power Apparatus and Systems, Vol. 94, No. 4, July/August 1975, pp. 1157-1166.

9 Choudhuri, S., Basu, S.K., Patra, S.P., "Polyphase Ground Distance Relaying by Phase Coincidence Principle", IEEE Transactions, PAS, 1973, pp. 626-634.

10 Cook, V., "Generalized Method of Assessing Polarizing Signals for the Polarized Mho Relay", Proc. IEE, Vol. 122, No. 5, May 1972, pp. 497-500.

11 Gallen, T.F., Breingan, W.D., Chen, M.M., "A Digital System for Directional Comparison Relaying", IEEE PES Summer Power Meeting, Los Angeles, Paper No. F 78 669-4, July 1978 pp. 1-8.

12 Gibert, J.G., Shovlin, R.J., "High Speed Transmission Line Fault Impedance Calculation Using a Dedicated Computer", IEEE Transactions on PAS, Vol. 94, No. 3, May/June 1975, pp. 872-883.

13 Gilbert, J.G., Udren, E.A., Sackin, M., "Evaluation of Algorithms for Computer Relaying", IEEE PES Summer Power Meeting, Mexico City, July 1977, Paper No. A 77 520-0, pp. 1-8.

14 Gilchrist, G.B., Rockefeller, G.D., Udren, E.A., "High Speed Distance Relaying Using a Digital Computer", IEEE Transactions on Power Apparatus and Systems, PAS-91 Vol. 3, May/June 1972, pp. 1235-1243.

15 Hamming, R., "Digital Filters", Englewood Cliffs, N.J., Prentice Hall [1977].

16 Hans Hoel, Humpage, W.D., "Composite Polar Charateristics in Multizone Systems of Phase Comparison", Proc. IEE, Vol. 113, No. 10, Oct. 1966, pp. 1631-1642.

17 Hope, G.S., Malik, O.P., Rasmy, M.E., "Digital Transmission Line Protection in Real time", Proc. IEE, Vol. 123, No. 12, Dec. 1976, pp. 1349-1354.

18 Horton, J.W., "The use of Walsh Functions for High Speed Digital Relaying", IEEE Publication No. 75CH1034-8 PWR, Paper No. A 75 582-7, IEEE PES Summer Meeting, San Francisco, July 1975, pp. 1-9.

19 Ingole, V.T., Sant, M.T., Paithankar, Y.G., "New Technique for Quadrilateral Distance Relay", Proc. IEE, 126(6), June 1974, pp. 464-473.

20 Jones, A.T., "Setting Response of Generalised Comparators for Distance Protection", Proc. IEE, Vol. 122, No. 5, May 1975, pp. 505-506.

21 Luckett, R.G., Munday, P.G., Murray, B.E., "A Substation Based Computer for Control and Protection", IEE Conference Publication No. 125, London, March 1975, pp. 252-260.

22 Lynn, P., "An Introduction to the Analysis and Processing of Signals", New York Wiley [1973].

23 Makino, J., Miki, Y., "Study of Operating Principles of Digital Filters for Protective Relays with Digital Computer", Paper No. C 75 1979, IEEE Winter Power Meeting, New York, January/February 1975.

24 Mann, B.J. and Morrison, I.F., "Digital Calculation of Impedance for Transmission Line Protection", IEEE Transactions on Power Apparatus and Systems, PAS-90 Vol. 1, January 1971, pp. 270-278.

25 McInnes, A.D., Morrison, I.F., "Real Time Calculation of Resistance and Reactance for Transmission Line Protection by Digital Computer", EE Transactions, Institute of Engineers, Australia, Vol. EE 7, No. 1, 1970, pp. 16-23.

26 Mclaren, P.G., "Static Sampling Distance Relays", Proc. IEE, Vol. 115, No. 3, March 1968, pp. 418-423.

27 Mclaren, P.G., Redfern, M.A., "Hybrid Phase Comparator Applied to Distance Protection", Proc. IEE, Vol. 122, No. 11, Nov. 1975, pp. 1295-1300.

28 Paithankar, Y.G., Deshpande, M.U., "New Technique for Comprehensive Analysis of Polyphase Relays", Proc. IEE, 1972, 119(8), pp. 1199-1200.

29 Paithankar, Y.G., Deshpande, M.U., "Polyphase Distance Relay", Proc. IEE, Vol. 120, No. 9, September 1973, pp. 1013-1015.

30 Parthasarthy, K., "Three Systsm and Single System Static Distance Relays", Proc. IEE, Vol. 113, No. 4, April 1966, pp. 641-651.

31 Phadke, A.G., Ibrahim, M., Hlibka, T., "A Digital Computer System for EHV Substations: Analysis and Field Tests", IEEE Transactions on PAS, Vol. 95, No. 1, Jan./Feb. 1976, pp. 291-301.

32 Phadke, A.G., Ibrahim, M., Hlibka, T., "Fundamental Basis for Distance Relaying with Symmetrical Components", IEEE Transactions, PAS, Vol. 96(2), 1977, pp. 635-646.

33 Ramamoorty, M., "A Note in Impedance Measurement Using Digital Computers", IEE-IERE Proc. (India), Vol. 9, No. 6 Nov./Dec. 1971, pp. 243-247.

34 Rockefeller, G.D., "Fault Protection with a Digital Computer", Trans. IEEE, Power Apparatus and Systems, Vol. PAS-94, No. 2, March/April 1975, pp. 544-550.

35 Rockefeller, G.D., "Zone Packaged Ground Distance Relay", IEEE Transactions PAS, Vol. 85 No. 10, Oct. 1966, pp. 1021-1044.

36 Sachdev, M.S., Baribeau, M.A., "A New Algorithm for Digital Impedance Relays", Paper No. F 79 248-6, IEEE PES Winter Meeting, February 1979, New York, N.Y., pp. 1-7.

37 Sachdev, M.S., "Protection of Power System Elements Using Programmable Digital Devices", Proceedings of the International Sysmposium on Water Resources Systems, Vol. 1, Section iv, December 1980, pp. vi-8-51 to vi-8-58.

38 Sachdev, M.S. (Coordinator), Breingan, W.D., Baird, T.C., Harbourt, C.O., Phadke, A.G., Russell, B.D., Udren, E.A. and Walker, L.N., "Computer Relaying Tutorial Text", IEEE Power Engineering Society Special Publication No. 79 EH0148-7-PWR, 1979, pp. 1-79.

39 Sonneman, W.K., Lenser, H.W., "Compensator Distance Relaying Principles and Operation", AIEE Transactions, Vol. 77, pt. III, June 1958, pp. 372-382.

40 Temes, G., "Modern Filter Theory and Design", A Wiley - Interscience Publication, New York, Wiley, [1973].

41 Wagner, C.F., Evans, R.D., "Symmetrical Components as Applied to the Analysis of Unbalanced Electrical Circuits", New York, McCraw Hill Book Co., 1933.

42 Walker, L.N., Ogden, A.D., Ott, G.E., Tudor, J.R., "Implementation of High Frequency Transistor Fault Detector", Paper No. 70CP 140-PWR, IEEE Winter Power Meeting, New York, January 1970.

43 Warrington, A.R. van C., "Protective Relay for Long Transmission Lines", AIEE Transactions, Vol. 62, 1943, pp. 261-268.

44 Wedepohl, L.M., "Polarised Mho Distance Relay", Proc. IEE, Vol. 112, No. 3, March 1965, pp. 525-535.

9. APPENDICES

A. EVALUATION OF RELAYING ALGORITHMS FOR RELIABILITY

Developments in digital processor technology stimulated interest in using digital processors as programmable protective relays. Design of distance relays received considerable attention from many researchers. Different algorithms for calculating impedances, (V/I) ratios, from digitized voltage and current samples have been proposed. Each algorithm listed in Table A.1 has its own merits and demerits. Selection of an algorithm for use in a distance relay design is influenced by the performance required of the relay. At times, the power system data is such that some algorithms encounter computer software overflow, underflow or division by zero when the data is processed. The relay algorithms listed in Table A.1 were tested using the fault data stored in files listed in Table A.2.

A.1 Reliability of the Relaying Algorithms

A computer program was written to test the algorithms listed in Table A.1. Each algorithm forms a separate subroutine in the main program. Fault data contained in files listed in Table A.2 was used for testing the algorithms. The results are presented in this section.

Table A.1 Digital distance relaying algorithms tested for reliability

NO.	ALGORITHM	SAMPLING RATE Hz
1	Rockefeller,Udren,Gilcrest	1440
2	Rockefeller,Udren,Gilcrest	720
3	Mann - Morrison	1440
4	Mann - Morrison	720
5	Miki - Makino	1440
6	Miki - Makino	720
7	Gilbert - Shovlin	1440
8	Gilbert - Shovlin	720
9	Full cycle Fourier analysis	1440
10	Full cycle Fourier analysis	720
11	Full cycle Fourier analysis	120
12	Half cycle Fourier analysis	1440
13	Half cycle Fourier analysis	720
14	Breingan	1440
15	Breingan	720
16	Breingan 3rd. Harmonic	720
17	McInnes - Morrison	1440
18	McInnes - Morrison	720
19	7X7 least error squares	720
20	7X9 least error squares	720
21	6X9 least error squares	720
22	4X7 least error squares	720
23	4X9 least error squares	720
24	6X9 least error squares	720
25	6X12 least error squares	720
26	McInnes - Morrison 3rd. Harmonic	720

Table A.2 Fault data files used for testing the relaying algorithms

NO.	DATA FILE	VOLTAGES	CURRENTS
(A)	AP3071A.DAT	6	6
(B)	AP1071A.DAT	6	6
(C)	AP1072A.DAT	3	3
(D)	AP2072A.DAT	3	3
(E)	AP1093A.DAT	6	6
(F)	AP2093A.DAT	6	6
(G)	AP3093A.DAT	6	6
(H)	AP1067A.DAT	6	6
(I)	AP2061A.DAT	6	6
(J)	AP2063A.DAT	6	6
(K)	AP3063A.DAT	6	6
(L)	AP2068A.DAT	6	6
(M)	AP3068A.DAT	6	6
(N)	AP4068A.DAT	6	6
(O)	AP5068A.DAT	6	6
(P)	AP6068A.DAT	3	3
(Q)	AP7068A.DAT	3	3
(R)	AP8068A.DAT	3	3
(S)	AP3062A.DAT	6	6
(T)	AP4062A.DAT	6	6

Each algorithm was tested with the data listed in Table A.2. It is not convenient to determine the number of times an algorithm fails when operations such as divisions by zero are encountered. An algorithm was, therefore, considered to have failed once if a division by zero was encountered while processing a set of data. The number of failures per data file for the algorithms are listed in Tables A.3 and A.4.

From the results listed in Tables A.3 and A.4, the reliability of the algorithms was calculated as:

$$\text{Reliability} = 1 - \text{p.u. failures}$$

$$\text{p.u. failures} = \frac{\text{tatal failures}}{\text{total number of data sets used}}$$

The p.u. failures and the estimated indices of reliability of algorithms are listed in Table A.5.

Table A.5 shows that the least error squares and the Fourier algorithms are generally more reliable than the other algorithms. This is because these algorithms use long data windows and hence provide good filtering. Algorithms using short data windows have poor filtering characteristics and are more likely to encounter computer software overflow, underflow or division by zero.

Table A.3 Number of algorithm failures - while processing data files

ALGORITHM TESTED	FAILURES PER DATA FILE									
	(A)	(B)	(C)	(D)	(E)	(F)	(G)	(H)	(I)	(J)
(1)	1	2	0	0	0	0	0	2	3	0
(2)	0	0	0	0	0	0	1	0	1	0
(3)	0	0	0	0	0	0	0	0	0	0
(4)	0	0	0	0	0	0	0	0	0	0
(5)	0	0	0	0	0	0	0	0	0	0
(6)	0	0	0	0	0	0	0	0	0	0
(7)	1	3	0	1	0	0	0	2	3	1
(8)	0	2	0	0	0	0	1	0	2	0
(9)	0	0	0	0	0	0	0	0	0	0
(10)	0	0	0	0	0	0	0	0	0	0
(11)	0	0	0	0	0	0	0	0	0	0
(12)	0	0	0	0	0	0	0	0	0	0
(13)	0	0	0	0	0	0	0	0	0	0
(14)	1	3	0	1	0	0	0	2	3	1
(15)	0	2	0	0	0	0	1	0	2	0
(16)	0	2	0	0	0	0	1	0	2	0
(17)	0	0	0	0	0	0	0	0	0	0
(18)	0	0	0	0	0	0	0	0	0	0
(19)	0	0	0	0	0	0	0	0	0	0
(20)	0	0	0	0	0	0	0	0	0	0
(21)	0	0	0	0	0	0	0	0	0	0
(22)	0	0	0	0	0	0	0	0	0	0
(23)	0	0	0	0	0	0	0	0	0	0
(24)	0	0	0	0	0	0	0	0	0	0
(25)	0	0	0	0	0	0	0	0	0	0
(26)	0	0	0	0	0	0	0	0	0	0

Table A.4 Number of algorithm failures - while processing data files

ALGORITHM TESTED	FAILURES PER DATA FILE									
	(K)	(L)	(M)	(N)	(O)	(P)	(Q)	(R)	(S)	(T)
(1)	2	2	2	3	3	0	0	0	1	3
(2)	0	1	0	2	3	0	0	0	0	0
(3)	0	0	0	3	1	0	0	0	0	0
(4)	0	0	0	1	1	0	0	0	0	0
(5)	0	0	0	3	1	0	0	0	0	0
(6)	0	0	0	1	1	0	0	0	0	0
(7)	2	3	2	3	3	0	0	0	2	3
(8)	0	1	0	3	3	0	0	0	0	1
(9)	0	0	0	0	1	0	0	0	0	0
(10)	0	0	0	0	0	0	0	0	0	0
(11)	0	0	0	0	0	0	0	0	0	0
(12)	0	0	0	0	0	0	0	0	0	0
(13)	0	0	0	0	1	0	0	0	0	0
(14)	2	3	2	3	3	0	0	0	2	3
(15)	0	1	0	3	3	0	0	0	0	1
(16)	0	1	0	3	3	0	0	0	0	1
(17)	0	0	0	1	3	0	0	0	0	0
(18)	0	1	0	2	3	0	0	0	0	0
(19)	0	0	0	0	1	0	0	0	0	0
(20)	0	0	0	0	0	0	0	0	0	0
(21)	0	0	0	0	0	0	0	0	0	0
(22)	0	0	0	0	0	0	0	0	0	0
(23)	0	0	0	0	1	0	0	0	0	0
(24)	0	0	0	0	0	0	0	0	0	0
(25)	0	0	0	0	0	0	0	0	0	0
(26)	0	1	0	2	3	0	0	0	0	0

Table A.5 Results for reliability of relaying algorithms

ALGORITHM NUMBER	TOATL DATA TESTED	TOTAL FAILURES	FAILURES P.U.	RELIABILITY
(1)	105	24	0.22857	77.142
(2)	105	8	0.07619	92.380
(3)	105	4	0.03809	96.190
(4)	105	2	0.01904	98.095
(5)	105	4	0.03809	96.190
(6)	105	2	0.01904	98.095
(7)	105	29	0.27619	72.380
(8)	105	13	0.12380	87.619
(9)	105	0	0.00000	100.00
(10)	105	0	0.00000	100.00
(11)	105	1	0.0095238	99.047
(12)	105	0	0.00000	100.00
(13)	105	1	0.0095238	99.047
(14)	105	29	0.27619	72.380
(15)	105	13	0.12380	87.619
(16)	105	13	0.12380	87.619
(17)	105	4	0.03809	96.190
(18)	105	6	0.057142	94.285
(19)	105	1	0.0095238	99.047
(20)	105	0	0.00000	100.00
(21)	105	0	0.00000	100.00
(22)	105	0	0.00000	100.00
(23)	105	1	0.0095238	99.047
(24)	105	0	0.00000	100.00
(25)	105	0	0.00000	100.00
(26)	105	6	0.057142	94.285

B. THE Z-TRANSFORM

Equation 3.1 which represents the output of a digital recursive filter is a difference equation. The method of z-transform can be used to derive the transfer function of the digital filters. The method is described briefly in this appendix.

The z-transform F(z) of any function f(n) is defined by the equation:

$$F(z) = \sum_{n=-\infty}^{\infty} f(n)z^n \qquad (B.1)$$

If $x(t) = \sum_{n=-\infty}^{\infty} x(n)\delta(t-n)$ is an arbitrary input signal and h(t) is its impulse response, the output y(t) can be expressed as:

$$y(t) = \sum_{n=-\infty}^{\infty} x(n)h(t-n) \qquad (B.2)$$

Equation B.2 is called the convolution of x(t) with h(t) and is generally written as:

$$y(t) = x(t)h(t) \qquad (B.3)$$

The z-transform of the output y(t) is given by:

$$Y(z) = \sum_{n=-\infty}^{\infty} y(n)z^n = \sum_{n=-\infty}^{\infty} z^n \sum_{m=-\infty}^{\infty} x(m)h(n-m) \qquad (B.4)$$

Substituting $z^n = z^m \; z^{n-m}$ and $p = n-m$; Equation B.4 reduces to:

$$Y(z) = \sum_{m=-\infty}^{\infty} x(m)z^m \sum_{p=-\infty}^{\infty} h(p)z^p \qquad (B.5)$$

By substituting $\sum_{m=-\infty}^{\infty} x(m)z^m = X(z)$ and $\sum_{p=-\infty}^{\infty} h(p)z^p = H(z)$ in Equation B.5, the following equation is obtained:

$$Y(z) = X(z)H(z) \qquad (B.6)$$

The z-transform H(z) of the impulse response h(t) is called the transfer function. In this technique, the transfer function of the sum of two functions is the sum of the transforms of the functions. For two systems with transfer function $H_1(z)$ and $H_2(z)$ in parallel, the combined transfer function is:

$$H(z) = H_1(z) + H_2(z) \qquad (B.7)$$

The combined transfer function of two systems connected in

series is given by:

$$H(z) = H_1(z)H_2(z) \qquad (B.8)$$

To illustrate the application of z-transform, consider a simple feedback system represented by:

$$y(t) = x(t) + h_1(t)y(t) \qquad (B.9)$$

The z-transform of Equation B.9 provides:

$$Y(z) = X(z) + H_1(z)Y(z) \qquad (B.10)$$

Solving Equation B.10 for Y(z)

$$Y(z) = \frac{X(z)}{1 - H_1(z)}$$

$$= H(z)X(z) \qquad (B.11)$$

where: $H(z) = 1/\{1-H_1(z)\}$

Equation B.11 demonstrates the use of z-transform for deriving the transfer functions from the difference equations representing systems with feedback.

Equation 3.33 of Chapter 3 describes the transfer function of a second order filter and is reproduced below:

$$H(z) = A_g \frac{1 + A_1 z^{-1} + A_2 z^{-2}}{1 + B_1 z^{-1} + B_2 z^{-2}} \qquad (B.12)$$

To find the frequency response of the filter, the term z in equation B.12 is replaced by $e^{jw\Delta T}$. The magnitudes and arguments of H(z), when the frequency is varied from zero to the Nyquist frequency, describe the frequency response of the filter.

C. DERIVATION OF THREE SAMPLE LEAST ERROR SQUARES MODEL

In this appendix Equations 4.6 and 4.7 of Chapter 4 are derived using the three sample least error squares pure sine wave model. The coefficients of the 6X9 least error squares filter are also listed.

C.1 Derivation of Eauations 4.6 and 4.7

A fundamental frequency voltage signal can be expressed as:

$$v(t) = V_p \sin(w_1 t + \theta) \qquad (C.1)$$

where:

V_p is the peak value of the voltage

w_1 is the fundamental frequency in radians

θ is the phase angle

t is the time in seconds

Equation C.1 when expanded leads to Equation C.2:

$$v(t) = V_p \cos(\theta)\sin(w_1 t) + V_p \sin(\theta)\cos(w_1 t) \qquad (C.2)$$

Substituting $V_p \cos(\theta)=B_1$ and $V_p \sin(\theta)=B_2$; Equation C.2 reduces to:

$$v(t) = B_1 \sin(w_1 t) + B_2 \cos(w_1 t) \qquad (C.3)$$

If ΔT is the intersampling interval, voltage $v(-\Delta T)$, $v(0)$ and $v(\Delta T)$ can be expressed as Equations C.4 to C.6. These equations are obtained by substituting, in Equation C.3 t by $-\Delta T$, 0, ΔT.

$$v_{-1} = B_1 \sin(-w_1 \Delta T) + B_2 \cos(-w_1 \Delta T) \qquad (C.4)$$

$$v_0 = B_1 \sin(0) + B_2 \cos(0) \qquad (C.5)$$

$$v_{+1} = B_1 \sin(w_1 \Delta T) + B_2 \cos(w_1 \Delta T) \qquad (C.6)$$

When the data is sampled at 1000 Hz, Equations C.4 to C.6 reduce to:

$$v_{-1} = -0.3681246B_1 + 0.9297765B_2 \qquad (C.7)$$

$$v_0 = 0.0000000B_1 + 1.0000000B_2 \qquad (C.8)$$

$$v_{+1} = 0.3681246B_1 + 0.9297765B_2 \qquad (C.9)$$

Equations C.7, C.8 and C.9 can be written in matrix form as:

$$[V] = [A]\ [B] \qquad (C.10)$$

where:

$$[A] = \begin{bmatrix} -0.3681246 & 0.9297765 \\ 0 & 1 \\ 0.3681246 & 0.9297765 \end{bmatrix}$$

$$[B] = \begin{bmatrix} B_1 \\ B_2 \end{bmatrix} \qquad [V] = \begin{bmatrix} v_{-1} \\ v_0 \\ v_{+1} \end{bmatrix}$$

The elements of the matrix B can be obtained by:

$$[B] = [A]^{\dagger}[V] \tag{C.11}$$

where: $[A]^{\dagger} = \left[[A]^T [A] \right]^{-1} [A]^T$

$[A]^{\dagger}$ is the three sample least error squares fit and its coefficients for the case of Equation C.10 are:

$$[A]^{\dagger} = \begin{bmatrix} -1.358227 & 0.000000 & 1.358227 \\ 0.340690 & 0.366430 & 0.340690 \end{bmatrix}$$

These are the coefficients used in Equations 4.6 and 4.7 of Chapter 4.

C.2 Coefficients of the 6X9 Least Error Squares Filter

The coefficients of the 6X9 least error squares filter

when data is sampled at 720 Hz are as follows[3]:

Coefficients of the real terms (cosine filter):

-0.2439 -0.1434 -0.0429 0.2294 0.4018
0.2294 -0.0429 -0.1434 -0.2439

Coefficients of the imaginary terms (sine filter):

-0.6750 0.3644 0.6212 0.3644 0.0000
-0.3644 -0.6212 -0.3644 0.6750

C.3 Additional Results of the Studies Conducted in Chapter 4

In this section some additional results of the studies conducted in Chapter 4 are given.

Figures C.1 to C.3 show the impedances and their phase angles calculated using the Mann and Morrison algorithm and Figures C.4 to C.6 depict the impedances and their phase angles calculated using the three sample least error squares sine wave algorithm. The fault voltages and currents in these cases were processed by second order (55-65 Hz) recursive filters. Figures C.7 to C.10 show the impedances and their phase angles (or R and X) calculated using the 6X9 least error squares algorithm and smoothed using second order lowpass digital recursive filters. These results have been discussed in details in Chapter 4.

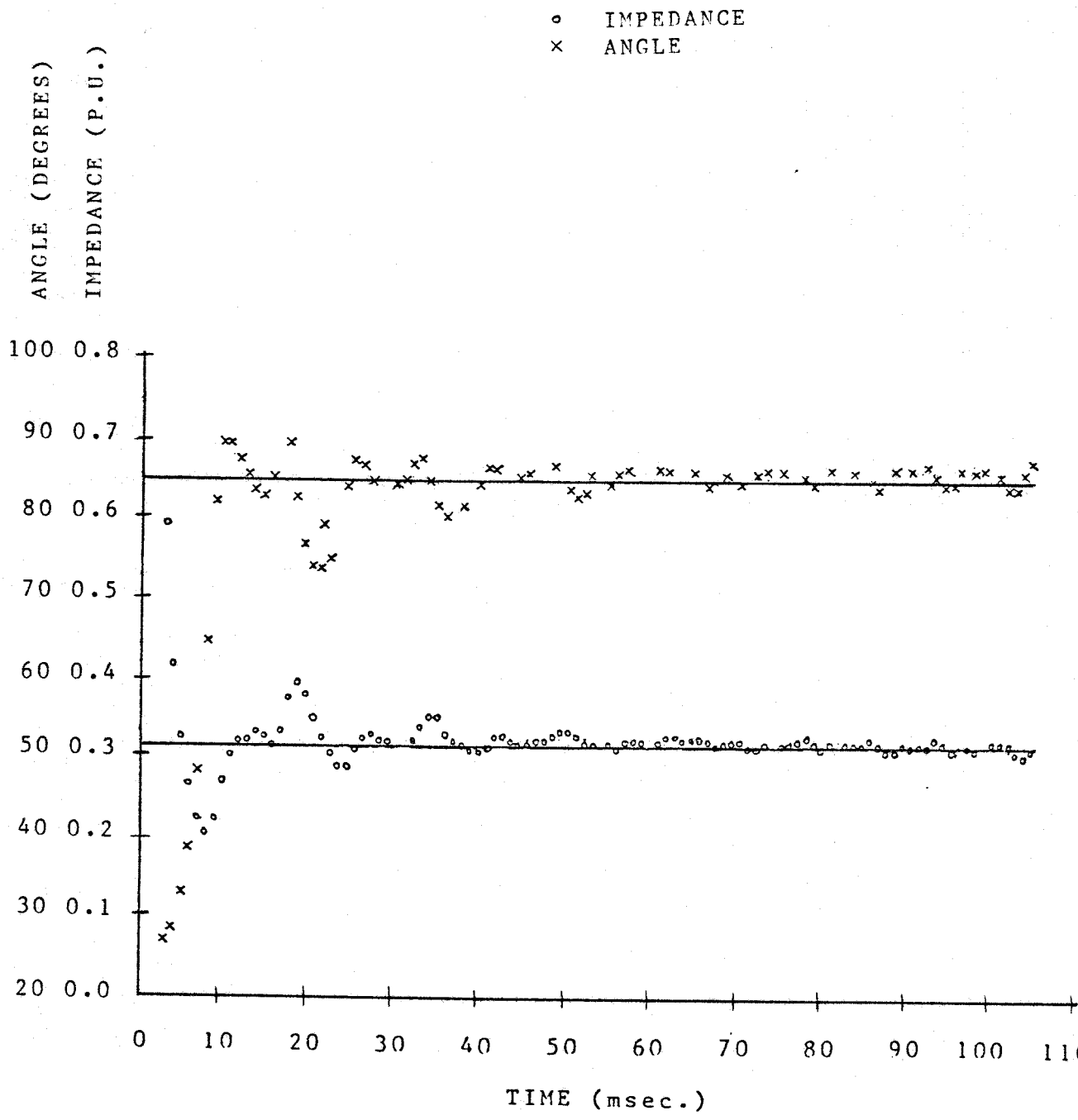

Figure C.1 Bandpass R-Filter (55-65) Hz with Mann and Morrison algorithm - fault incidence at 30 degrees

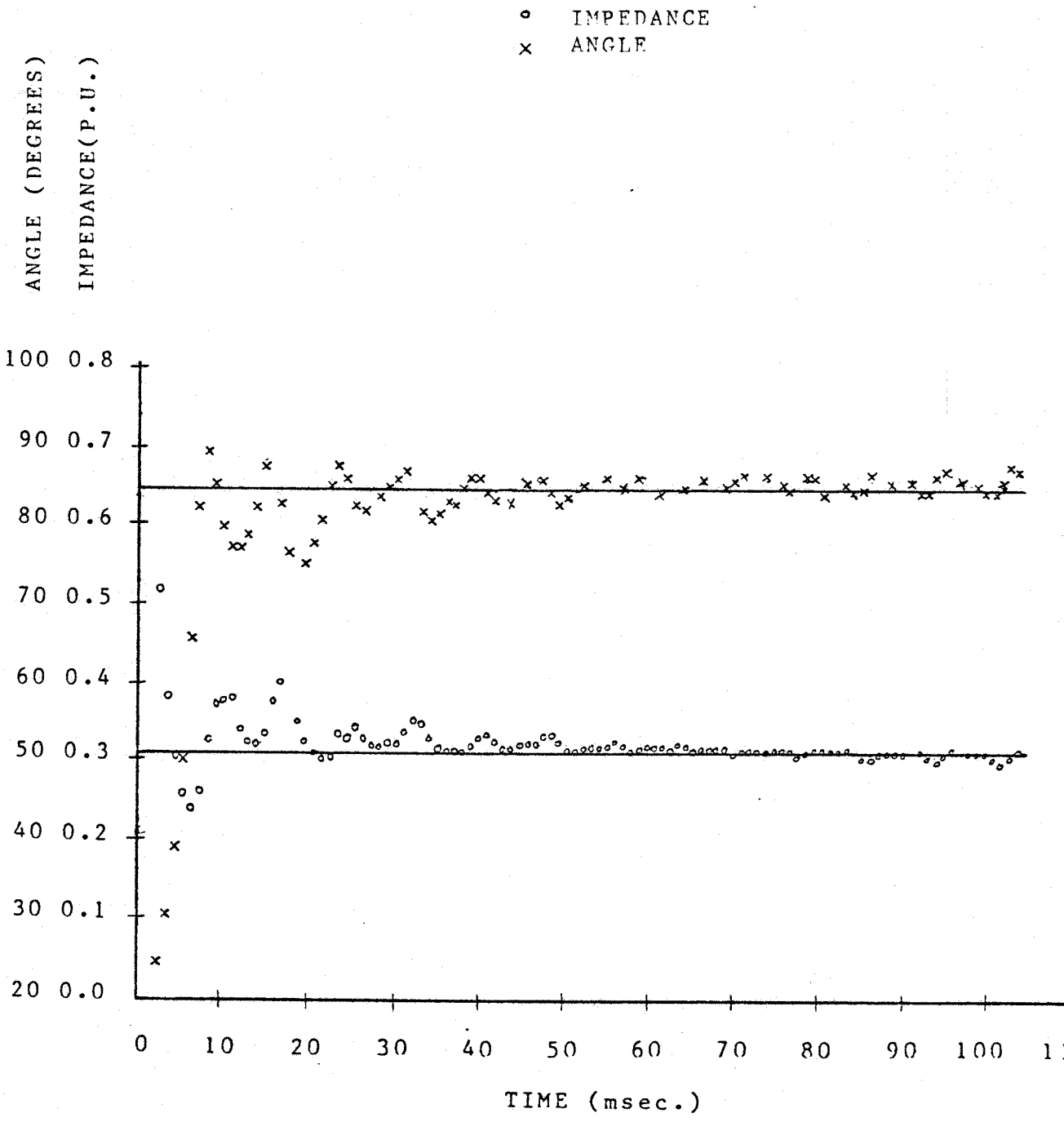

Figure C.2 Bandpass R-Filter (55-65) Hz with Mann and Morrison algorithm - fault incidence at 60 degrees

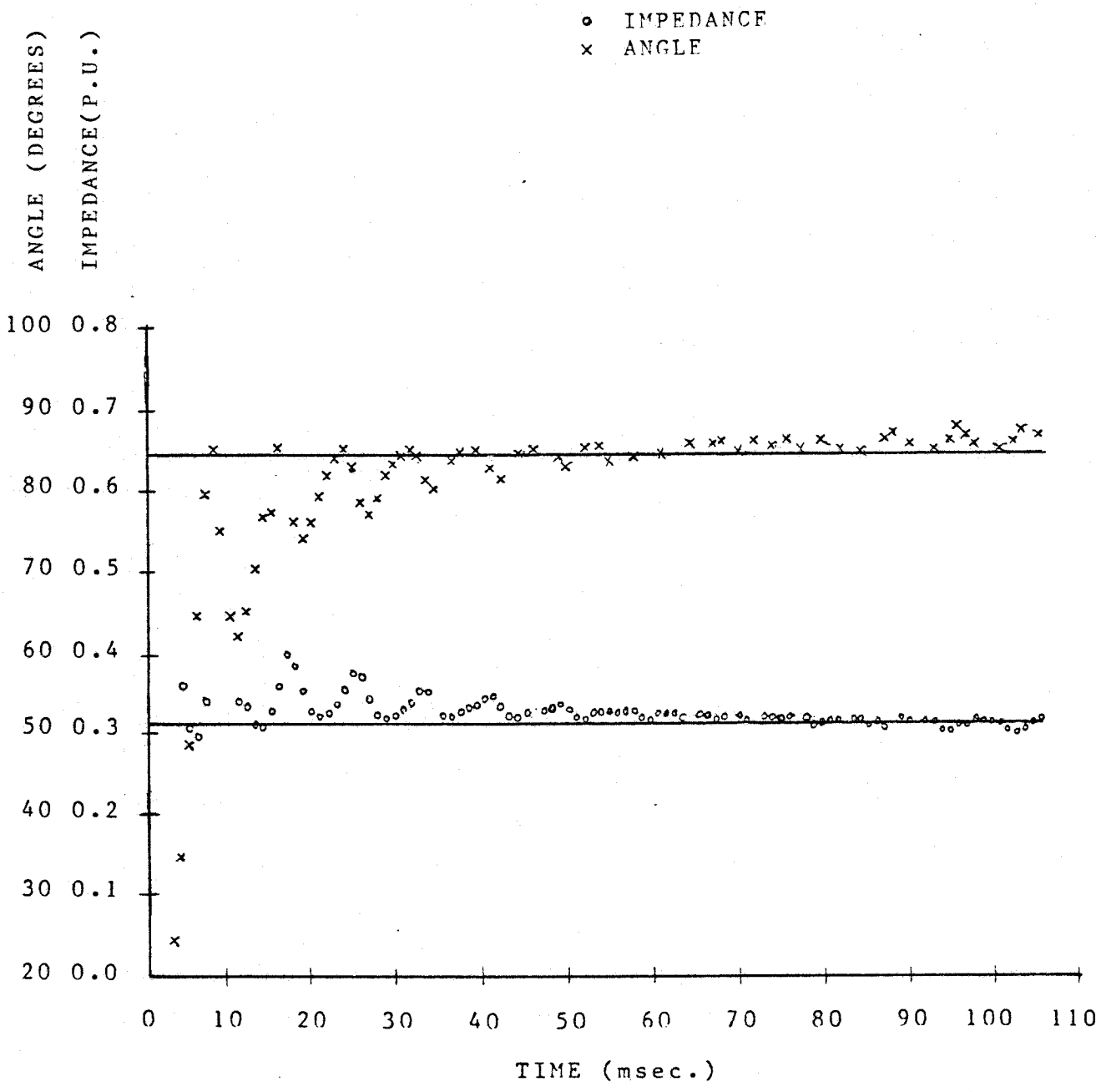

Figure C.3 Bandpass R-Filter (55-65) Hz with Mann and Morrison algorithm - fault incidence at 90 degrees

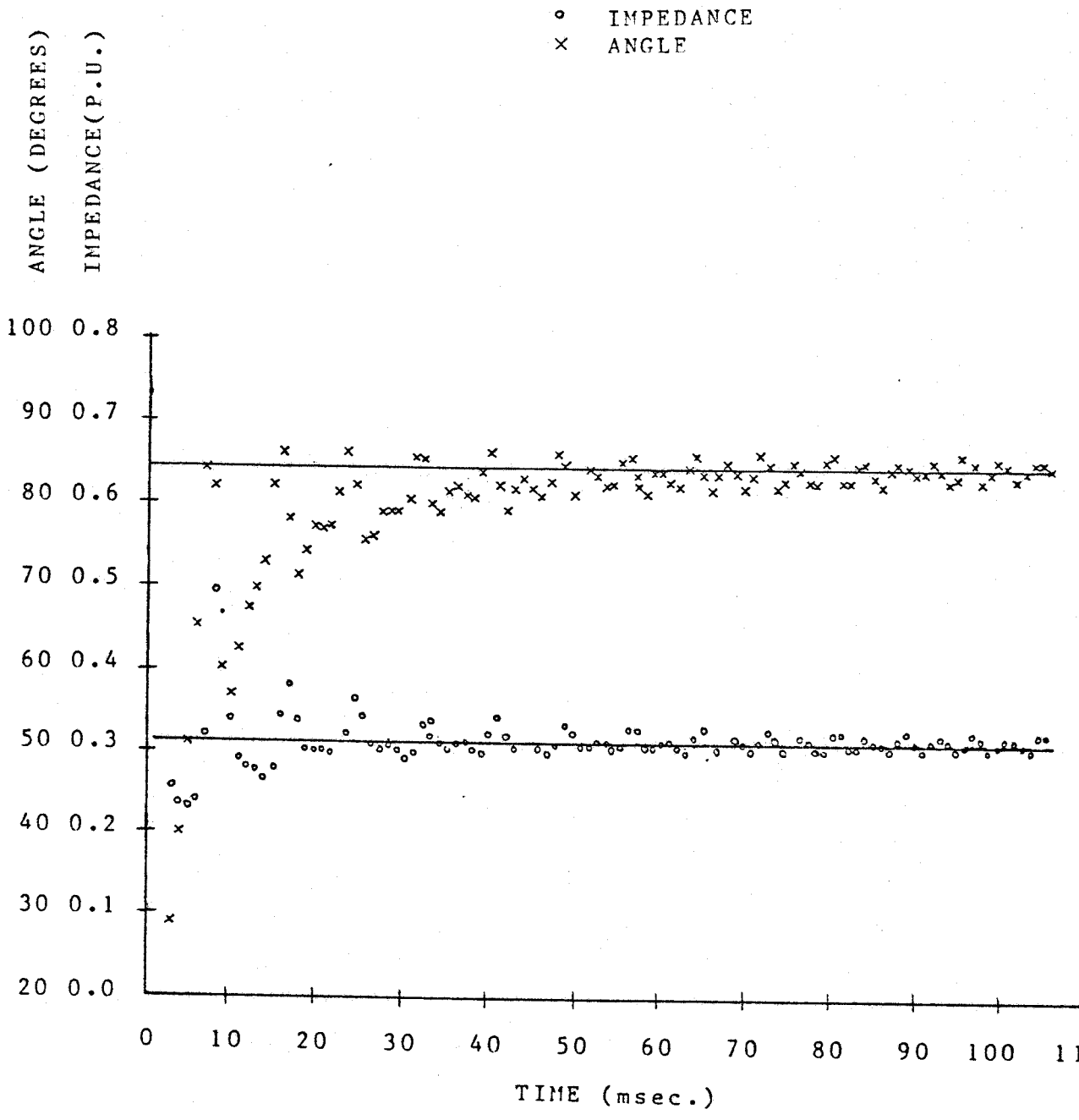

Figure C.4 Bandpass R-Filter (55-65) Hz with least error squares pure sine wave algorithm - fault incidence at 30 degrees

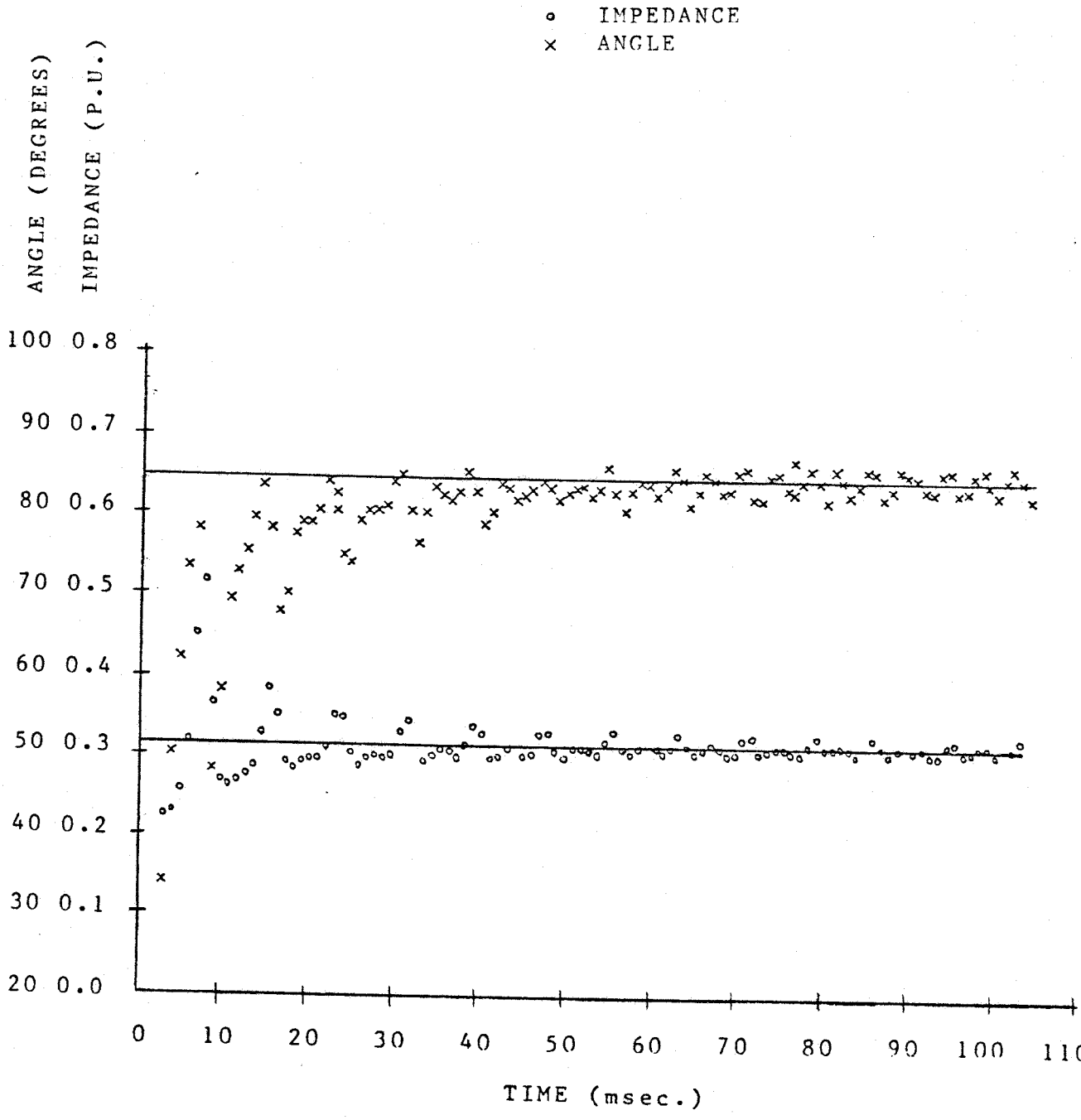

Figure C.5 Bandpass R-Filter (55-65) Hz with least error squares pure sine wave algorithm - fault incidence at 60 degrees

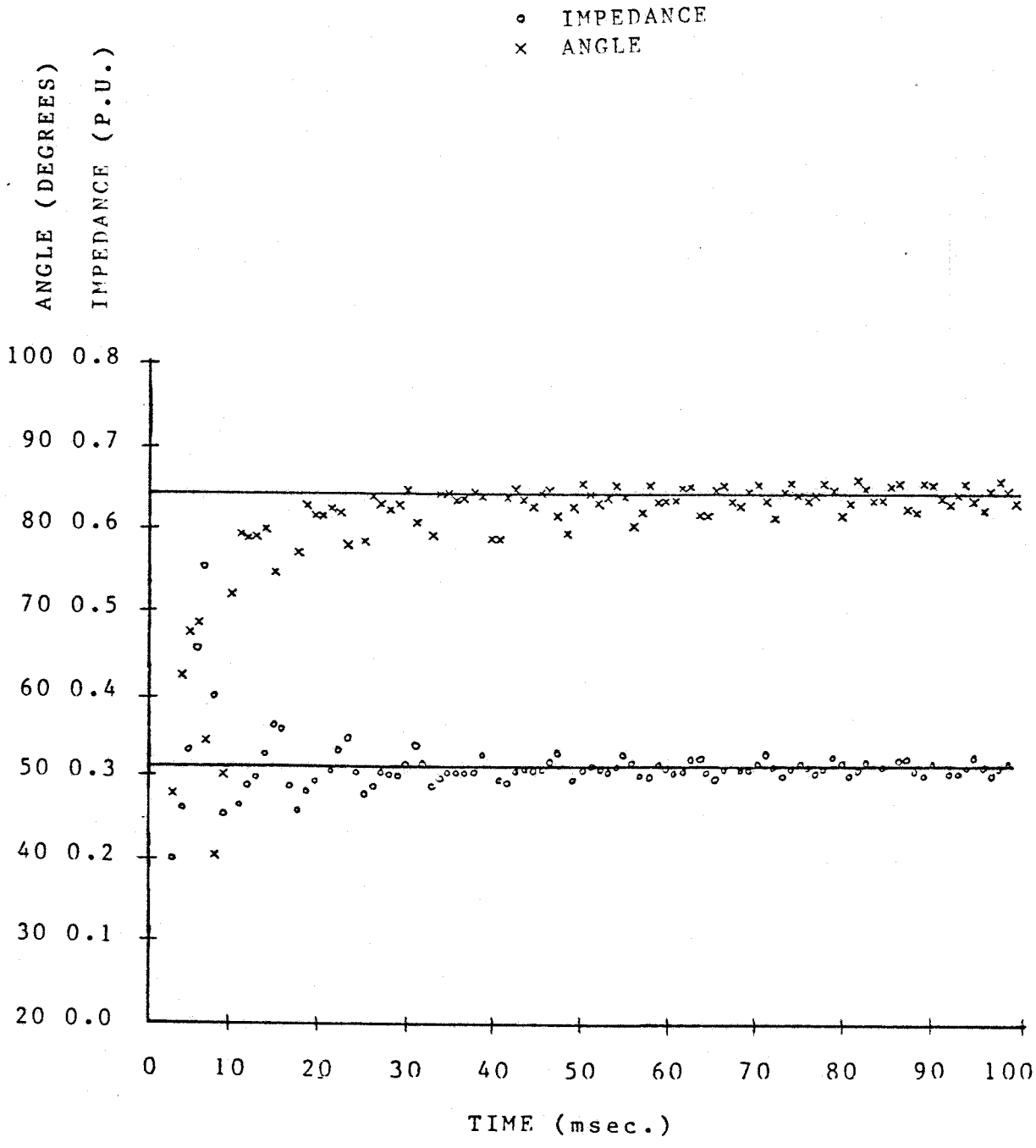

Figure C.6 Bandpass R-Filter (55-65) Hz with least error squares pure sine wave algorithm - fault incidence at 90 degrees

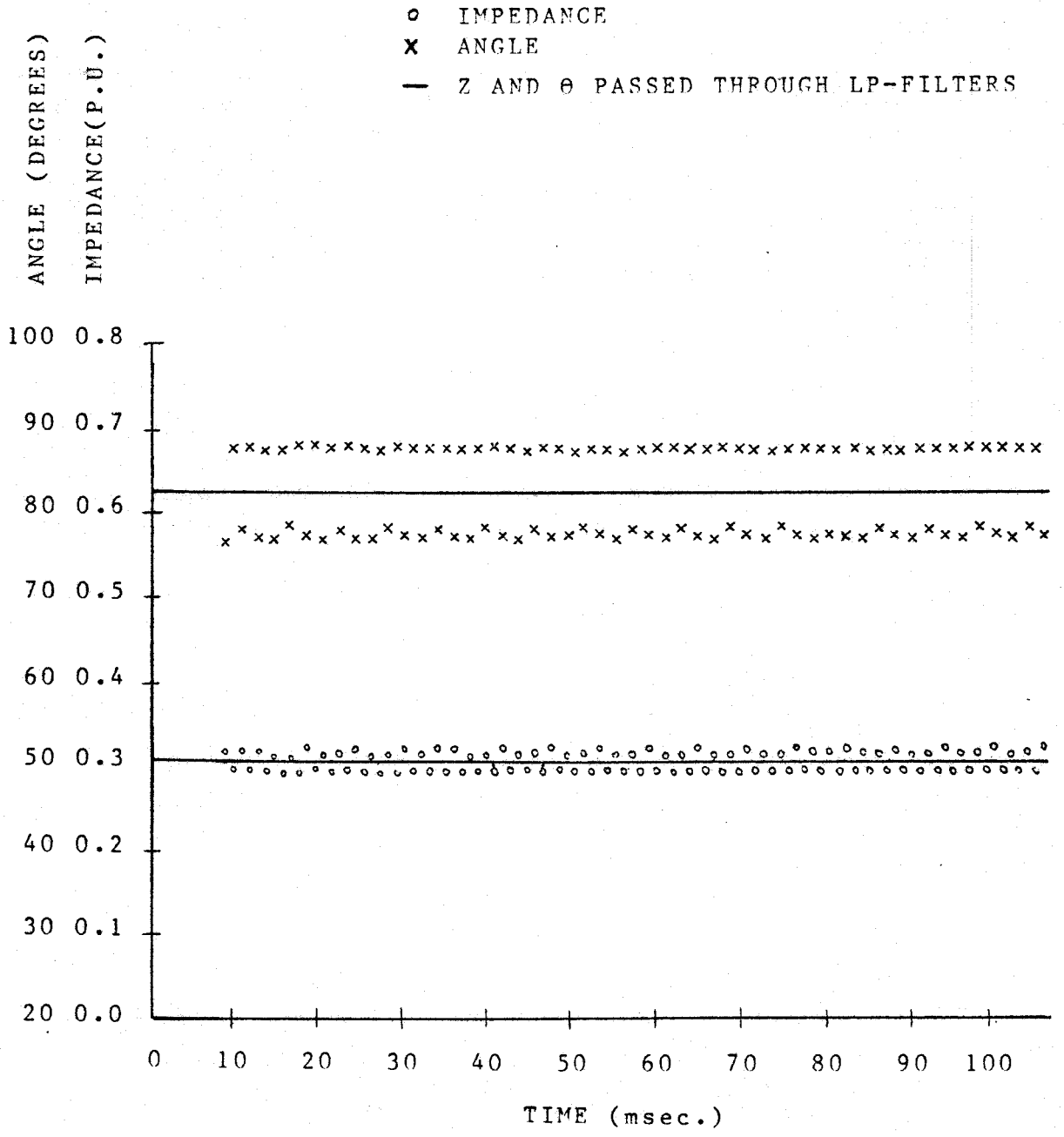

Figure C.7 6X9 least error squares algorithm with 10 Hz lowpass recursive filter - fault incidence at 30 degrees

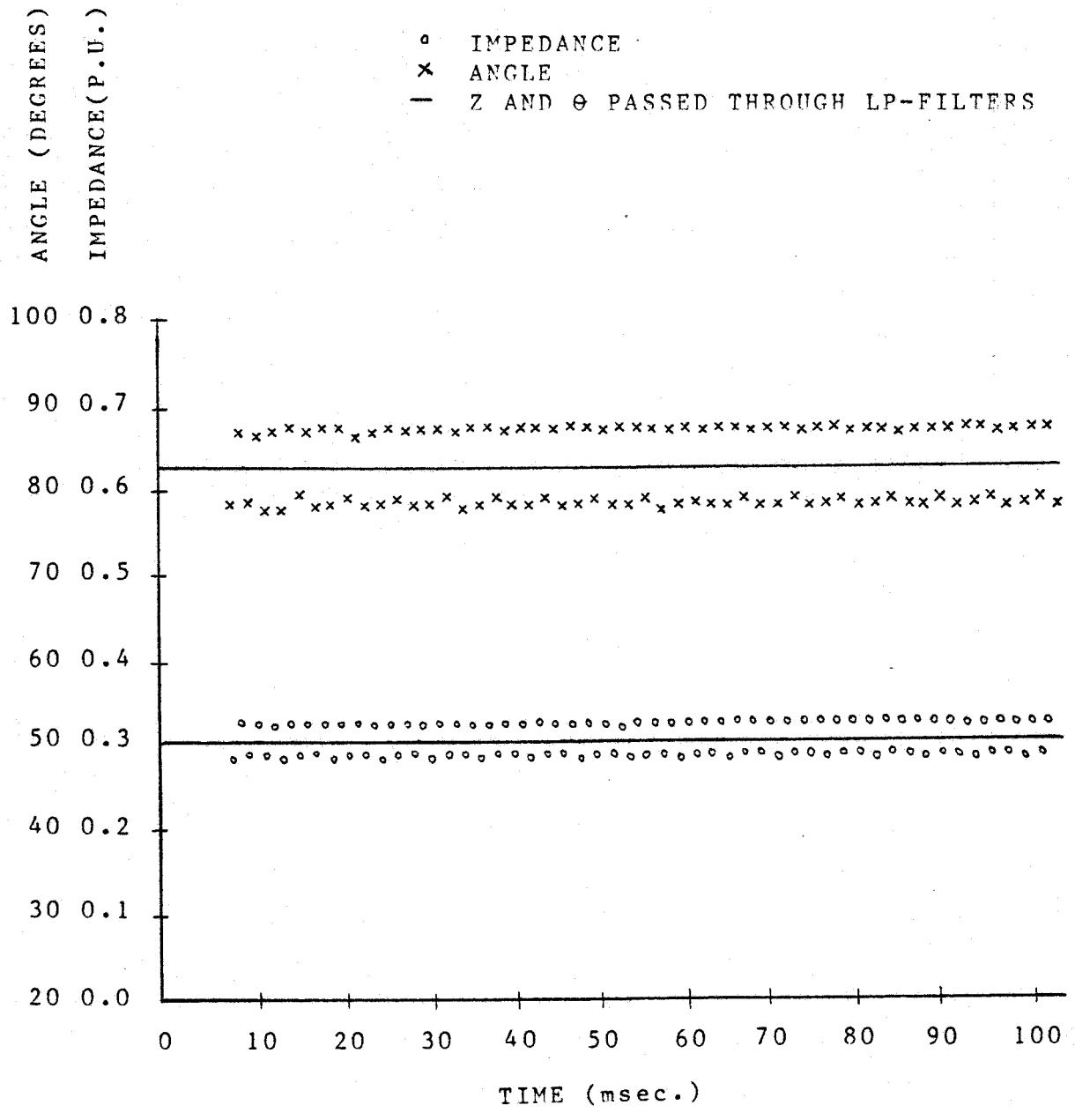

Figure C.8 6X9 least error squares algorithm with 10 Hz lowpass recursive filter - fault incidence at 60 degrees

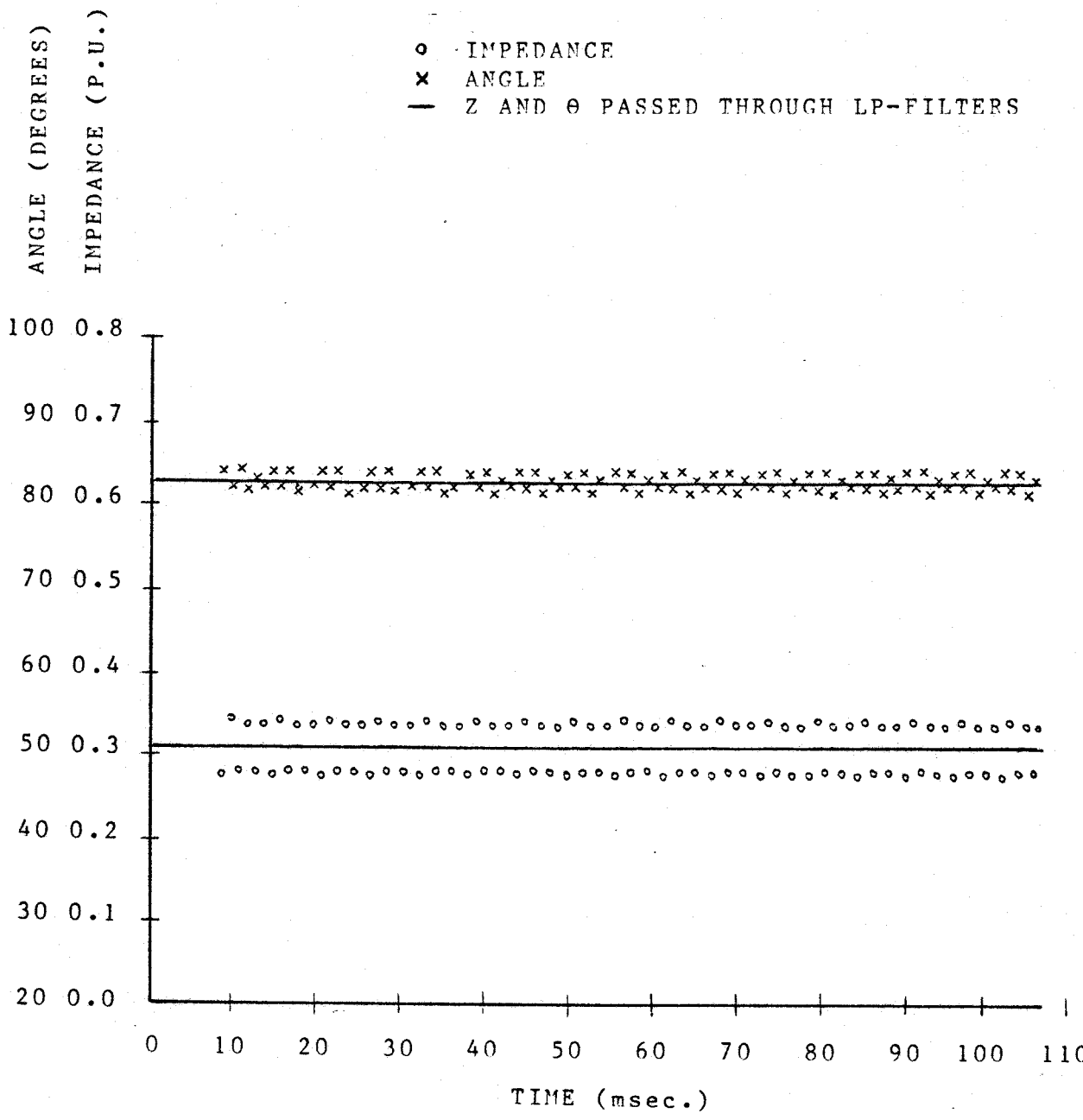

Figure C.9 6X9 least error squares algorithm with 10 Hz lowpass recursive filter - fault incidence at 90 degrees

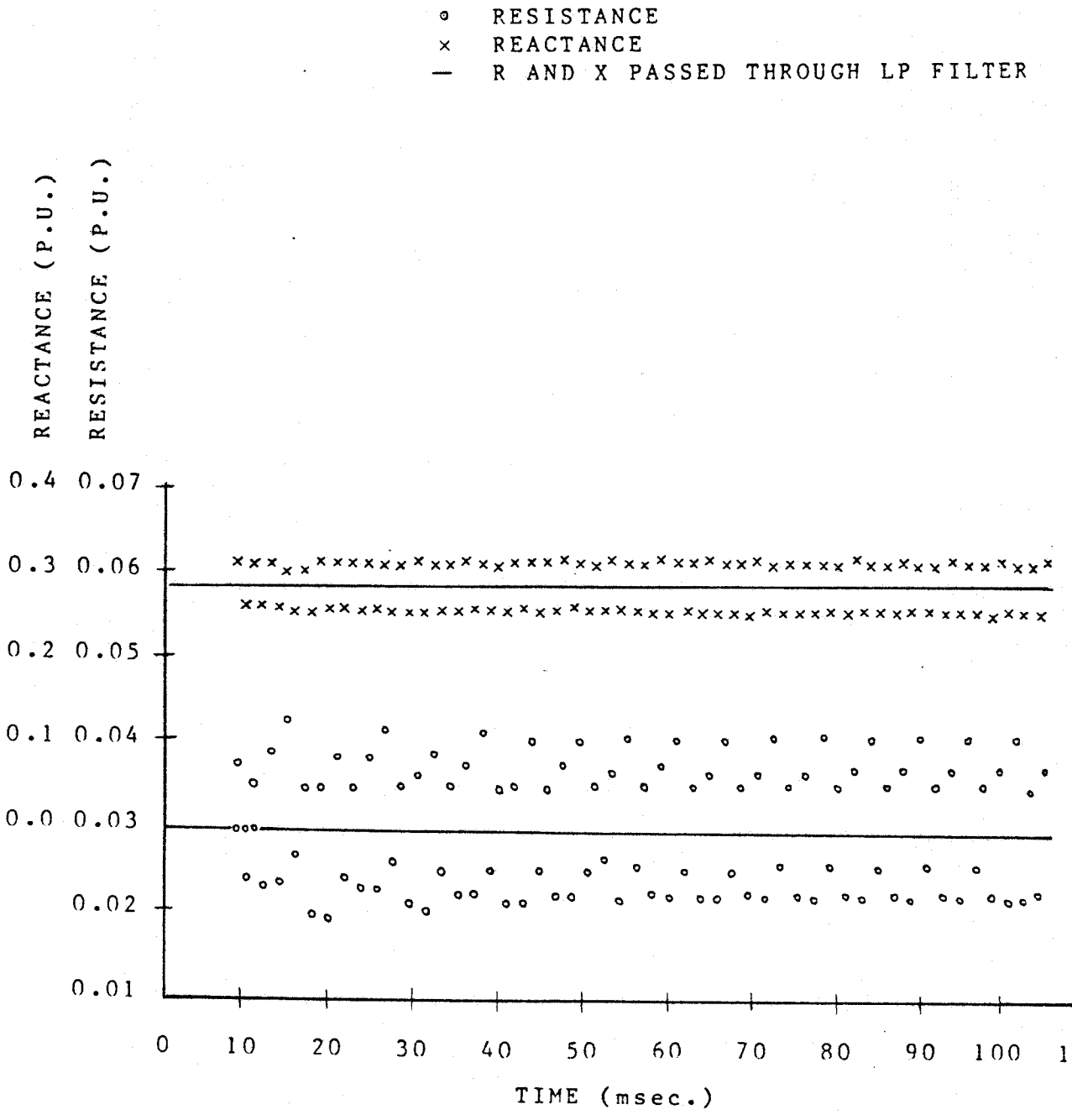

Figure C.10 6X9 least error squares algorithm with 10 Hz lowpass recursive filter - fault incidence at 120 degrees

D. DERIVATION OF GENERAL EXPONENTIAL SMOOTHING

Equation 5.6 of Chapter 5 represents a technique for revising the coefficients of general exponential smoothing at the end of a sampling interval. Complete details of this process are given in Reference 7. A brief derivation is given in this appendix for ready reference of the reader.

Assume that the data vector, x(t), can be represented by:

$$x(t) = A_1 f_1(t) + A_2 f_2(t) + \ldots\ldots A_m f_m(t) + e(t)$$

$$= \{ \sum_{i=1}^{m} A_i f_i(t) \} + e(t) \qquad (D.1)$$

where:

$A_i(t)$ is the ith data coefficient

$f_i(t)$ are the known functions of time

$e(t)$ is the noise in the signal

m represents the degrees of freedom

The A_i coefficients of this equation are determined such that the squared sum of the residuals defined by Equation D.2 is minimum:

$$\sum_{j=0}^{n} B^j [x(n-j) - A(n)f(n-j)]^2 \qquad (D.2)$$

where: n is the number of data samples

A matrix of weighted fitting functions, F(n), and the data vector, g(n), are defined as follows:

$$F(n) = \sum_{j=0}^{n} B^j f(-j) f^T(-j)$$

$$= F(n-1) + B^n f(-n) f^T(-n) \qquad (D.3)$$

$$g(n) = \sum_{j=0}^{n} B^j x(n-j) f(-j)$$

$$= x(n) f(0) + BL^{-1} g(n-1) \qquad (D.4)$$

In this equation L is the state transition matrix which generates successive values of fitting functions $f(t) = Lf(t-1)$. The minimum discounted squared residual is obtained when:

$$F(n)A(n) = g(n) \qquad (D.5)$$

Since the fitting function, F(n), has an inverse $F^{-1}(n)$, the coefficients A(n) are:

$$A(n) = F^{-1}(n) g(n) \qquad (D.6)$$

The fitting function matrix, F(n) reaches a steady state when $f_i(t) < B^{-t/2}$ for all i and the steady state matrix F

is given as:

$$F = F(\infty) = \sum_{j=0}^{\infty} B^j f(-j) f^T(-j) \qquad (D.7)$$

Using Equations D.5 and D.7, the steady state solution of Equation D.4 is obtained to be:

$$FA(n) = x(n)f(0) + BL^{-1}FA(n-1) \qquad (D.8)$$

A(n) is obtained by pre-multiplying both sides of this equation by F^{-1}.

$$A(n) = x(n)F^{-1}f(0) + BF^{-1}L^{-1}FA(n-1) \qquad (D.9)$$

Term $F^{-1}f(0)$ is usually designated as h and is called the smoothing vector. Its coefficeints are constant for a particular model. Designating $BF^{-1}L^{-1}F$ by H, Equation D.9 reduces to:

$$A(n) = hx(n) + HA(n-1) \qquad (D.10)$$

Pre-multiply Equation D.7 by L^{-1} and post-multiply the

result by $\left[L^T\right]^{-1} L^T$, the following equation is obtained:

$$L^{-1} F \left[L^T\right]^{-1} L^T = \sum_{j=0}^{\infty} B^j [L^{-1} f(-j)][L^{-1} f(-j)]^T L^T$$

$$= \frac{1}{B}[F - f(0)f^T(0)]L^T \qquad (D.11)$$

Hence $H = BF^{-1}L^{-1}F = [I - F^{-1}f(0)f^T(0)]L^T$ (D.12)

Because $h = F^{-1}f(0)$, H is given by

$$H = L^T - h\,[Lf(0)]^T \qquad (D.13)$$

Substituting the value of H in Equation D.10; A(n) is given by:

$$A(n) = hx(n) + [L - h\{Lf(0)\}]^T A(n-1)$$

$$= hx(n) + L^T A(n-1) - h[Lf(0)]^T A(n-1) \qquad (D.14)$$

Since $[Lf(0)]^T A(n-1) = S(n-1)$ was the previous output, substituting it in Equation D.14 leads to Equation D.15:

$$A(n) = L^T A(n-1) + h[x(n) - S(n-1)] \qquad (D.15)$$

This is Equation 5.6 of Chapter 5.

D.1 Numeriacl Values for the State Transition Matrix and the Smoothing Vector

Numerical values for the state transition matrix and the smoothing vector for a voltage or current modelled by Equation 5.9 are listed in this section. The sampling interval in this case is assumed to be 30 electrical degrees. The coefficients of the smoothing vector for this case and three different values of the smoothing constant 'a' are given below.

$$[L] = \begin{bmatrix} 1 & 0 & 0 & 0 \\ 1 & 1 & 0 & 0 \\ 0 & 0 & 0.8603 & 0.5000 \\ 0 & 0 & -0.500 & 0.8603 \end{bmatrix}$$

a	0.25	0.10	0.05
B	0.93061	0.97400	0.98726
h_1	0.12949	0.05024	0.02503
h_2	0.00457	0.00066	0.00016
h_3	0.04113	0.00605	0.00148
h_4	0.12052	0.04977	0.02499

D.2 Additional Results of the Studies Conducted in Chapter 5

In this section some additional results of the studies conducted in Chapter 5 are given.

Figures D.1 to D.3 depict the impedances and their phase angles calculated using the Mann and Morrison algorithm and smoothed using the single exponential smoothing. Figures D.4 to D.6 show the impedances and their

phase angles calculated using the three sample least error squares algorithm and smoothed using the single exponential smoothing. The data in these cases was processed by the (55-65 Hz) bandpass recursive filters. These results have been discussed in details in Chapter 5.

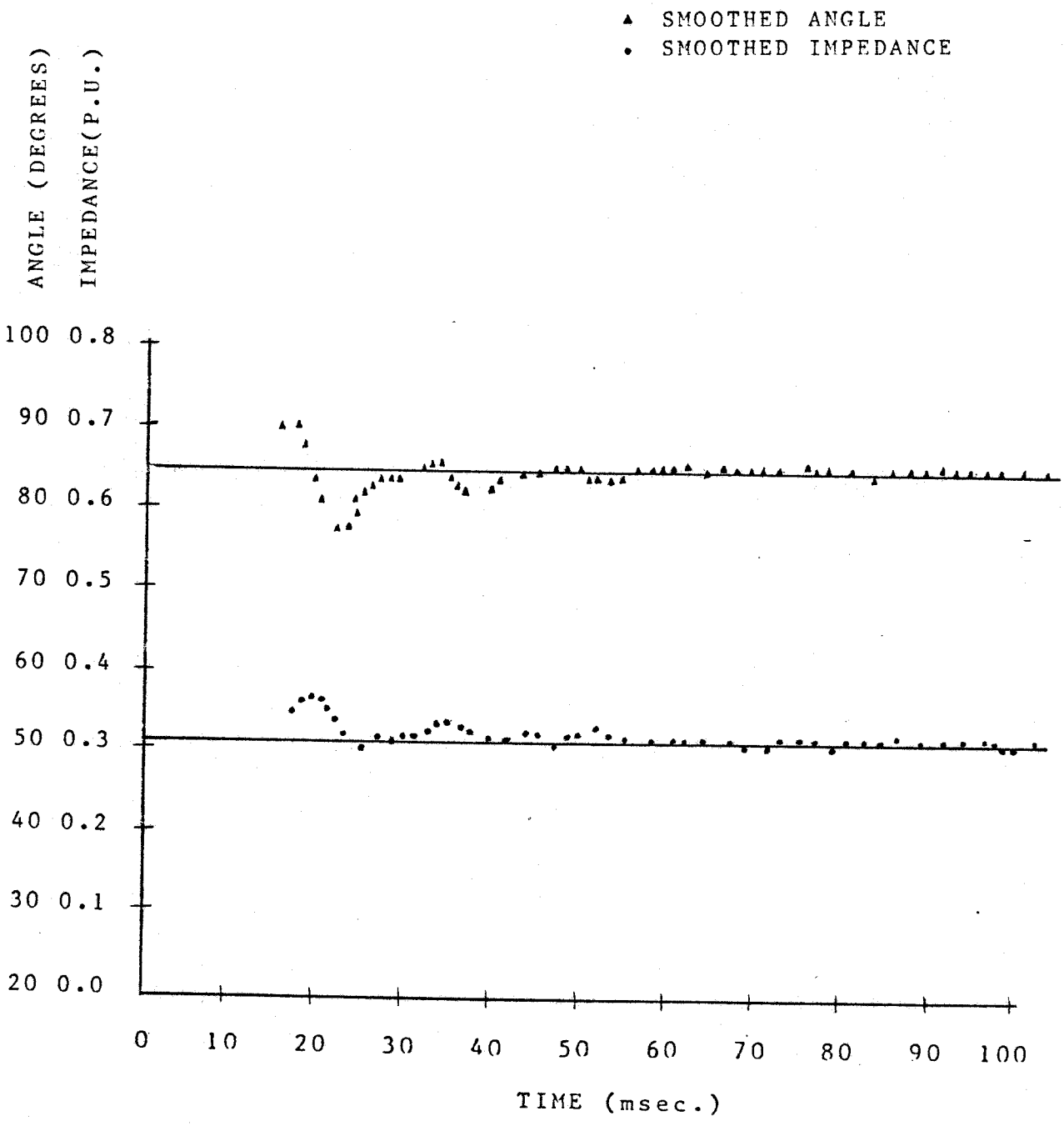

Figure D.1 Bandpass R-Filter (55-65 Hz) + Mann and Morrison Algorithm + Single Exponential Smoothing (a=0.3) - fault incidence at 30 degrees

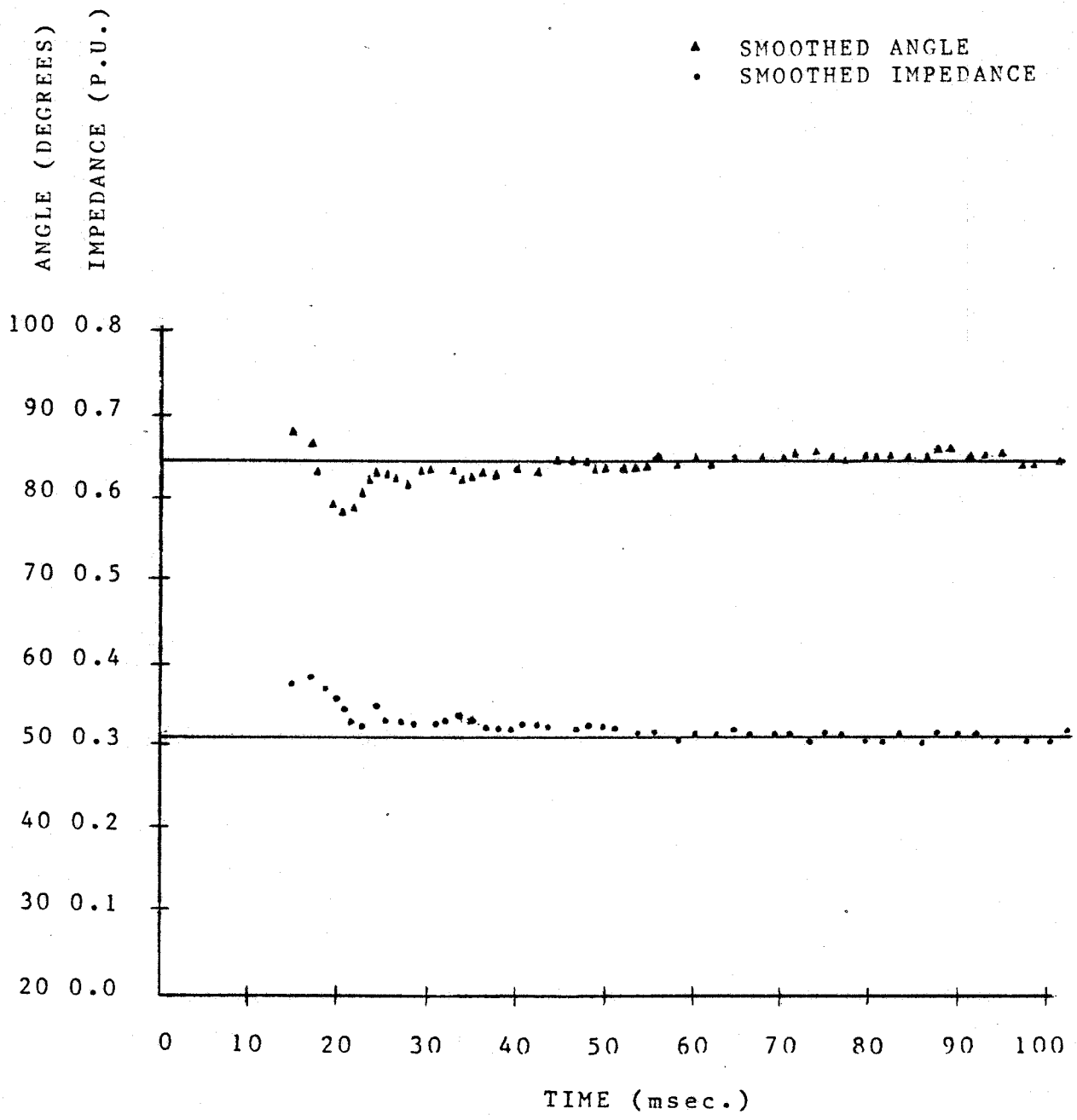

Figure D.2 Bandpass R-Filter (55-65 Hz) + Mann and Morrison Algorithm + Single Exponential Smoothing (a=0.3) - fault incidence at 60 degrees

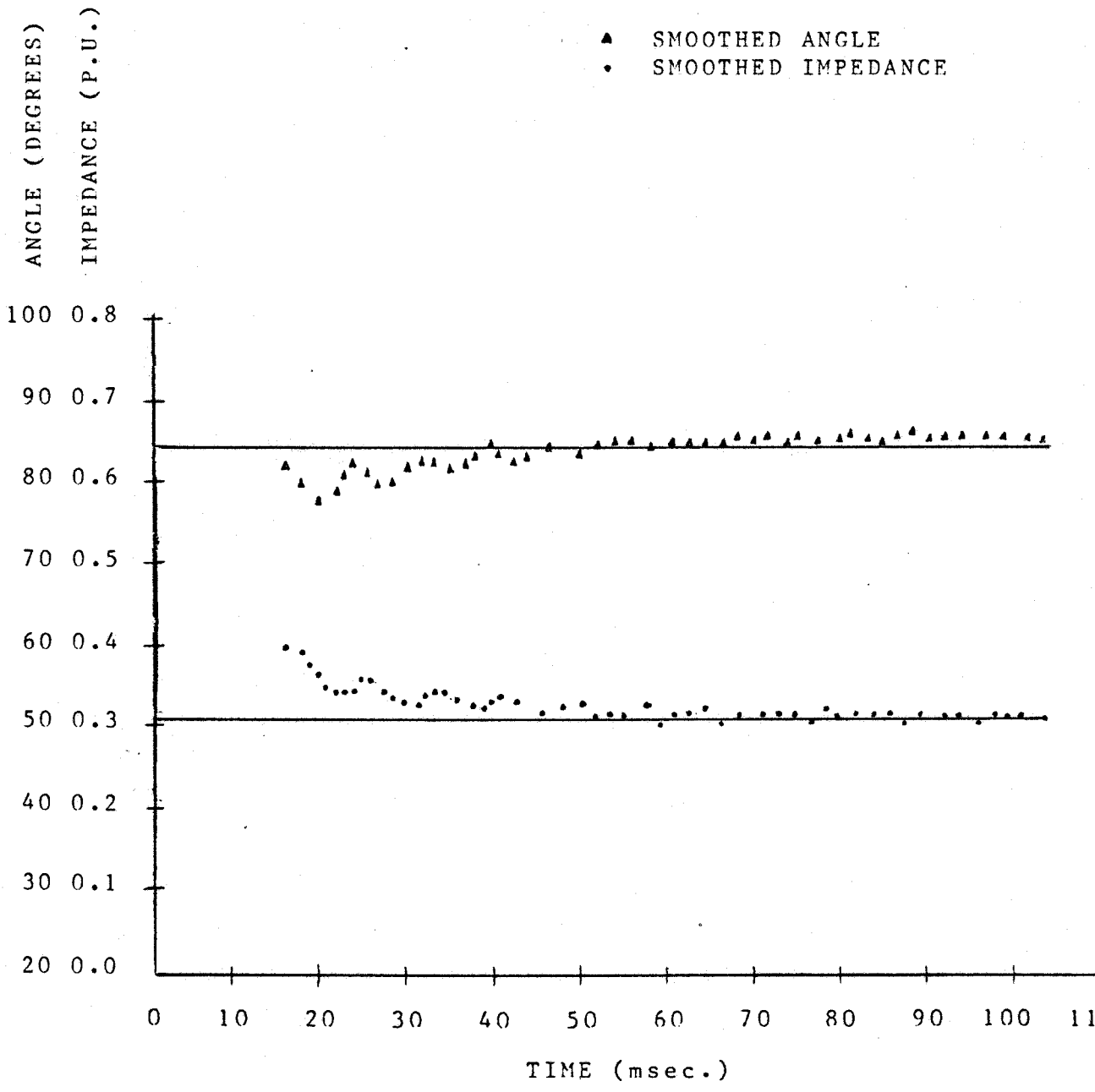

Figure D.3 Bandpass R-Filter (55-65 Hz) + Mann and Morrison Algorithm + Single Exponential Smoothing (a=0.3) - fault incidence at 90 degrees

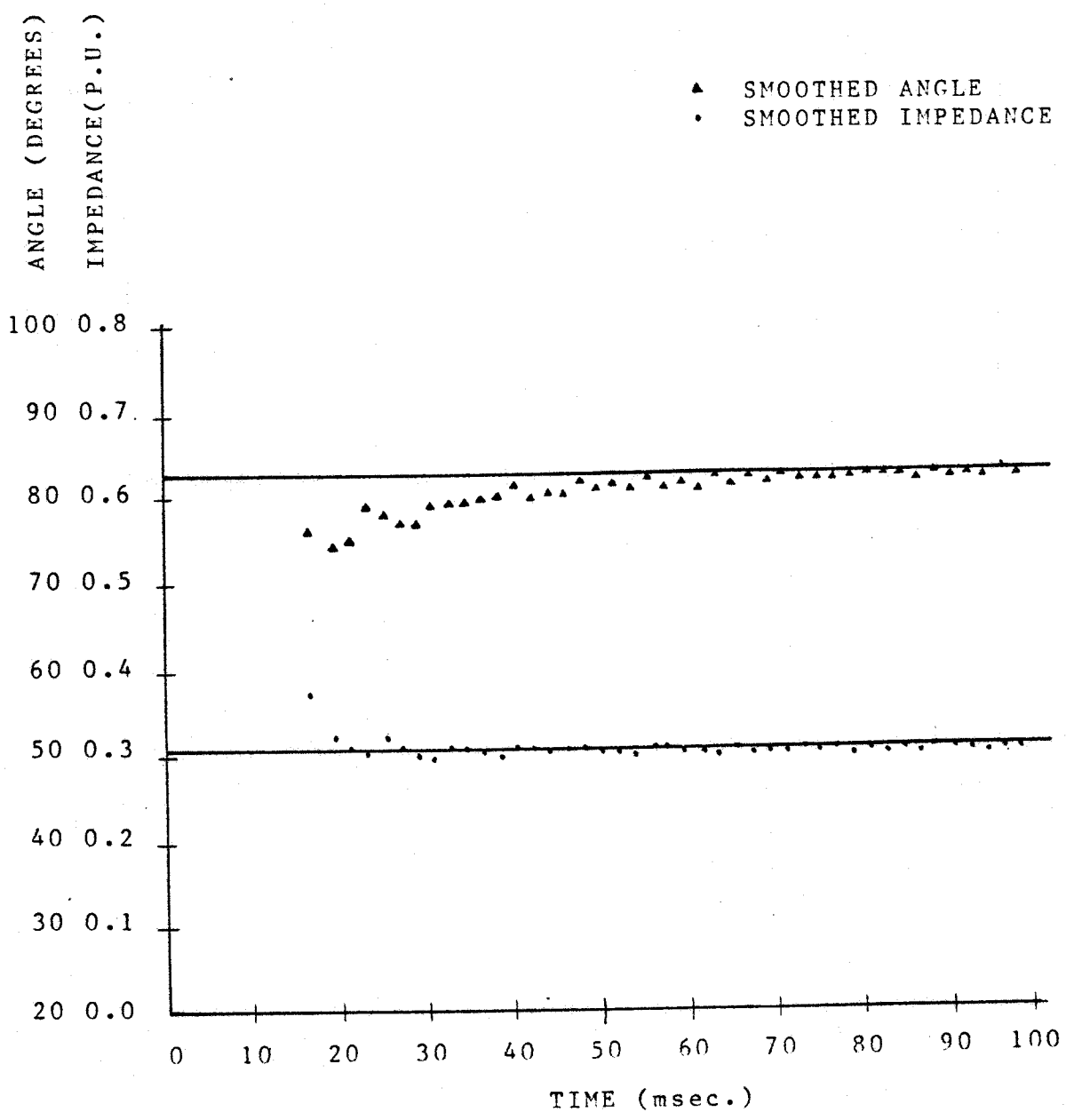

Figure D.4 Bandpass R-Filter (55-65 Hz) + Least Error Squares Pure Sine Wave Model + Single Exponential Smoothing (a=0.3) - fault incidence at 30 degrees

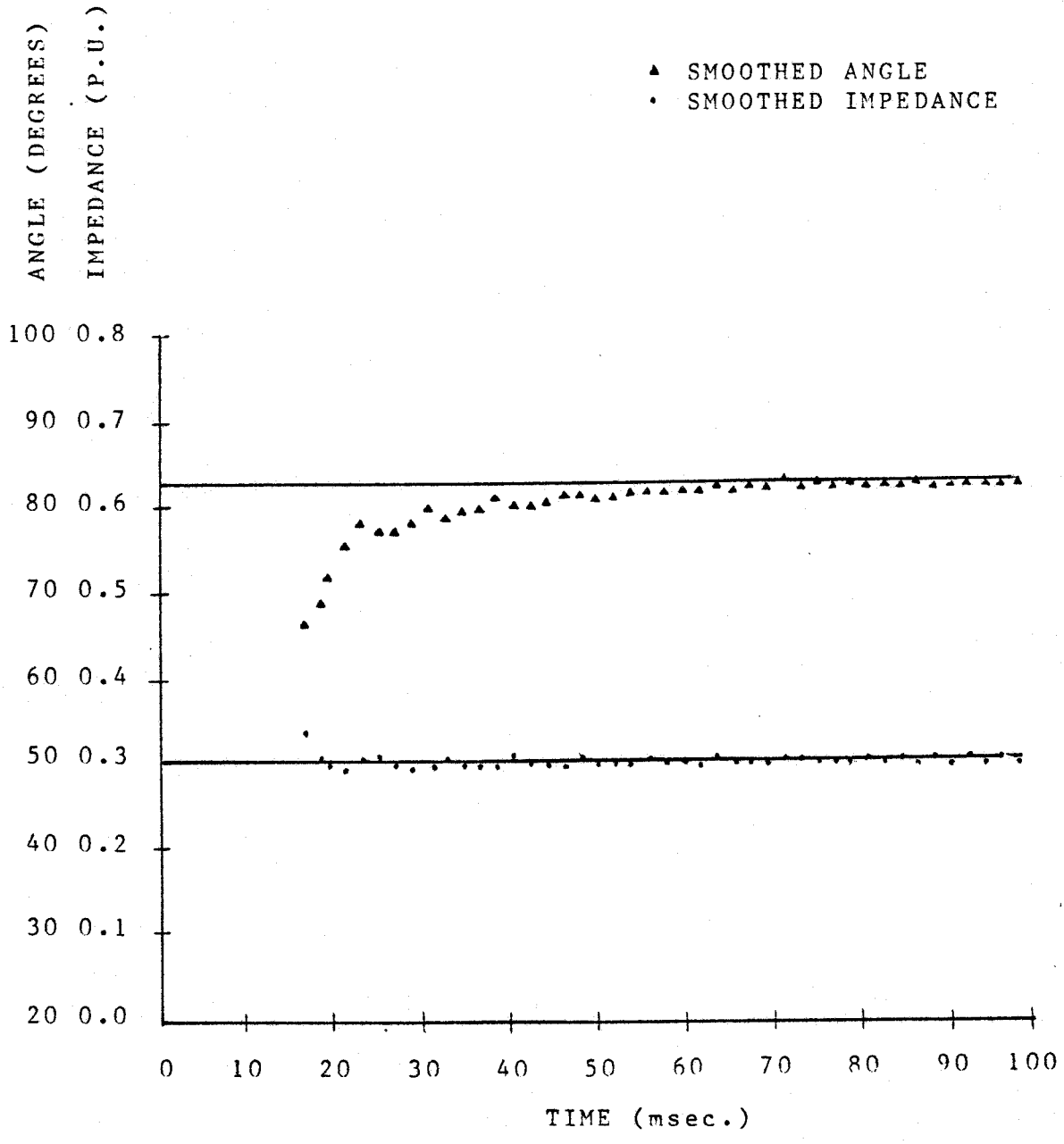

Figure D.5 Bandpass R-Filter (55-65 Hz) + Least Error Squares Pure Sine Wave Model + Single Exponential Smoothing (a=0.3) - fault incidence at 60 degrees

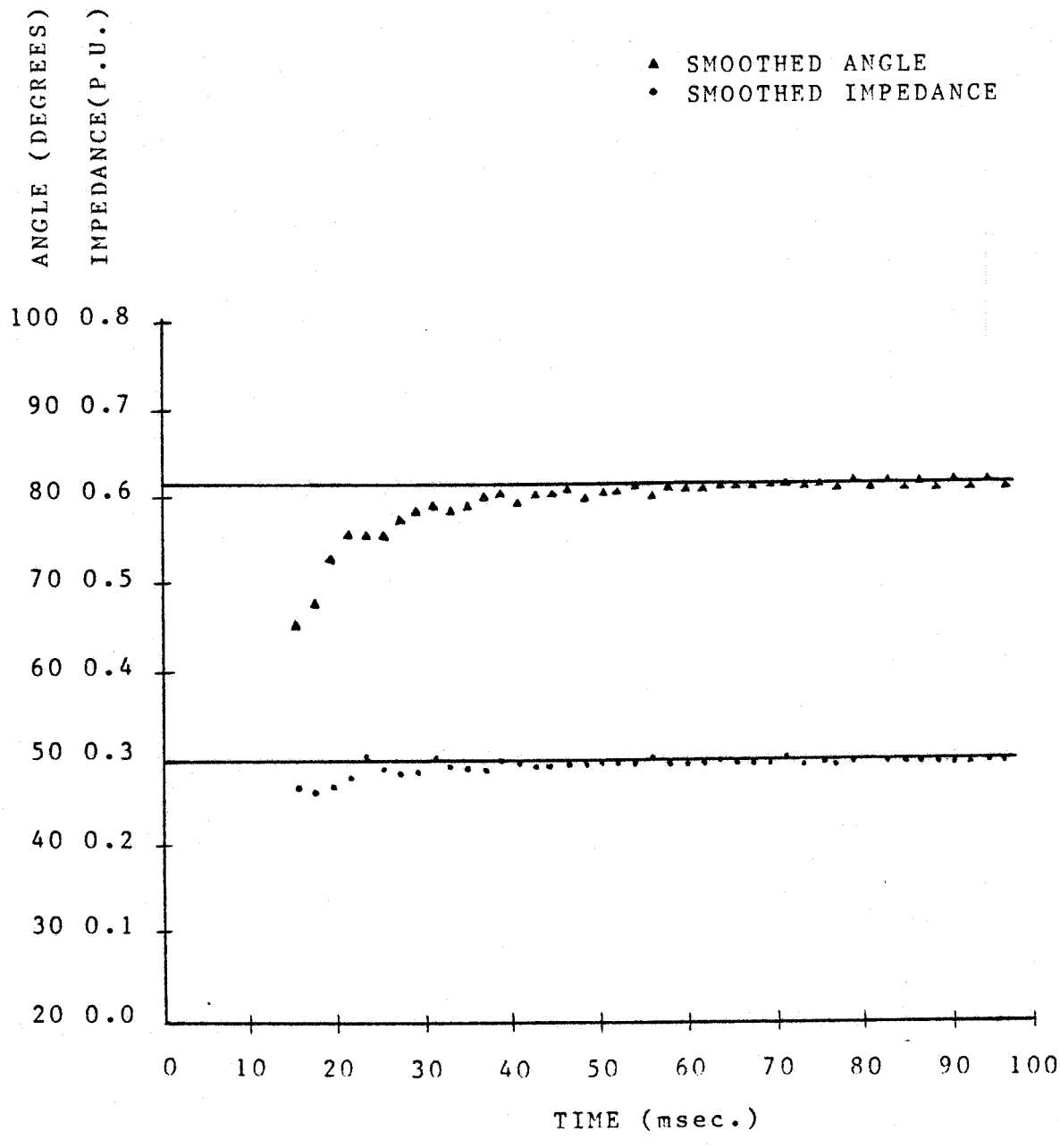

Figure D.6 Bandpass R-Filter (55-65 Hz) + Least Error Squares Pure Sine Wave Model + Single Exponential Smoothing (a=0.3) - fault incidence at 90 degrees

E.1 Parameters of the Power Systems Shown in Figures 4.1 and 6.1

The parameters of the power systems shown in Figures 4.1 and 6.1 are given below. All values are in p.u. on 275 kV and 75 MVA basis.

Generators

positive sequence reactance $X_1 = 0.2$ p.u.

negative sequence reactance $X_2 = 0.1$ p.u.

zero sequence reactance $X_0 = 0.1$ p.u.

Transformers

positive sequence reactance $X_1 = 0.1$ p.u.

negative sequence reactance $X_2 = 0.1$ p.u.

zero sequence reactance $X_0 = 0.1$ p.u.

Transmission Lines of Figure 6.1

positive sequence impedance $Z_{L1} = 0.143+j0.508$ p.u.

negative sequence impedance $Z_{L2} = 0.143+j0.508$ p.u.

zero sequence impedance $Z_{L0} = 0.326+j1.390$ p.u.

Transmission Line of Figure 4.1

positive sequence impedance $Z_{L1} = 0.0004127+j0.004127$ p.u.

negative sequence impedance $Z_{L2} = 0.0004127+j0.004127$ p.u.

zero sequence impedance $Z_{L0} = 0.001238+j0.01238$ p.u.

Bus Voltages

voltages at the buses 2 and 4 are assumed to be 1.0 p.u.

E.2 A Technique to Modify the Filter Coefficients

The coefficients of the 6X9 least error squares filter can be modified to include the relay setting impedance Z_r. The technique used to modify the filter coefficients is given in this section.

Consider that the row vectors [A] and [B] represent the orthogonal filters such that:

$$I_p \cos(\theta) = \underset{1x9}{[A]} \; \underset{9x1}{[I]} \qquad (E.1)$$

$$I_p \sin(\theta) = \underset{1x9}{[B]} \; \underset{9x1}{[I]} \qquad (E.2)$$

where: [I] is the colum vector representing nine sampled values of a current

Now consider that the relay setting impedance is:

$$Z_r = R + jX \qquad (E.3)$$

Also $I_p Z_r$ is given by:

$$\begin{aligned} I_p Z_r &= \{I_p \cos(\theta) + jI_p \sin(\theta)\}(R + jX) \\ &= \{RI_p \cos(\theta) - XI_p \sin(\theta)\} + j\{XI_p \cos(\theta) + RI_p \sin(\theta)\} \end{aligned} \qquad (E.4)$$

Substituting for $I_p\cos(\theta)$ and $I_p\sin(\theta)$ from Equations E.1 and E.2, the following equations are obtained.

$$I_p Z_r = R\,[A][I] - X\,[B][I] + jX\,[A][I] + jR\,[B][I]$$
$$= [R[A] - X[B]][I] + j[X[A] + R[B]][I] \qquad (E.5)$$

The real and imaginary components of $I_p Z_r$ can then be obtained by using the row vectors $[C] = [R[A]-X[B]]$ and $[D] = [X[A]+R[B]]$.

This technique saves computation time when the product $I_p Z_r$ is computed in the real time mode.